2016

DIFFERENTIAL GENE EXPRESSION IN EQUINE CARTILAGINOUS TISSUES AND INDUCED CHONDROCYTES

Emma N. Adam
University of Kentucky, eadam9387@gmail.com
Digital Object Identifier: http://dx.doi.org/10.13023/ETD.2016.343

STUDENT AGREEMENT:

I represent that my thesis or dissertation and abstract are my original work. Proper attribution has been given to all outside sources. I understand that I am solely responsible for obtaining any needed copyright permissions. I have obtained needed written permission statement(s) from the owner(s) of each third-party copyrighted matter to be included in my work, allowing electronic distribution (if such use is not permitted by the fair use doctrine) which will be submitted to UKnowledge as Additional File.

I hereby grant to The University of Kentucky and its agents the irrevocable, non-exclusive, and royalty-free license to archive and make accessible my work in whole or in part in all forms of media, now or hereafter known. I agree that the document mentioned above may be made available immediately for worldwide access unless an embargo applies.

I retain all other ownership rights to the copyright of my work. I also retain the right to use in future works (such as articles or books) all or part of my work. I understand that I am free to register the copyright to my work.

REVIEW, APPROVAL AND ACCEPTANCE

The document mentioned above has been reviewed and accepted by the student's advisor, on behalf of the advisory committee, and by the Director of Graduate Studies (DGS), on behalf of the program; we verify that this is the final, approved version of the student's thesis including all changes required by the advisory committee. The undersigned agree to abide by the statements above.

Emma N. Adam, Student

Dr. James N. MacLeod, Major Professor

Dr. Daniel Howe, Director of Graduate Studies

DIFFERENTIAL GENE EXPRESSION IN EQUINE CARTILAGINOUS TISSUES AND INDUCED CHONDROCYTES.

_____

DISSERTATION

_____

A dissertation submitted in partial fulfillment of the
requirements for the degree of Doctor of Philosophy in the
College of Agriculture, Food and Environment
at the University of Kentucky

By
Emma Noble Adam
Lexington, Kentucky
Director: Dr. James N. MacLeod, Professor of Veterinary Science
Lexington, Kentucky
2016

ABSTRACT OF DISSERTATION

DIFFERENTIAL GENE EXPRESSION IN EQUINE CARTILAGINOUS TISSUES AND INDUCED CHONDROCYTES.

Degenerative joint disease, or osteoarthritis, is a major cause of lameness and morbidity in horses, humans, and dogs. There are no truly satisfactory cures for this widespread problem and current treatments all have limitations or unwanted side effects.

New cell-based strategies to repair joint surface lesions have generated a high level of interest, but have yet to achieve the full restoration of articular cartilage structure and function. Currently used therapy cells include autologous chondrocytes and adult mesenchymal cells such as bone marrow derived cells and adipose derived cells. Unfortunately, the resultant repair tissue is biomechanically inferior fibrocartilage. A critical gap in knowledge in this regard is a limited understanding of the specific cellular phenotype of normal, robust articular chondrocytes.

This thesis examines the global mRNA transcriptome of equine articular cartilage to test the hypothesis that adult articular chondrocytes have a unique gene expression profile. In the first part of the study, RNA-sequencing was used to compare the mRNA transcriptome of normal adult articular cartilage with five other cartilaginous tissues. From these comparisons, locus level gene expression and alternative splicing patterns have been identified that clearly distinguish articular cartilage. In the second part of the study, fetal (interzone, cartilage anlagen chondrocytes, dermal fibroblasts) and adult (bone marrow derived, adipose derived, articular chondrocytes, dermal fibroblasts) primary cells were grown in culture and stimulated to differentiate into chondrocytes. The chondrogenic differentiation potential as assessed by matrix proteoglycan and the expression of cartilage biomarker genes was highly variable among cell types. Together, these results advance our understanding of the specific phenotype of articular chondrocytes and the potential of prospective therapeutic progenitor cells to differentiate into articular chondrocytes. This new knowledge will improve efforts to optimize cell-based therapies for osteoarthritis and the repair of joint cartilage lesions.

KEYWORDS: Horse, Transcriptome, Cartilage, Regenerative Medicine, Interzone

Emma Adam

July 25th, 2016

DIFFERENTIAL GENE EXPRESSION IN EQUINE CARTILAGINOUS TISSUES

AND INDUCED CHONDROCYTES.

By

Emma Noble Adam

Dr. James MacLeod

Director of Dissertation

Dr. Daniel Howe

Director of Graduate Studies

July 25th, 2016

ACKNOWLEDGEMENTS

The Odyssey of this PhD program has been the ride of a lifetime. Firstly, I thank the continued loving support of my family; Chris Adam, Grace Adam and Dave Kingett. Among their many talents, they have provided moral support and an amazing tolerance of my impecuniary pursuits.

For this opportunity I am immensely grateful to my mentor, and now friend, Jamie MacLeod. Jamie is an exemplary PhD mentor showing a dedication to his students and an honesty of spirit that is rare indeed. I look forward to further research projects together. I would also like to thank the solid support and help of Walter and June Zent. Their friendship and support is hard to measure.

I thank my committee members for their support and help whenever I needed it, and to Ernie Bailey for helping me into the world of genomics. My lab colleagues, past and present deserve significant mention. Drs. Stephen Coleman, Jennifer Janes, Parvathy Thampi, Scottie DePriest, as well as Rachael Lowney have been an immense source of support, help, and have offered interesting discussions for our work. Thank you to Dr. Robert Flight for his insightful help at a time of crisis, and to Josh Lambert and Arnie Stromberg for steering me straight and answering all of my questions. Thanks to my dear colleagues, Xinan Liu and Yi Zhang, for their computational expertise and patience with me.

At the University Farm and at the Veterinary Diagnostic Lab I would like to thank Kevin Gallagher, Chad Tucker, and Jamie Howard. Their expertise and caring attention to their work has made this thesis the richer.

There are likely many people I have failed to mention by name, so I will suffice to say that during my PhD I am grateful to the myriad of interactions, friendships and collaborations that have made it the enriching journey that it has been.

TABLE OF CONTENTS

LIST OF TABLES

LIST OF FIGURES

Chapter 1

Introduction

Articular cartilage exists on the end of bones to form synovial joints that allow smooth, pain-free, and low friction movement between adjoining bones. It provides tensile strength and resists compressive forces during weight bearing and locomotion. It is a unique tissue where form and function combine to produce remarkable biomechanical properties.

Cartilage is avascular, aneural and alymphatic and exists in a physiologic hypoxia – '*physioxia*' (physioxia refers to a physiologic oxygen tension of 1 - 11%)[1,2]. Articular cartilage is described as 'hyaline', a word that takes it derivation from the Greek word meaning transparent or glassy in appearance. This is nothing more than a gross description that belies the pleiotropic and complex architecture of the tissue, the components and organization of which hold the key to its remarkable biomechanical properties. Other adult cartilages that fall under this classification include nasal septum, tracheal rings and part of the ear pinna cartilage. However, unlike these cartilages, articular cartilage is devoid of a surface perichondrium, being interlocked to the subchondral bone on one side and gliding with the articular cartilage of the opposing bone surface.

Like all cartilage, articular cartilage is composed of an extracellular matrix (ECM) elaborated by the resident chondrocytes that make up a small percentage of the mass of the tissue. In articular cartilage, this is estimated to be ~ 2% by mass[3]. Typically, adult mammalian articular cartilage is 1 - 4 mm thick and has a zonal appearance histologically[4]. These characteristics are relatively conserved across species with diarthrodial joints, and equine and human articular cartilage are

of comparable thickness[5]. A brief background of the makeup of articular cartilage is vital to understanding the challenges faced when considering this tissue in both health and disease.

Zones of Articular Cartilage

Figure 1.1 depicts the four basic zones seen in articular cartilage histologically.

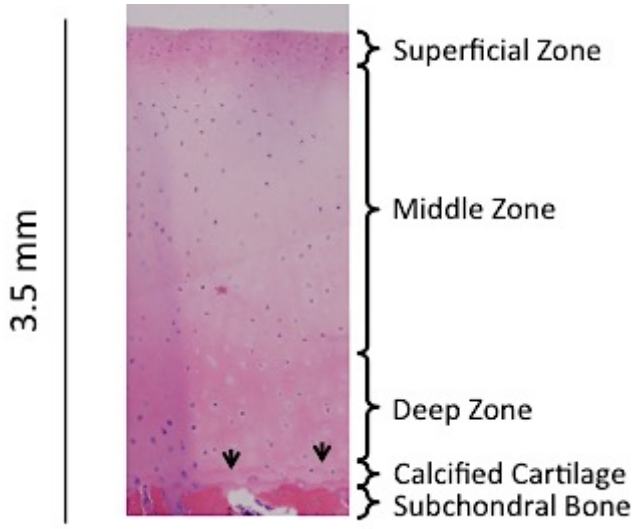

Figure 1.1*. Photomicrograph of a section of equine medial femoral condyle (age 15 months) depicting articular cartilage and subchondral bone stained with hematoxylin and eosin. Arrow heads pointing downwards localize the so-called 'tidemark' that marks the junction of the Deep Zone and Calcified Cartilage.*

The *superficial (tangential) zone* consists of a relatively dense population of flattened chondrocytes, with collagen fibers oriented in parallel to the gliding surface. These parallel fibers are thought to be the apex of collagen arcs which span the depth of the tissue according to the model proposed by Benninghoff in 1925[6]. As such, the superficial layer protects the deeper layers from erosion, optimizing surface gliding with its superior tensile strength and by interacting with synovial fluid. Here collagen fibrils, primarily of Collagen type II and Collagen type IX, are thinner than in the rest of the matrix.

The *middle (transitional) zone* is the anatomical and functional bridging zone between the superficial and deep zones. In a somewhat gradient fashion, from the articular surface to the underlying subchondral bone, chondrocyte density decreases, chondrocyte volume increases,

and the proteoglycan content in the matrix increases. This zone has robust resistance to compressive forces and thicker collagen fibrils are seen in oblique orientations histologically.

The *deep zone* has the lowest water content, highest proteoglycan content, and largest diameter of collagen fibrils that are seen to radiate from the subchondral bone with a perpendicular orientation. The paradigm of lowest water content in spite of the highest proteoglycan content is thought to be related to the flow of water through the cartilage along this gradient to transport and distribute nutrients to chondrocytes[4]. The deep zone offers the greatest resistance to compressive forces. Chondrocytes in this zone are typically arranged in short columns parallel to the collagen fibrils.

Beneath the deep zone in a mature individual is the *calcified cartilage.* This zone anchors the cartilage to the underlying subchondral bone and chondrocytes are more sparse. The so-called *tidemark* is a refractive histological feature observed at the junction between the deep and the calcified layers.

Extracellular Matrix

In addition to structural zones defined histologically, the matrix exhibits localized variation in molecular composition. Immediately around the chondrocyte is the *pericellular matrix*. The pericellular matrix is an important transducer of biomechanical and biochemical signals for the chondrocyte to respond to its environment[7]. While small at only 1 – 2μm thick, it is distinguished by a relative abundance of Collagen type VI in addition to types II and IX. The *territorial matrix* is immediately adjacent to the pericellular matrix. It has a fine network of collagen fibrils thought to protect the pericellular matrix from mechanical stress[3]. The remaining category and vast majority of the ECM is termed *interterritorial,* and is largely responsible for the biomechanical properties of articular cartilage.

Collagen makes up ~ 60% of the dry weight of cartilage, of which collagen type II comprises 90-95%. For this reason, Collagen type II is a traditional biomarker of all cartilaginous tissues. Other collagens molecules are present, types I, IV, V, VI, IX and XI, but in comparison these make up only a minor proportion of articular cartilage's total collagen composition.

The second largest group of macromolecules in articular cartilage is proteoglycans, accounting for 10-15% of the tissue's wet weight. Because they are heavily glycosylated and sulfated with a high negative charge density, they remain separated from each other by anionic repulsion and also capture the 65 - 80% water content of articular cartilage. This water content is central to articular cartilage's ability to resist compressive forces making the proteoglycan content hugely important. Proteoglycans found in abundance in articular cartilage include chondroitin sulfate, keratin sulfate, and aggrecan. All of these interact with Collagen type II, further enhancing the structural complexity of articular cartilage. Aggrecan is the major articular cartilage proteoglycan, and represents another traditional biomarker of this tissue.

As noted, articular cartilage is a heterogeneous tissue[8]. Morphological differences in chondrocytes between the histologically-defined zones, as well as different matrix molecular profiles elaborated by chondrocytes under different biomechanical forces add complexity to the investigation of chondrocyte cell biology. Chondrocytes from different locations within the same joint, from different, but homologous joints, and from allogeneic joints have been used to obtain chondrocytes for cell-based therapies in clinical medicine. Additionally, chondrocytes from different cartilaginous tissues, such as nasal septum, have been considered suitable replacement chondrocytes for articular cartilage lesions[9]. Only limited consideration has been given to the likelihood that different cartilaginous tissues will have functionally distinct populations of chondrocytes. Similarities and differences between the cell biology of articular

chondrocytes relative to chondrocytes in other hyaline cartilages in the body or their developmental progenitors represent a major knowledge gap. Given the great challenges that diseases of articular cartilage pose, global analyses of gene expression at a transcriptome level may provide important new insight with potential clinical relevance.

Osteoarthritis

The highly differentiated function and minimal mitotic activity of chondrocytes along with the avascular nature of cartilage are cited as the biggest factors responsible for cartilage's extremely limited intrinsic repair capacity[10]. Over time, wear and tear on articular cartilage from normal movement can exceed the tissue's repair capacity. Cartilage degradation is compounded by trauma, intense athletic activity, infection, and age-associated chondrocyte senescence[11]. The resulting progressive loss of articular cartilage leads to osteoarthritis (OA) and compromised joint function. This is a common condition in mammalian species, with major clinical significance for humans, horses and dogs. In humans, OA is one of the most widespread causes of musculoskeletal pain, economic loss and disability[11-13]. Nearly 27 million adults in the United States as of 2008, were estimated to have Doctor diagnosed OA[12,13]. In horses, OA is the number one cause of retirement from an athletic career[14]. In spite of decades of research and clinical intervention efforts, OA continues to represent a major medical challenge and the restoration of articular cartilage remains a huge unmet clinical need.

Current therapies for articular cartilage lesions include pain- and inflammation relieving medications, joint injections with corticosteroids and/or synthetic hyaluronic acid, surgical debridement of the lesion, and ultimately, in humans, prosthetic joint replacement[5,14]. None of these therapies, however, effectively recapitulate articular cartilage or fully restore normal

diarthrodial joint function. In addition, these therapies include the potential for distinct and unwanted side-effects, some of which can have substantial clinical significance[15-17]. A further complication is that repair tissue in articular lesions is often poorly integrated, highly cellular fibrocartilage with abnormally high amounts of collagen type I and less than normal amounts of collagen type II. Repair tissue architecture does not resemble that of normal cartilage and its functional lifespan is limited and counted in years[18-22]. Figure 1.2 illustrates damaged articular tissue in the femorotibial (stifle) joint of a horse viewed arthroscopically and a histological section of the type of fibrocartilage repair tissue that often forms in such a lesion.

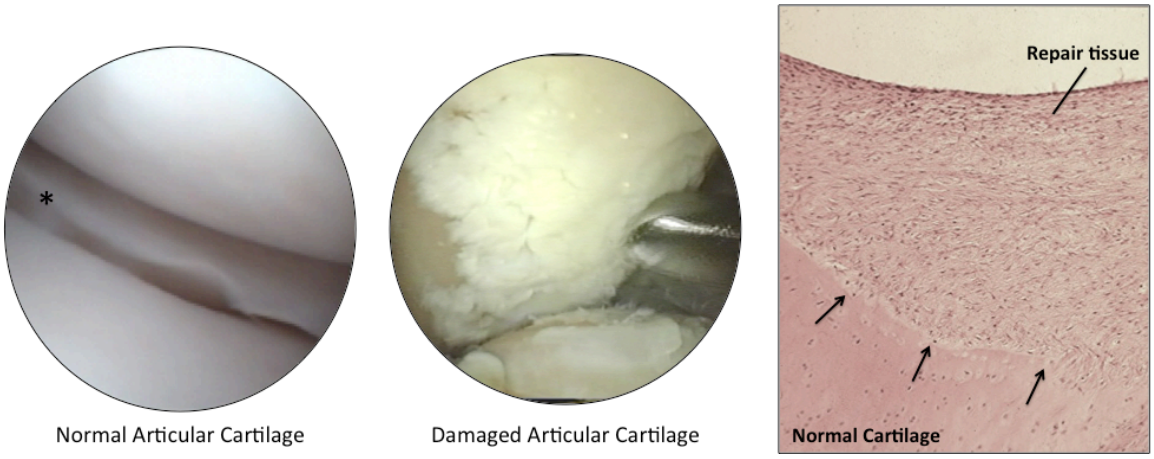

***Figure 1.2**. Left: Arthroscopic view of normal articular cartilage with an interposed meniscus(*). Center: Arthroscopic view of severely damaged cartilage. The cartilage is white, with the metal probe on the right of the image indenting the soft, damaged cartilage matrix. The adjacent yellow colored tissue is exposed subchondral bone. Right: Hematoxylin and eosin stained histological section of fibrocartilage repair tissue illustrating poor integration with adjacent normal articular cartilage tissue (arrows). Images courtesy of Dr. Dean Richardson, University of Pennsylvania, and Dr. Lisa Fortier, Cornell University.*

A reduction in morbidity and more rapid return to activity in humans with cartilage lesions has been demonstrated with autologous chondrocyte implantation (ACI), first introduced in the early 1990's[23]. Therapy cells are generated from autologous chondrocytes harvested surgically and digested from their native matrix. The original concept was that increased cell density

within the lesion site would augment the repair process. In order to generate the large numbers of cells needed for the procedure, chondrocytes must be expanded as monolayer cultures *in vitro* and implanted into the defect during a subsequent surgery. Improvements on this technique have included a periosteal 'bandage' attached over the lesion, as well as the incorporation of various engineered matrices (Matrix-assisted Autologous Chondrocyte Implantation, MACI) to augment retention and physical protection of the transplanted cells[19,24].

Unfortunately, chondrocytes expanded in monolayer culture readily lose their differentiated phenotype[25]. This dedifferentiation phenomenon is cited as a major reason for their failure to recapitulate native articular cartilage at implantation. However, even with efforts to re-differentiate these cells after expansion, the surgical results are little improved[26]. In an effort to use chondrocytes from more accessible sites, nasal septum cartilage has been harvested to generate autologous joint therapy cells[27-30]. *In vitro* reports suggest nasal septum chondrocytes can generate neocartilage that has attractive characteristics and an equine *in vivo* model experiment is said to be underway[9]. However, the evaluation of the neocartilage generated was limited to a few output measures and was not subject to biomechanical testing.

In addition to the problem of cellular dedifferentiation with ACI/MACI techniques, the desire to avoid two surgical interventions led to the investigation of mesenchymal stem cells as therapy cell sources. Mesenchymal stem cells attracted attention because they proliferate readily and can be induced to become chondrocyte-like under chondrogenic conditions *in vitro.* Cells that have these properties can be obtained from a variety of tissue sources, but for the focus of this discussion the two more mainstream sources are bone marrow aspirates and adipose tissue[28]. Adipose tissue is typically abundant and readily harvested in humans [31,32]. Bone marrow

aspirate can be obtained with minimal intervention as well[33]. Human nucleated, plastic-adherent cells with appropriate mesenchymal stem cell surface markers ($CD29^+$, $CD44^+$, $CD166^+$, $CD105^+$, $CD45^-$, $CD34^-$) have been shown to be capable of tri-lineage differentiation[34]. Tri-lineage differentiation has been considered a 'gold standard' characteristic in many studies for demonstrating the multipotency of mesenchymal cells. Different induction media and protocols are used to stimulate these cells to exhibit adipocyte, osteocyte, or chondrocyte biomarker gene expression or biosynthetic capability[35,36]. In spite of much promise, the clinical results to date of induced-chondrocyte implantation have been little better than microfracture techniques or ACI/MACI. Repair tissue generated retains fibrocartilage characteristics that do not restore normal articular cartilage form or function[37,38].

Cell surface markers and cellular characteristics of equine mesenchymal stem cells are not exactly the same as those found in humans and remain ill-defined[39-43]. Recent studies published also no longer perform tri-lineage differentiation to demonstrate "stemness" [36,37,44-47]. Despite a paucity of quality research to demonstrate efficacy and optimize protocols, these standard approaches are widely used in equine clinical practice to harvest cells from adipose tissue and bone marrow aspirates for clinical use[37,47].

Developmental Cells of Interest – Interzone.

The continued search for more 'appropriate' and efficacious cell types to use in cartilage regeneration led to consideration of studies from the field of developmental biology[48]. Joint formation is an early embryonic process that is nearing completion in day 7.5 in chick embryos, day E14.5 in mouse embryos[49] and appears to occur in the limb joints of equine fetuses progressively from proximal to distal within a short window between days 35 and 55 of their

~340 day gestation[50] (*Adam and MacLeod, unpublished data*).

As limb buds are developing, condensations of pre-cartilaginous mesenchyme form in the bud. These condensations are termed *anlage* (pl: *anlagen*) from the German word that means to 'layer on'. Under the control of Homeobox transcription factors, cells stop expressing Collagen type I and hyaluronan and start expressing N-cadherin, tenascin-C and other adherence molecules under a *Sox 9* governed Transforming Growth Factor-β, Wnt/β-catenin signaling cascade[51-53]. The *Sox* triad (*Sox 5, 6* & *9*) of transcription factors is required for chondrocyte differentiation and comes into play at this stage[51].

The location of future distal limb joints can be appreciated under light microscopy in chicks around day 6 of incubation due to differential optical characteristics. At this stage, the so-called *interzone* is developing at nascent joint sites; an event first described in 1925 by Fell[54]. More recently, elegant vital dye staining studies strongly suggest that the interzone cells are not differentiated anlage cells, as once thought, but migrate from an adjacent location to demarcate the developing joint site locations[49]. This group identified these cells by their expression of the previously defined and accepted interzone biomarker genes *Wnt9A* (cited in earlier literature as *Wnt14*), *GDF5*, *Gli3*, *CD44* and *COL2A*. The investigators went on to show that interzone derived cells acquired a round chondrocyte-like appearance and expressed high levels of additional articular cartilage biomarkers *COL9* and *ACAN* when cultured *in vitro*. Elegant lineage tracing studies in mice followed the trail to test whether interzone cells were indeed joint progenitors that ultimately form articular cartilage. Initial lineage studies suggested that articular chondrocytes in the interphalangeal joints of mice were derived from cells that had expressed *GDF5*[55]. Hyde *et al*, used Matrillin-1 positive cells to trace lineage. Matrillin-1 is an ECM protein found in anlage, but not in articular cartilage cells. The data indicated that interzone cells went on to become not only articular cartilage, but also related intra-articular structures such as

ligaments and the synovial membrane[56].

Further corroborative studies with conditional knock-out mice revealed that disrupting the normal TGFβ/ Wnt/β-catenin signaling cascade, or surgically ablating this tissue resulted in defective joint formation or an absence of joint formation[49,57-61]. Taken together, these studies firmly established the interzone as containing joint progenitor cells, although its continued existence in mammals as a residual population of joint stem cells remains a matter of active debate[62-64].

Experiments in our lab were the first to indicate that interzone tissue may also be of interest for articular cartilage repair. The experiments were performed in axolotls, an aquatic salamander that retains interzone tissue into adulthood as one of its pedamorphic characteristics. Radical resection of half of the tibiofibulo-tarsal joint interzone and adjacent cartilage that formed the medial condyle of the distal femur achieved spontaneous and full restoration of the joint structure and function over 24 weeks[65]. Furthermore, when interzone-rich tissue explants were placed in critical sized long bone defects in the tibia, remarkably, a *de novo* joint was formed. Control transplants with skin and skeletal muscle did not result in closure of the defect or the generation of a new joint[66]. Cellular and molecular details of the repair process are not well understood, being significantly hampered by the absence of an axolotl reference genome and the inability to culture axolotl cells *in vitro*. As such, it is unclear as to the balance between the interzone-rich tissue cellular contribution to the repair process versus paracrine regulatory mechanisms that orchestrate other cell types to achieve tissue repair, or both.

Studies of interzone tissues in mammals are limited due to the period in development when they exist – that is *in utero*. Mouse embryos have provided significant insight through utilization of the many inducible *cre*-recombinase genetic mutants that are available or can be generated.

However, interzone tissue volumes in the murine embryo are extremely limited and as such equine embryos offer a more robust source of interzone for *in vitro* studies. Our lab has been able to develop a protocol to harvest embryos and fetuses from mares that is performed standing with the mare under light sedation. The epitheliochorial equine placenta makes flushing the fetus from the gravid uterus by lavage a relatively easy and non-invasive procedure. We have harvested fetuses of 45 - 68 days of gestation with this technique. Figure 1.3 shows a 46 day equine fetus collected in this manor (described more fully in Chapter 3). Histology reveals that developing skeletal structures including diarthrodial joints are already apparent and fairly well organized, even at this very early gestational age.

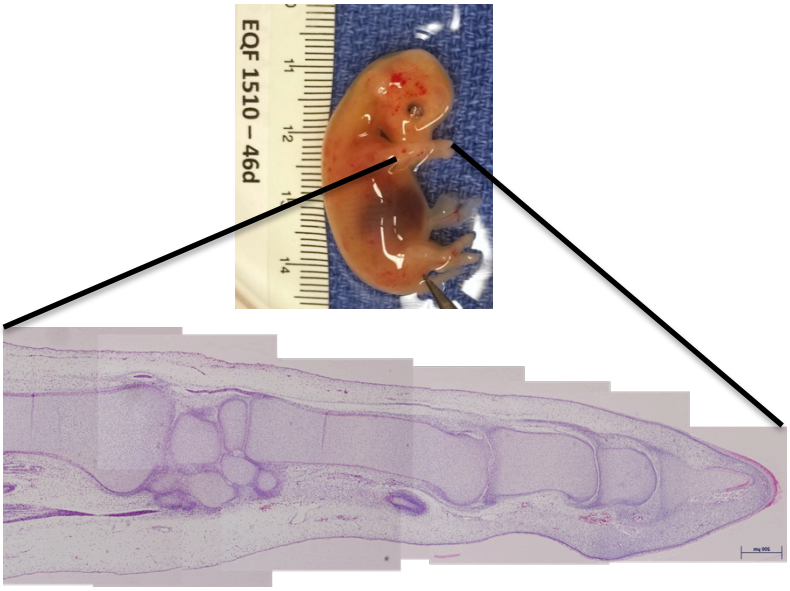

Figure 1.3. A 46 day gestational age equine fetus, with the forelimb (mid-radius to third phalanx) shown below as a composite of photomicrographs from hematoxylin and eosin stained sections. Ongoing cavitation of the joints at this stage in development is clearly seen. The scale bar is 200μm. The length of limb shown is approximately 3mm.

New technologies

What is evident from published descriptions of the molecular phenotypes for the cells and tissues already discussed is that much of these characterizations are based on a limited number of marker genes or protein products. The fundamental disappointment of cells that show promising chondrogenic behavior *in vitro,* but then fail to achieve this potential *in vivo* may

partially reflect shortcomings of the limited assessments applied.

With the advent of high throughput sequencing platforms and the establishment of annotated reference genomes, the opportunity to assess gene expression on a transcriptome level has become a reality. The equine genome was sequenced in 2007 and has been a catalyst for equine research in many areas[67]. Being able to scrutinize the expression of traditional biomarker gene lists, while concurrently having the entire transcriptome data of the cell or tissue is a powerful scientific resource. Next generation sequencing (NGS) has enabled this quantitative and qualitative data resource to become a reality for many laboratories, and has rapidly gained traction for gene expression studies in all fields of research. This technology emerged from efforts to sequence the human genome, and the transition to solid phase technology has enabled a massive increase in throughput – hence the term Next Generation. Importantly, these advances have come with a concurrent and substantial cost decrease per nucleotide base, making it ever more accessible to scientists. However, the gargantuan amount of primary data generated, concerns over false discovery rate detection, and the pitfalls of imperfect reference genomes with limited annotation make these data a challenge to work with.

With each breakthrough in technology, we can look back and reflect on the limitations of earlier studies. Only 15 years ago, equine gene expression analyses were still being performed with cumbersome Northern blotting techniques[16]. However, it is vital to remember that each former increment was a necessary stepping-stone along the path of discovery and past efforts should be commended, not condemned, for dealing with the limitations of their time. On a whole tissue mRNA transcriptome level, it is easy to see how we might uncover limitations of our path so far in divining a genuine, robust articular cartilage therapy cell. However, *a priori,* we need a better understanding of normal adult articular cartilage to have a "gold standard" by which to

compare. The nuances of gene expression and synthesis of tissue restricted mRNA splice variants has long been in our research vocabulary. Twenty years ago, our lab published data on an articular cartilage restricted mRNA variant of fibronectin, termed the (V+C)- isoform[68]. Prior to this, alternatively spliced type II procollagen was reported and its significance in embryonic development considered by the authors[69]. Since then, evidence for tissue-restricted gene expression being more than a loci level difference in expression has mounted. Regulation at the level of mRNA splicing is now recognized and widely accepted as a major molecular mechanism of cellular specificity[70]. Work performed in our lab by Hestand *et al* was able to illustrate this with RNA-seq data from a group of 16 different human tissues[70]. As expected, almost 40% of protein-coding gene loci were commonly expressed across all sixteen tissues – what might be termed 'housekeeping genes. Equally unsurprising was the much smaller subset of gene loci expressed in a tissue-restricted pattern – the 'biomarker' genes, such as Collagen type II in articular cartilage. However, a surprising result was that approximately 65% of expressed, multi-exon genes contained at least one tissue-restricted splice-junction. These data confirm that tissue-restricted alternative splicing is widespread, including gene loci with a broad pattern of expression. That is, those genes expressed in many tissues but with a unique and tissue-restricted splice variant. RNA sequencing data has proven to be very efficient in discovering mRNA transcript variants with high levels of resolution. Before this technology and associated computational analytical methods, much of the complexity in the mRNA transcriptome went undetected.

To date there are numerous transcriptome studies in various areas of science. However, in terms of cartilage research, they are very limited. Although isolating high quality RNA from cartilage is challenging, cartilage is a tissue that lends itself to the generation of 'clean'

transcriptome data. Unlike most other tissues, it is not a composite of several cell types, such as endothelium, nervous tissues, epithelium etc. Cartilage consists of just chondrocytes and matrix, although the chondrocytes may exhibit gene expression differences according to their location in different types of cartilage or within different zone in articular cartilage[8,71]. Our lab has generated microarray data comparing different cartilage tissues at different ages, stages of maturation and repair tissue[18,72,73]. These studies highlighted the utility of global gene expression in observing stark differences between tissues traditionally observed to be somewhat similar. Similarly, microarray expression data have examined murine cartilage formation which confirmed gene expression data regarding developmentally important genes such as *COL2A1, ACAN, BMP8A, GDF5*, and N-cadherin (*NCAD*) and identified less well known candidates such as *SOX11* and *TRPV4*[74]. To date there are a limited numbers of studies using RNA-seq transcriptome data generated from adult cartilage tissue. One such study was performed to compare transcriptomic signatures in aging cartilage[75]. In discussion with one of the authors of this paper, it is worth noting that they expressed the difficulty experienced in obtaining equine tissues in a timely fashion and that they were at the mercy of slaughterhouses for their experimental samples. Their study suffered from these issues as their RNA quality was sub-optimal and suffered significant attrition of reads during threshold trimming according to quality score thresholds. The data did demonstrate, however, an over-representation of genes with reduced expression relating to ECM, matrix synthetic enzymes and growth factors in cartilage from the older horses (>15 years old) compared with the young horses (4 years old). Additionally, they identified a reduction in Wnt signaling-pathway genes in ageing cartilage.

Priority Knowledge Gaps and Questions

The studies presented here are designed to address identified gaps in articular chondrocyte cell biology, specifically in relation to unique patterns of gene expression. Experiments reported in Chapter 2 test the hypothesis that articular cartilage exhibits a unique tissue-restricted pattern of loci-level gene expression and alternative splicing. These data are used in Chapter 3 to gain new insight into the proficiency of different adult and fetal cell progenitor cell types stimulated to form chondrocytes with an articular-type phenotype. In doing this we will test the hypothesis that interzone cells have a chondrogenic potential that exceeds that of adult bone marrow derived and adipose derived mesenchymal stem cells. Finally, Chapter 4 will reflect on work performed so far and elaborate on a promising RNA-seq data set resulting from work performed in Chapter 3. Several future directions will also be proposed.

Chapter 2 Gene Expression Patterns That Distinguish Equine Articular Cartilage From Other Cartilaginous Tissues.

Introduction

Degenerative joint disease (DJD) is the number one cause of lameness and cause for retirement from athletic pursuits in all equine breeds, regardless of athletic discipline[76]. There are no current cures for advanced articular cartilage degeneration and treatments range from non-steroidal anti-inflammatory drugs, intra-articular corticosteroids, surgical debridement, autologous chondrocyte implantation, and intra-articular mesenchymal stem cell therapy [14-17,35,37]. None of these modalities, however, can fully repair damaged articular cartilage and restore joint surface integrity, and some have severe long-term detrimental effects [14,17,77]. DJD, or osteoarthritis (OA) as it is usually termed in humans, is an equally serious problem for physicians, who are seeing an ever increasing number of patients with this condition[5]. As such, the functional restoration of damaged articular cartilage remains an unmet, very important and growing clinical need[35,37].

A major limitation to healing joint surface lesions is the inability to produce a robust chondrocyte in the repair tissue that can integrate with, and function as a normal articular chondrocyte synthesizing appropriate cartilage matrix [18,64,71,72]. Articular defects in horses and other mammals fill partially with a fibrocartilaginous tissue that is rich in collagen type I, highly cellular[18], poorly organized, and woefully unable to integrate with the adjacent native tissue. As such, it restores only a fraction of the biomechanical properties associated with normal articular cartilage and, worse still, is less durable, starting to fray and detach with wear and tear.

Based on structural differences among cartilaginous tissues, comparative *in vitro* studies using expanded primary chondrocytes, and efforts to differentiate stem cells into chondrocytes, it is clear that not all chondrocytes are equivalent on a molecular biology level [26,64]. Further knowledge on the cellular and molecular phenotype of normal articular chondrocytes should provide new opportunities to advance therapeutic options. Comprehensive gene expression profiles and a determination of unique, tissue-restricted expression patterns of articular chondrocytes relative to progenitor cells and other cartilaginous tissues may provide valuable functional insights, with clinical implications.

Transcriptome shotgun sequencing or RNA-sequencing (RNA-seq) is a relatively new and widely adopted high-throughput technology that enables robust characterization of RNA transcripts in a sample on both qualitative and quantitative levels[78-81]. Cartilage is a tissue that is difficult to extract significant quantities of high quality RNA from due to the dense matrix encasing the relatively sparse population of cells that both hinders access to them and complicates chemical extraction of RNA. An important benefit, however, is the relatively homogenous population of cells compared to tissues that are vascularized, innervated, and have connective tissue planes that result the inclusion of multiple cell types within a tissue sample. As such, RNA sequencing of articular cartilage will provide specific transcriptome level expression data for chondrocytes at both a loci level, as well as splicing variants for this unique tissue.

RNA-seq has the capacity to generate genome wide data for loci level expression as well as the ability to resolve distinct splicing patterns. It is a data driven tool where the observer is guided by the data rather than examining a pre-determined list of genes. Using the MapSplice software developed in our group[81], we recently analyzed RNA-seq data from 16 human tissues[82]. The data revealed unique and tissue-restricted splicing patterns from gene loci that had a broad

pattern of expression across the tissues. These nuances would not have been detected without the ability to parse splicing events at this level. These studies found that all 16 tissues had hundreds of tissue-restricted splice variants. These unique exon splices provided refinements and additions to the tissue-specific gene expression patterns that are currently used to characterize different cell types. Using these analytical approaches, we proposed for the current project that mRNA sequencing on a transcriptome level could define a sensitive and specific "transcriptome fingerprint" of equine adult articular cartilage.

There is a limited whole transcriptome level data for normal articular cartilage. Some reports exist where the technique has been used to examine aging equine cartilage[75], transfected equine chondrocytes *in vitro*[83], and to evaluate certain nuances of disease states that affect skeletal development[84,85]. Earlier microarray-based profiling studies of equine samples compared neonatal cartilage, adult articular cartilage, and articular repair tissue, but had the limitations of pre-selected gene arrays and no splice variant analyses[18,72,73].

This chapter compares equine adult articular cartilage on an mRNA transcriptome level with five other cartilaginous tissues. Nasal septum is a stable adult hyaline cartilage that, due to its grossly similar appearance to articular cartilage, has been selected for clinical applications as a donor tissue for joint therapies[27,29,86]. The mammalian articular cartilages that are routinely studied (human, equine, bovine, rodent and rabbit) show some zonal heterogeneity in terms of cell morphology, gene expression and, not surprisingly, matrix composition[4,7,8,62,71,87-92]. Human nasal septum cartilage shares some degree of heterogeneity with articular cartilage, but this is manifest in subtle regional variations, such as rostral versus caudal [3,86,93,94]. With these factors in mind, nasal septum was selected as a stable adult cartilaginous tissue for comparison to elucidate adult articular cartilage specific transcriptome features.

Unlike the altricious young of humans, newborn foals are precocious neonates. Within hours of birth they are fully able to ambulate and follow theirs dams at some speed. Yet, their skeleton is still immature at birth with incomplete ossification of many bones, active epiphyseal plates, and considerable long bone growth yet to accomplish. Their joints contain immature cartilage that is different from adults in terms of cellularity, matrix composition, and depth[73,95,96]. The articular cartilage appears very similar to the underlying transient cartilage of the epiphysis, which will be replaced by bone through the completion of endochondral ossification. As such, gross anatomical and histological distinctions between 'articular' and 'epiphyseal' cartilage are difficult at this point, with the two tissues forming a continuum due to ongoing joint development and cartilage maturation in the postnatal period. Yet, the underlying cell biology must reflect a process that defines whether chondrocytes remain as permanent articular cartilage or undergo hypertrophy as transient chondrocytes. Comparing these tissues to adult articular cartilage could, therefore, provide insight into the transcript phenotype of a cell destined to become a robust and stable adult articular chondrocyte.

Finally, recent studies in chickens, mice, and horses have identified embryonic/fetal progenitor cells that generate structures of the synovial joint: the articular cartilage, synovial membrane, and intra-articular structures such as menisci[59,66,90]. Because these appear at future joint locations in the rudimentary condensed mesenchyme, and separate segments of the developing cartilaginous anlagen, they are termed *interzone* cells. Lineage tracing studies have further supported observations that they go on to make the structures of the synovial joint [56,97]. They are distinguished from anlagen cells by the absence of Matrillin-1 expression, a biomarker for anlagen chondrocytes[56,98]. Earlier studies in our lab using axolotl salamanders initiated our interest in interzone tissue[65,66]. Unlike mammals, the interzone persists in the distal limb joints of these amphibians into adulthood. The experiments indicated that interzone-derived cells

contributed to a remarkable regeneration of a partially ablated femorotibio-fibular joint, and created a *de novo* joint in a critical sized diaphyseal bone defect. Since interzone cells are considered to be the progenitor source of articular chondrocytes, these cells along with the transient chondrocyte population of the anlagen make appropriate tissues against which to compare adult articular cartilage.

To test our hypothesis that adult articular cartilage has a unique tissue-restricted pattern of gene expression compared to other cartilaginous tissues, we addressed the following aims. Firstly, we compared the mRNA transcriptome of adult articular cartilage with a paired adult tissue, (nasal septum), neonatal articular cartilage, neonatal epiphyseal cartilage, fetal interzone-rich tissue, and the adjacent fetal anlage tissue. Secondly, we identified tissue-restricted mRNA transcripts and splice junctions that are unique to adult articular cartilage when compared to the five comparison tissues. An overall objective was to identify specific transcript features of adult mammalian articular cartilage that define a gold standard by which to assess the functional phenotype of articular chondrocytes.

Materials and Methods

Fetal Samples

Fetuses were obtained from seven pregnant mares scheduled for euthanasia for reasons unrelated to this project under an IACUC-approved protocol. Gestational ages ranged between 57 and 66 days of the ~340 day gestation. The fetuses were harvested from the uterus immediately post-mortem in a sterile fashion and immediately washed in ice-cold sterile nuclease-free phosphate buffered saline (PBS) with 2% (v/v) amphotericin B (Gibco, Cat# 15290026) and 2% (v/v) penicillin/streptomycin (Gibco, Cat# 15070063). Forelimbs were removed from the trunk and soft tissues were dissected, using aseptic technique, from the skeletal elements with the aid of a dissecting microscope from the proximal radius distally. Anlage cartilage was harvested *en bloc* from both forelimb and hindlimb, but only forelimb tissue was used in this experiment, with the remaining tissue being snap frozen and stored. Anlage tissue (EQF-ANL) was excised adjacent to the bony collar at the primary center of ossification mid-radius to the widest point of the distal radial metaphysis (Figure 2.1a and b). An additional anlage sample was harvested from the proximal third metacarpus from just distal to carpometacarpal joint to the proximal edge of the emerging metacarpal ossification center. The intervening section of tissue, the developing interzone-rich carpus, was further debrided of any ligamentous structures on the palmar aspect of the joint and retained as the interzone-rich sample (EQF-IZ) for this study. Tissues were labeled, snap frozen in liquid nitrogen, and stored at -80^{o}C until RNA extraction.

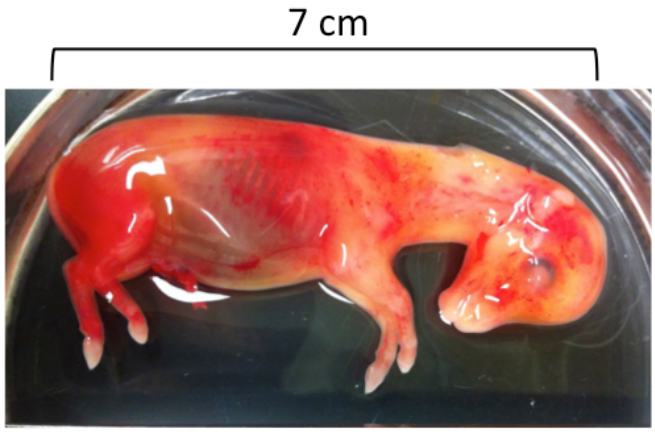

***Figure 2.1a**. Image of an equine fetus at 58 days of gestation. The crown-rump length is 7cm.*

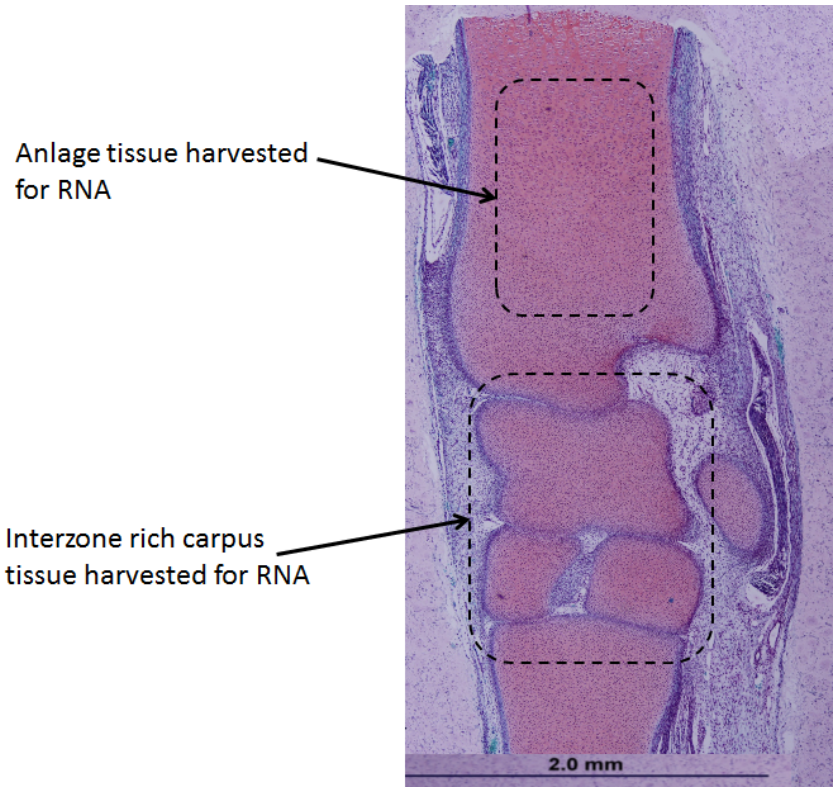

***Figure 2.1b**. Safranin-O stained oblique longitudinal section of a 65 day gestation equine carpus. This section of the limb is not ossified at this stage of development – the radius was sectioned adjacent to the bony collar appearing mid-radius. The joint spaces are cavitated and the interzone cells lining the joint spaces are visible as densely placed nuclei (blue-purple) along the joint spaces. The cartilage anlagen are rich in proteoglycan matrix as evidenced by the red Safranin-O stain uptake. This image depicts the sites of tissue harvested for RNA extraction and sequencing as indicated.*

Neonatal Samples

Equine neonatal cartilage had previously been harvested from neonatal joints and stored at -80°C [72]. Foals between 0 and 9 days old, where owner-elected euthanasia was performed for health reasons unrelated to this study, were used. Immediately post-mortem, the femorotibial joints were opened aseptically. Cartilage was harvested from the distal femoral condyles and proximal tibial plateau. The articular cartilage was collected as shavings from the joint surface to a depth estimated at 1-2 mm, where transection of small blood vessels in the cartilage matrix was first visible as small specks of blood (Figure 2.2a). These small vessels indicated that the epiphyseal cartilage had been reached. Epiphyseal cartilage samples were then collected as additional shavings down towards the ossification front, but leaving enough margin to avoid the hypertrophic cartilage. Cartilage shavings were rinsed thoroughly with ice-cold sterile nuclease-free PBS with 2% antimycotic and 2% penicillin/streptomycin to remove blood contamination, drained, and snap frozen. Prior to total RNA extraction, the cartilage shavings were reduced to a powder by direct impacts to the still frozen tissue.

Figure 2.2b shows the histologic appearance of neonatal and young adult articular cartilage.

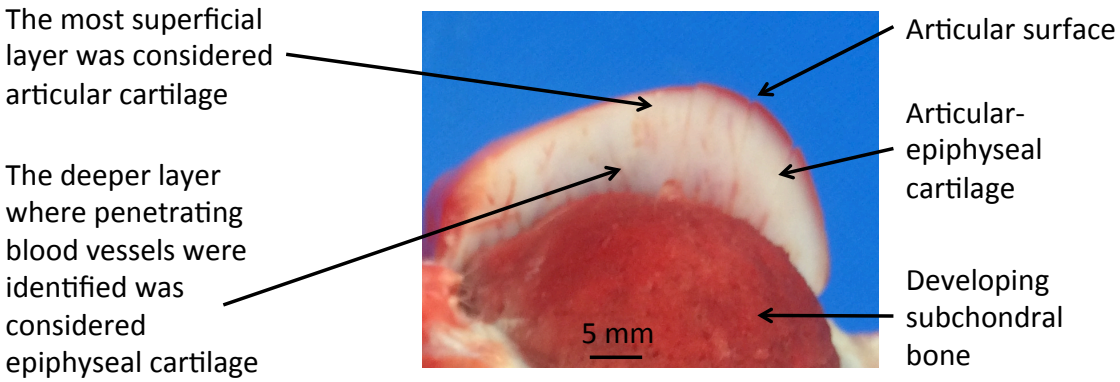

***Figure 2.2a**. Photomicrograph composite of neonatal day-old articular-epiphyseal cartilage from the medial femoral condyle depicted (right). The total cartilage layer was up to 10mm thick over this condyle.*

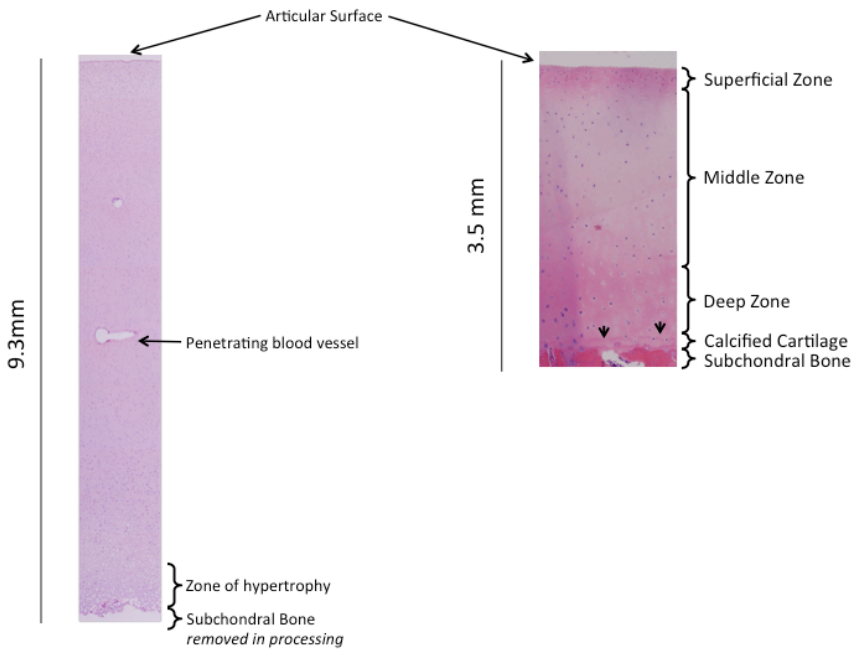

Figure 2.2b *Left: Composite photomicrograph image of neonatal equine articular-epiphyseal cartilage from the medial femoral condyle (postnatal age day 0). Right: Composite photomicrograph of young adult (~15 months) articular cartilage from the medial femoral condyle. The images are scaled relative to one another. Endochondral ossification continues postnatally to replace the remaining epiphyseal cartilage as long bones near the end of their longitudinal growth phase, resulting in just articular cartilage on the subchondral none surface. Both images are H & E stained.*

Adult Samples

Adult articular cartilage and nasal septum cartilage samples were obtained from horses donated to the University for owner-elected euthanasia under an IACUC approved protocol. Immediately post-mortem, the femorotibial joints were aseptically opened and articular cartilage from the distal femoral condyles and proximal tibial plateau was shaved off to the depth of the calcified layer. Figures 2.3 a-d illustrate the articular cartilage of the distal femoral condyle and use of a scalpel to collect cartilage shavings. Cartilage shavings were rinsed in ice-cold sterile nuclease-free PBS with 2% antimycotic and 2% penicillin/streptomycin, drained, and snap frozen. To obtain the nasal septum, the head was removed at the atlanto-occipital joint, the mandible and

maxilla removed with a transverse cut through the region of the diastema, followed by the head being sectioned in a dorsal-ventral paramedian plane just off the midline (see Figure 2.4a). The whole nasal septum was removed and the mucosa squeezed to remove blood and assist in cooling the tissue. The sample was copiously rinsed with ice cold sterile nuclease-free PBS with 2% antimycotic and 2% penicillin/streptomycin. Using aseptic technique, the mucosa was stripped off the entire septum and the underlying perichondrium meticulously removed. Given reports of variation in human nasal septums[94], the same region of nasal septum cartilage was collected in all biological replicates. This section was removed, minced, rinsed again and snap frozen. Articular and nasal septum cartilage samples were powdered prior to RNA extraction as described above. Figure 2.4b illustrates the histological appearance of adult nasal septum tissue.

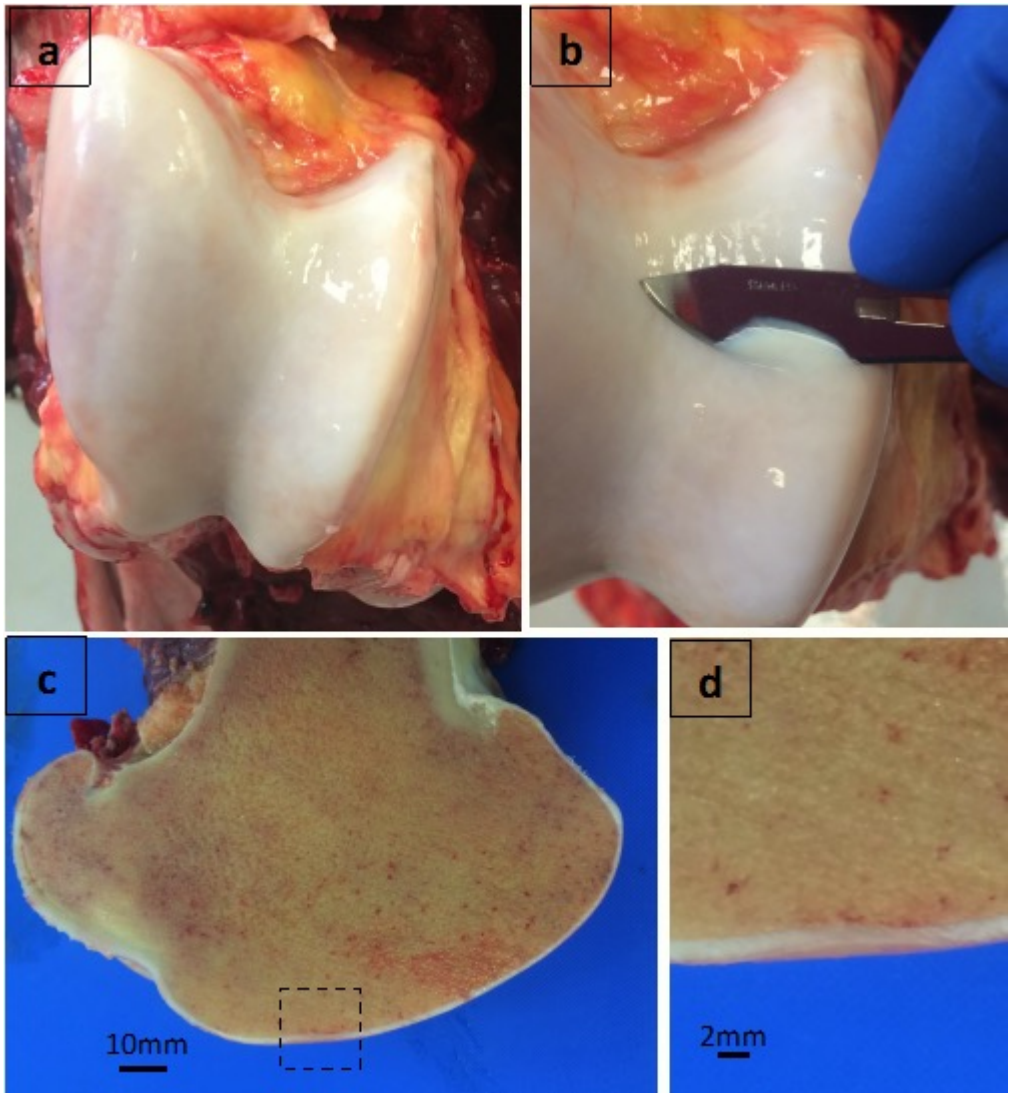

***Figures 2.3 a-d**. Images of an adult equine left distal femur. (a) Surface of the articular cartilage over both trochlea ridges of the distal femur. The joint capsule, patella, menisci and cruciate ligaments have been removed. Note the glassy white appearance of normal intact cartilage. (b) Photograph showing a No. 22 scalpel blade being used to slice off cartilage. Cartilage is removed down to the level of the calcified cartilage. (c) Parasagittal section of the medial condyle/trochlea ridge of the distal femur. The thin layer of articular cartilage covering the articular surface is clearly seen in this image. The area in the outlined area (dashed box) is shown at a higher magnification in image d. (d) Image of the articular cartilage/subchondral bone shown at higher magnification to better appreciate the thickness of the articular cartilage at this location.*

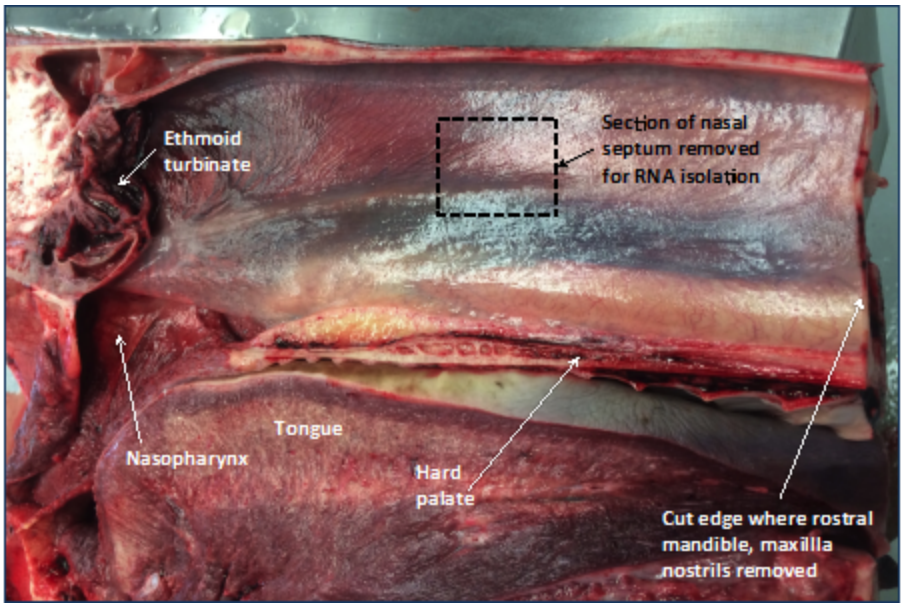

Figure 2.4a *– Photograph of an equine head sectioned in the parasagittal plane to show the right side of the nasal septum. The rostral mandible and maxilla are removed prior to sectioning (left side of image). The dashed box outlines the area routinely harvested for RNA isolation as described above. Note the rich vasculature in the mucosa. This is adherent to the perichondrium and present on both sides of the septum.*

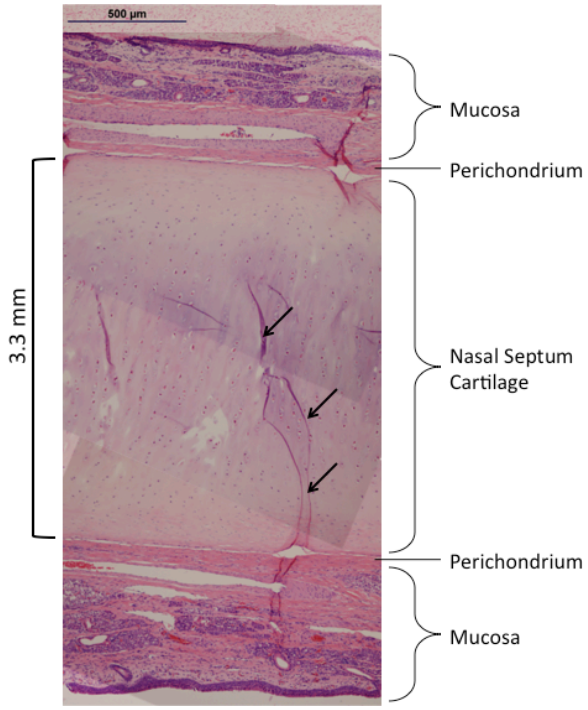

Figure 2.4b*. Composite photomicrograph illustrating the histological appearance of adult nasal septum typical of the region harvested for RNA in this chapter. The tissue is challenging to handle when sectioned. The arrows point to artifact lines caused by tissue folding.*

RNA Isolation, Quality Assessment, Sequencing, and Mapping Pipeline

RNA Isolation

Frozen tissue (fetal) and frozen powdered cartilage (neonatal and adult) samples were thawed in an aliquot of QIAzol® (Qiagen, Cat# 79306) during intermittent homogenization on ice. Total RNA was isolated using variations of acid guanidinium thiocyanate/phenol/chloroform extraction routinely used in our laboratory[18]. All samples were processed with a final RNeasy silica gel column purification (Qiagen RNeasy Mirco Kit, Qiagen, Cat# 74004), ethanol precipitated, and re-solubilized in nuclease-free water.

Quality Assessment

Quantitative and qualitative parameters of the RNA preparations were assessed using a NanoDrop ND-1000 spectrophotometer and a Bioanalyzer 2100 (Agilent Technologies, Eukaryotic Total RNA Nano & Pico Series II). Only samples with NanoDrop quality thresholds of $A_{260/280}$ ratios between 1.7 - 2.0, and $A_{260/230}$ ratios between 1.8 - 2.1 were taken forward for qualitative assessment. Qualitative assessment of RNA sample integrity was performed on an Agilent Technologies Bioanalyzer 2100. Depending on the RNA concentration, either Nano Chips or Pico Chips were used and concentrations of RNA were similar for all samples on the same chip. Each chip had a positive control RNA sample that had a known RIN of 9.9 - 10. Only samples with an Agilent RNA integrity number (RIN) of ≥ 7.0 were carried forward for sequencing.

RNA-Sequencing

RNAseq Library Preparation

RNAseq libraries were constructed using the TruSeq HT Stranded RNA Sample Preparation Kit (Illumina San Diego, CA). PolyA+ RNA was selected from 1 μg of total RNA (or the total amount available if less than 1 μg), then first-strand synthesis was performed using random hexamer primers and SuperScript II™ reverse transcriptase (Life Technologies). Further sample preparation of the double-stranded DNA included blunting ends, ensuring the addition of a 3'-end A-tail and finally, ligation of indexed adaptors. The adaptor-ligated double-stranded cDNA was amplified by PCR for 12 cycles with Kapa HiFi polymerase (Kapa Biosystems, Woburn, MA). The final libraries were quantitated using Quant-it© (Life Technologies, Grand Island, NY) and the average size determined on an AATI Fragment Analyzer (Advanced Analytics, Ames, IA). The libraries were diluted to a final concentration of 5nM. The 5nM dilution was further quantitated by qPCR on a BioRad CFX Connect Real-Time System (Bio-Rad Laboratories, Inc. CA).

Cluster Generation and Sequencing

Strand-specific sequencing of RNA was performed on all 38 samples using a paired-end mRNA-seq protocol (http://www.illumina.com/technology/paired_end_sequencing_assay.ilmn) at the Keck Center, University of Illinois with the goal of generating >30 million reads per sample.

Briefly, the final pools of libraries were loaded onto lanes of an 8-lane flow cell© for cluster formation using an automated proprietary system that creates clonal clusters from single molecule DNA templates – the cBot 2 System™ (Illumina©). In this system cDNA fragments are isothermally amplified after their capture by complementary adapter oligonucleotides that are covalently bound to the surface of Illumina flow cells©. These proprietary flow cells facilitate access of bound DNA to enzymes and ensure high stability of the surface-bound template as

well as low non-specific binding of fluorescently-labeled nucleotides. Attached DNA fragments are extended and bridge amplified creating hundreds of millions of clusters. Each cluster contains approximately 1,000 identical copies of a single DNA template molecule.

The bar coding system, based on the indexed adapters mentioned above, allows samples to be pooled, sequenced, and then traced back to the original sample identity. Samples were then sequenced on an Illumina© HiSeq2500 with version 4 SBS sequencing reagents from both ends of the molecules for a total read length of 100nt from each end. The run generated .bcl files that were then converted into de-multiplexed compressed fastq files using bcl2fastq v2.17.1.14 Illumina©Conversion Software. A secondary pipeline decompressed the fastq files, generated plots with quality scores using FastX Tool Kit, and generated a report with the number of reads per sample/library. Finally, de-multiplexed fastq files were .tgz compressed and posted to a password-secured sFTP site for downstream processing.

Once these files were downloaded from the University of Illinois server to the University of Kentucky, quality control for each sample was performed with FastQC v0.11.5. Trimmomatic Version 0.36 [99] (http://www.usadellab.org/cms/?page=trimmomatic) in the paired-end mode to perform a variety of tasks on the raw RNA-seq data that included cutting Illumina® adapter.

Mapping & Annotation

The trimmed RNA-seq reads were aligned onto NCBI EquCab2.0 Annotation Release 102 (chromosomes 1-31, M, X, Un) using MapSplice 3.0 Beta [81,99]. Default settings were used. Reads were considered as mapped only when alignments for both ends of a read pair were assigned, and at least half of the read bases mapped. For example, for 100bp paired end reads, a read pair is considered as mapped only when alignments for both ends is more than 100 bases out of the total 200 bases for the pair (non-truncated). If reads were truncated on the basis of low quality

score and/or mismatches, they were retained and mapped if they were truncated by <50% and, thus, in the case of 100bp reads, >50bp in length. The maximum number of mismatched bases permitted in the aligned region was set as a ratio relative to the length of the mapped read. This ratio was set at 0.06. In other words, for a 100bp read the maximum number of mismatches tolerated would be 6. In addition to canonical splice junction discovery, detection of semi-canonical and non-canonical splice junctions was enabled.

A genome-wide background level of read alignment was determined by adding a 1Kb 'buffer' regions to the 5' and 3' ends of gene loci coordinates to account for untranslated regions and potential errors in gene structure annotation. A background of 0.09 was calculated using the intergenic regions from all 38 samples and described as per base coverage over all the intronic and intergenic regions across the genome. Coverage for each gene loci minus the 0.09 background constant was then reported as nucleotides per base of exonic length and normalized to the individual sample out of the total sample set of 38 that generated the largest number of reads from the sequencing protocol described above.

For analysis of these data, the samples were grouped into the six experimental groups (3 sets of paired tissues) according to tissue type:

- Fetal Interzone-Rich Carpus (EQF-IZ)
- Fetal Anlage Cartilage (EQF-ANL)
- Neonatal Articular Cartilage (EQN-AC)
- Neonatal Epiphyseal Cartilage (EQN-EPI)
- Adult Articular Cartilage (EQA-AC)
- Adult Nasal Septum (EQA-NA)

All pseudogene loci were included in the analyses. Due to conserved sequences, measuring transfer RNA gene expression is frequently confounded by multiple alignments of individual reads[100]. As such, tRNA loci were excluded from the analyses.

Differential Gene Expression Analyzed at the Loci Level

Paired *t*-tests were calculated to generate *p*-values for differential expression between the paired intra-age group adult samples (EQA-AC and EQA-NA). Unpaired *t*-tests were calculated to generate *p*-values for the comparison of gene expression in adult articular cartilage to each of the other four tissues. Gene loci with zero expression across all samples were excluded from the analysis. For the purposes of fold change calculations, any locus where group average coverage (average of the biological replicates in each group) was <1 was nominally assigned the value of '1'. This avoided the inflation of fold change values when it was log transformed. For each comparison of genes expression, volcano plots were generated to visualize the results. For these plots, *p*-values were Log_{10} transformed and the negative Log_{10} value plotted on the *y*-axis. Log_2 transformations were performed on fold change values and plotted on the *x*-axis using JMP version 10 software (SAS Institute Inc.).

Differentially Expressed Loci Level Gene Lists – Five Differentially Expressed Gene Lists.

Lists of differentially expressed gene loci (DEG) were generated by comparing expression in adult articular cartilage (EQA-AC) to each of the other five experimental groups. These comparisons are depicted schematically in Figure 2.5. Thresholds for significance were: $p<0.05$, average group expression level ≥ 2 in both comparison groups, and a fold change ≥ 2. The *p*-values were not adjusted to account for false discovery rates (FDR). FDR conversion was determined (not shown), but left so few significant differences that comparisons depicted in

Figure 2.5 were made with the original lists. These gene lists are referred to as the '5 DEG lists' from hereon.

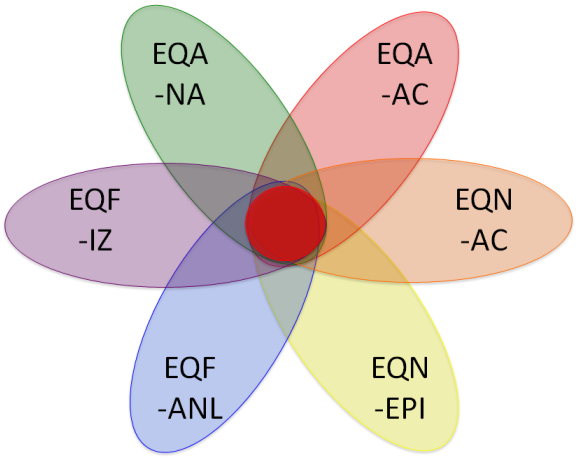

Figure 2.5. *Diagram illustrating the comparisons made between gene expression in adult articular cartilage and the other five tissue groups. The red center to the schematic 'flower' represents gene loci that are differentially expressed between adult articular cartilage and each (all) of the other 5 tissue types.*

Analyses of Data to Determine Gene Loci Expression Characterizing Adult Articular Cartilage.

Figure 2.6, below, is a schematic representation of the workflow for the loci-level analyses performed. The goal was to define a gene expression profile that characterizes the unique features of loci level gene expression in adult articular cartilage relative to other cartilaginous tissues.

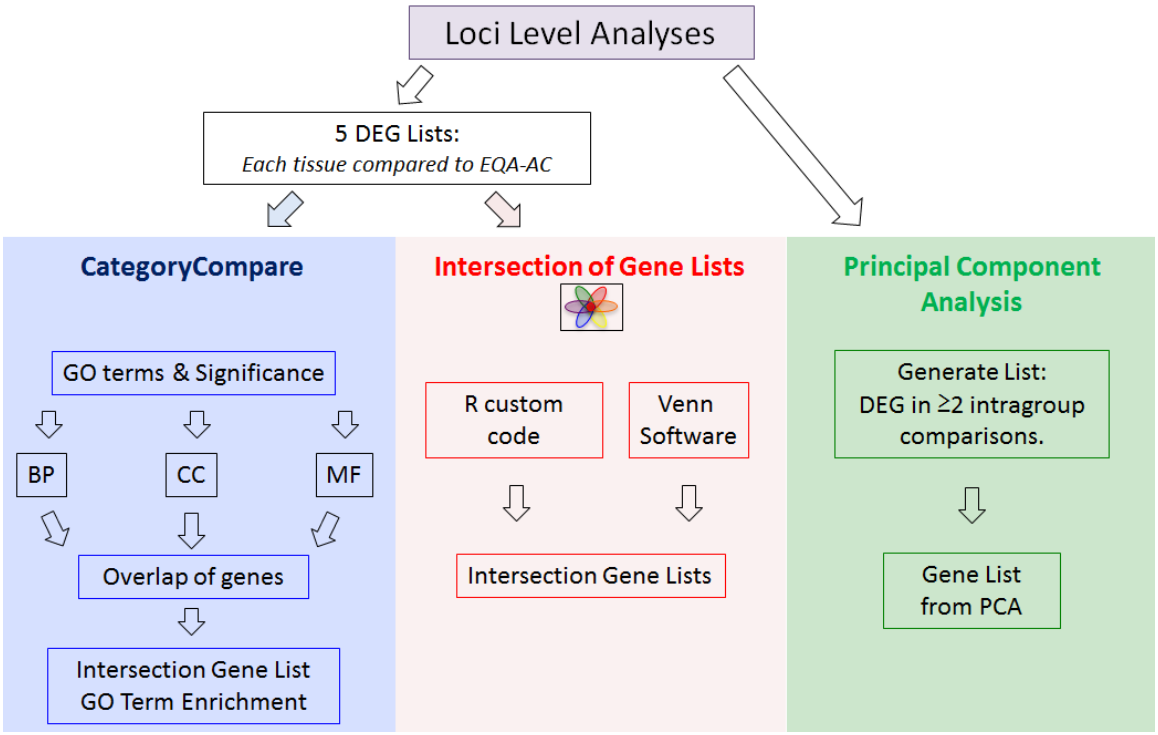

Figure 2.6. *Schematic diagram of work flow for the analyses of gene loci that are differentially expressed between adult articular cartilage and the other five tissue types.*

In the absence of a way to compare all gene loci across 38 samples (6 groups) simultaneously, the analyses were broken down and performed as follows:

1) Gene Ontology Category Comparison - *CategoryCompare*.
2) Establishing intersecting genes - two methods.
    a. Using custom R code.
    b. Using online Venn diagram software.
3) Principal component analysis.

Analysis 1. Gene Ontology Category Comparison - *CategoryCompare*

The comparison of enriched genes via GO category comparison has been shown to better represent changes in biological processes or signaling pathways under different biological

conditions[101]. *CategoryCompare* software was used for this analysis[101]. This software was designed to analyze high-throughput '–omics data in cross-sample and cross-platform comparison at the annotation level. To further investigate the gene ontology of differentially expressed genes in articular cartilage, an additional assessment was performed. In addition to enriched GO categories, individual genes from the comparisons were also identified.

GO Mapping Construction

Equine specific gene-Gene Ontology annotations for NCBI EquCab 2.0 Annotation Release 102 were downloaded from AgBase (http://www.agbase.msstate.edu/cgi-bin/download.pl?submit=download&file=horse_ga.zip) and expanded to include all non-specific annotations using the *buildGOmap* function from the *clusterProfiler* Bioconductor package version 2.4.3 (https://www.bioconductor.org)[102]. Full mappings were generated separately for each GO category (biological process [BP], molecular function [MF], and cellular component [CC]). For each gene list generated, gene ontology enrichments were calculated with hypergeometric enrichment tests using v0.99.158 of *CategoryCompare2* (Flight RM, (2016) https://dx.doi.org/10.6084/m9.figshare.3381253.v1). All annotated genes in the equine genome were used as the background. Hypergeometric testing detects whether items selected from a sample are higher than would be expected by chance, relative to how may items have the same attribute in the background sample[103]. GO terms with ≥5 and ≤500 genes annotated were considered. A weight for edges between GO terms was used. This is a way to account for the degree of shared gene annotation calculated by the average of their Jaccard and overlap similarities[104]. Edges with weights less that 0.8 were removed, followed by *cluster_walktrap* algorithm application to define groups of GO terms[105]. The results for each GO category were then combined to allow determination of which list had which GO terms enriched. GO terms with uncorrected *p*-values 0.0001 and at ≥2 genes in the input gene list were retained for

further investigation. GO terms that were enriched in all five DEG lists were examined and genes annotated to them were derived.

Analysis 2. Intersecting Genes.

Using the five DEG lists generated from comparing EQA-AC to each of the other cartilaginous tissues, it was proposed that loci in common would represent genes that were differentially expressed between EQA-AC and *all of the other five tissues*. As such, these genes, consistently up-regulated or down-regulated, would define unique gene expression characteristics of adult articular cartilage. Recognizing that different analytical strategies do not always yield concordant results, two different methods were used.

***Analysis 2.2*: Intersection of the 5 DEG using custom R code.**

Custom code, written in R programming language (https://www.r-project.org), was employed to capture the list of intersecting genes from the 5 DEG lists.

***Analysis 2.2*: Intersection of the 5 DEG lists using Venn diagram software**

An online Venn diagram tool capable of uploading 5 gene lists was used to determine common genes among the 5 DEG lists (http://bioinformatics.psb.ugent.be/webtools/Venn/). The expression of this intersecting list of gene loci was interrogated as to whether it could segregate adult articular cartilage from the other tissues by principal component analysis.

3. Principal Component Analysis.

Principal component analysis (PCA) is a statistical representation of data composed of possibly related variables to a set of uncorrelated variables called principal components. Intra-age group comparisons were performed for each of the three age groups (fetal, neonate, and adult). Genes that were significantly differentially expressed between paired tissues in more than one

comparison were carried forward for PCA computation. For example, Gene *X* being differentially expressed in a comparison of EQF-IZ and EQF-ANL, as well as between EQN-AC and EQN-EPI would be retained. The number of components in the PCA was equal to the gene expression data for this group of genes. These principal components are successively assigned starting with the first (principal component 1, PC1), which has the largest possible variance. This first component therefore accounts for the greatest amount of variability in the data. The data are represented graphically in two or three-dimensional graphs with different principal components along the *x-, y-* and *z*-axes. Different principal components will array the experimental groups differently. The principal components that are used in any analysis are those that segregate the data to best describe differences among experimental groups. PCA is a mathematical analysis, not a biological analysis. However, it's elegance lies in the fact that the relationships are derived using the large data sets. Principal components are not in the format of genes *per se,* because the transformed data is a numerical matrix. Each gene locus contributed to the PCA by their coefficients, and the coefficients were calculated by the correlation of the genes between different samples. Genes with small correlations result in large coefficients in principal components. This gives more weight to the PCA.

Visualizing Data

Overlapping gene ontology results and intersecting gene sets were summarized as *UpSet* plots using *UpSetR* software[106]. Heatmaps were generated using the *colorRampPalette* function in the *circlize* package v.0.3.5[107] and plotted using *ComplexHeatmap* package v1.6.0[108].

Expression of Genes Established as Traditional Articular Cartilage Biomarkers

A selection of established biomarker genes that have classically been used in scientific research to characterize articular cartilage by either high expression or very low expression were examined in the RNA-seq data. These include genes with anticipated high expression (*ACAN, BOC, COL2A1, COL9A1, COL9A2, COL9A3,* and *COMP*) and genes with anticipated very low expression (*COL1A1, COL10A1*). Gene expression comparisons were performed pairwise with each locus in each tissue type being compared to EQA-AC. Statistical analyses were performed with a one-way analysis of variance and significance was set at $p<0.05$.

Analysis of Transcript Variants from the Same Gene Locus

Alternative splicing modules (ASMs) were detected using DiffSplice v0.1.1[78]. Figure 2.7 illustrates the ASM concept of the DiffSplice software. The image shows a simple 3-exon protein-coding gene. For this gene locus, two transcript isoforms are produced based on an exon skipping event. Path 1 generates a transcript that includes Exon 2. Path 2 generates a transcript where Exon 2 is excluded from the mature mRNA transcript. The alternative splicing module (ASM) unit is defined as the region between the divergence and convergence of transcript paths. Any given gene locus may have more than one ASM and any ASM may have more than two pathway possibilities. Splicing events documented include exon skipping, intron retention, alternative splice donor sites, alternative splice acceptor sites, and alternative transcription start or stop sites. Splice junctions were detected if the sum of the path coverage depth was >20 across 34 of the 38 samples. If these criteria were satisfied, the junction was included in an ASM structure. For differential isoform transcription, an ASM was considered significant if the square root of the Jenson-Shannon Divergence (sqrtJSD, JSD*) was >0.1 and the False Discovery Rate was <0.01. The JSD* is a metric applied to significance for non-parametric distributions and takes

into consideration ratios of the different ASM pathways that are independent of sample coverage depth[78,80,81].

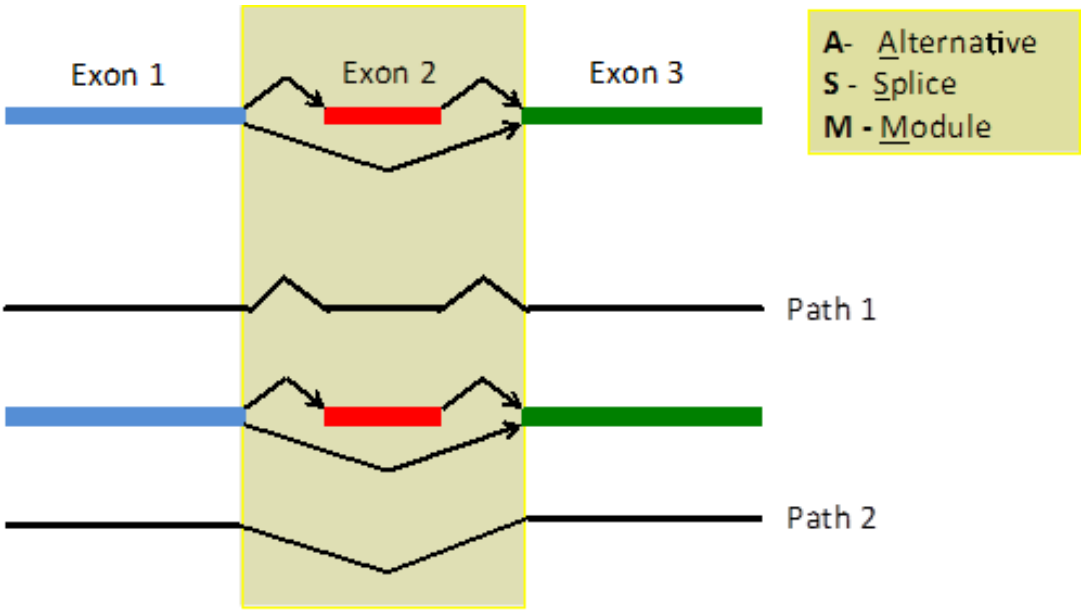

Figure 2.6. *A schematic of the Alternative Splice Module that is the functional unit of DiffSplice software. The image shows a simple 3 exon protein coding gene. For this gene, there are 2 transcript isoforms based on an exon skipping event. Path 1 generates a transcript that includes Exon 2. Path 2 generates a transcript where Exon 2 is excluded from the mature mRNA transcript. The alternative splicing module (ASM) unit is defined as the region between the divergence and convergence of transcript paths. This is outlined in yellow in this schematic example.*

Results

Samples

A total of 38 RNA samples were obtained as described in the Materials and Methods section (Table 2.1). A minimum of 500ng of ethanol precipitated total RNA was sent for sequencing for each sample.

Sample Description		Age	Biological Replicates
Equine Fetus (EQF)	Interzone-rich carpus (EQF-IZ)	57 - 66 days of gestation	n = 7
	Anlage Cartilage (EQF-ANL)		
Equine Neonate (EQN)	Articular Cartilage (EQN-AC)	0 - 9 days old	n = 7
	Epiphyseal Cartilage (EQN-EPI)		
Equine Adult (EQA)	Articular Cartilage (EQA-AC)	22 - 51 months old	n = 5
	Nasal Septum Cartilage (EQA-NA)		

Table 2.1. *Table summarizing the sample set from which the RNA-seq data was generated.*

RNA-sequencing data

The average fragment length of the library prepared for sequencing was 270nt (range 130-520nt). A total of 1,195,212,253 paired-end reads were generated from the 38 samples submitted for sequencing. This resulted in an average of 31,452,954 paired-end reads per sample (Range: 30,321,950 – 83,085,262 paired reads). The average Phred score was above 30 for every base in both the forward and reverse. The percentage of reads that mapped unambiguously to NCBI Equcab2.0 Annotation Release 102 averaged 96.34%. Table 2.2 summarizes these data.

sample	EQF-IZ-1	EQF-IZ-2	EQF-IZ-3	EQF-IZ-4	EQF-IZ-5	EQF-IZ-6	EQF-IZ-7	Highest	Lowest	Average
unique paired alignment reads	94.59%	94.12%	93.34%	94.38%	94.06%	94.05%	93.45%	94.59%	93.34%	94.00%
multiple paired alignment reads	1.9442%	2.2783%	2.8387%	2.0156%	1.9679%	2.0630%	2.4176%	2.84%	1.94%	2.22%
unmapped reads (pair)	3.4673%	3.6037%	3.8220%	3.6002%	3.9743%	3.8878%	4.1353%	4.14%	3.47%	3.78%
mapped reads (pairs)	96.53%	96.40%	96.18%	96.40%	96.03%	96.11%	95.86%	96.53%	95.86%	96.22%

sample	EQF-ANL-1	EQF-ANL-2	EQF-ANL-3	EQF-ANL-4	EQF-ANL-5	EQF-ANL-6	EQF-ANL-7	Highest	Lowest	Average
unique paired alignment reads	93.91%	92.45%	86.78%	93.48%	93.53%	94.09%	93.55%	94.09%	86.78%	92.54%
multiple paired alignment reads	2.6833%	3.8263%	9.3200%	3.3403%	2.5271%	2.4001%	2.7995%	9.32%	2.40%	3.84%
unmapped reads (pair)	3.4052%	3.7198%	3.8977%	3.1812%	3.9439%	3.5118%	3.6500%	3.94%	3.18%	3.62%
mapped reads (pairs)	96.59%	96.28%	96.10%	96.82%	96.06%	96.49%	96.35%	96.82%	96.06%	96.38%

sample	EQN-AC-1	EQN-AC-2	EQN-AC-3	EQN-AC-4	EQN-AC-5	EQN-AC-6	EQN-AC-7	Highest	Lowest	Average
unique paired alignment reads	95.29%	94.88%	94.95%	94.39%	94.10%	95.20%	95.14%	95.29%	94.10%	94.85%
multiple paired alignment reads	1.5233%	1.5935%	1.6614%	1.9684%	1.7311%	1.5219%	1.7212%	1.97%	1.52%	1.67%
unmapped reads (pair)	3.1866%	3.5247%	3.3897%	3.6423%	4.1667%	3.2805%	3.1408%	4.17%	3.14%	3.48%
mapped reads (pairs)	96.81%	96.48%	96.61%	96.36%	95.83%	96.72%	96.86%	96.86%	95.83%	96.52%

sample	EQN-EPI-1	EQN-EPI-2	EQN-EPI-3	EQN-EPI-4	EQN-EPI-5	EQN-EPI-6	EQN-EPI-7	Highest	Lowest	Average
unique paired alignment reads	95.70%	95.22%	94.64%	94.73%	94.52%	95.77%	95.52%	95.77%	94.52%	95.16%
multiple paired alignment reads	1.5523%	1.6515%	1.8095%	1.8826%	1.7526%	1.3735%	1.6733%	1.88%	1.37%	1.67%
unmapped reads (pair)	2.7439%	3.1259%	3.5542%	3.3920%	3.7307%	2.8568%	2.8036%	3.73%	2.74%	3.17%
mapped reads (pairs)	97.26%	96.87%	96.45%	96.61%	96.27%	97.14%	97.20%	97.26%	96.27%	96.83%

sample	EQA-AC-1	EQA-AC-2	EQA-AC-3	EQA-AC-4	EQA-AC-5	Highest	Lowest	Average
unique paired alignment reads	94.95%	94.44%	94.14%	94.40%	94.74%	94.95%	94.14%	94.53%
multiple paired alignment reads	1.3560%	1.4560%	1.3238%	1.3525%	1.5888%	1.59%	1.32%	1.42%
unmapped reads (pair)	3.6931%	4.1023%	4.5346%	4.2522%	3.6664%	4.53%	3.67%	4.05%
mapped reads (pairs)	96.31%	95.90%	95.47%	95.75%	96.33%	96.33%	95.47%	95.95%
sample	EQA-NA-1	EQA-NA-2	EQA-NA-3	EQA-NA-4	EQA-NA-5	Highest	Lowest	Average
unique paired alignment reads	95.43%	95.03%	93.15%	95.22%	92.11%	95.43%	92.11%	94.19%
multiple paired alignment reads	1.4188%	1.4881%	2.2896%	1.5723%	3.0722%	3.07%	1.42%	1.97%
unmapped reads (pair)	3.1481%	3.4811%	4.5634%	3.2083%	4.8131%	4.81%	3.15%	3.84%
mapped reads (pairs)	96.85%	96.52%	95.44%	96.79%	95.19%	96.85%	95.19%	96.16%

Table 2.2. *A summary of mapping statistics for the 38 sample data set.*

Background intergenic coverage was 0.09 nt/base, which was subtracted from normalized nt/base coverage values for analyses of expression. Prior to this correction, $\log_2$ coverage histograms were bimodal reflecting the inclusion of loci with very low expression levels (data not shown). Background correction of expression yielded modal histograms for the average coverage per tissue type. These data are shown in Figures 2.8 a-f. The similar shape of the histograms suggests that these samples did not suffer from inter-group technical bias. In these graphs, Log_2 coverage is plotted on the *x*-axis and on the *y*-axis coordinate indicates the number of gene loci with that level of expression. In the absence of broadly accepted rationale for defining coverage thresholds, these graphs were used as a guide. Across the full dataset, a coverage depth of ≥2nt/exonic base was estimated to capture >95% of the gene loci that have foreground expression (Figure 2.9).

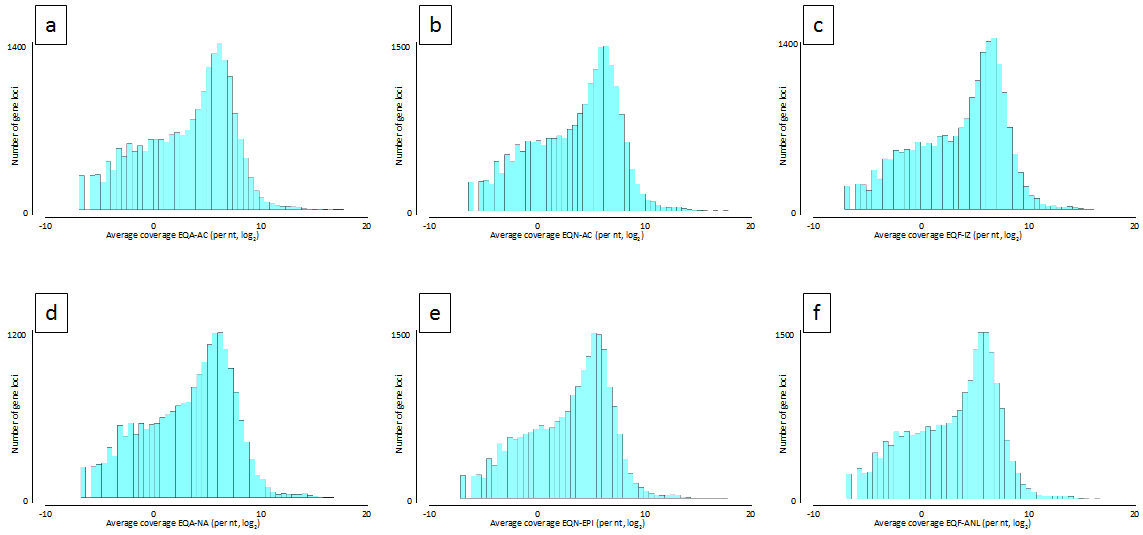

Figures 2.8 a-f. *Histograms showing log_2 average coverage for each sample type (x-axis) against the number of genes (y-axis). Note that there are minor scale differences on the y-axis scales. (a) EQA-AC, (b) EQN-AC, (c) EQF-IZ, (d) EQA-NA, (e) EQN-EPI, (f) EQF-ANL.*

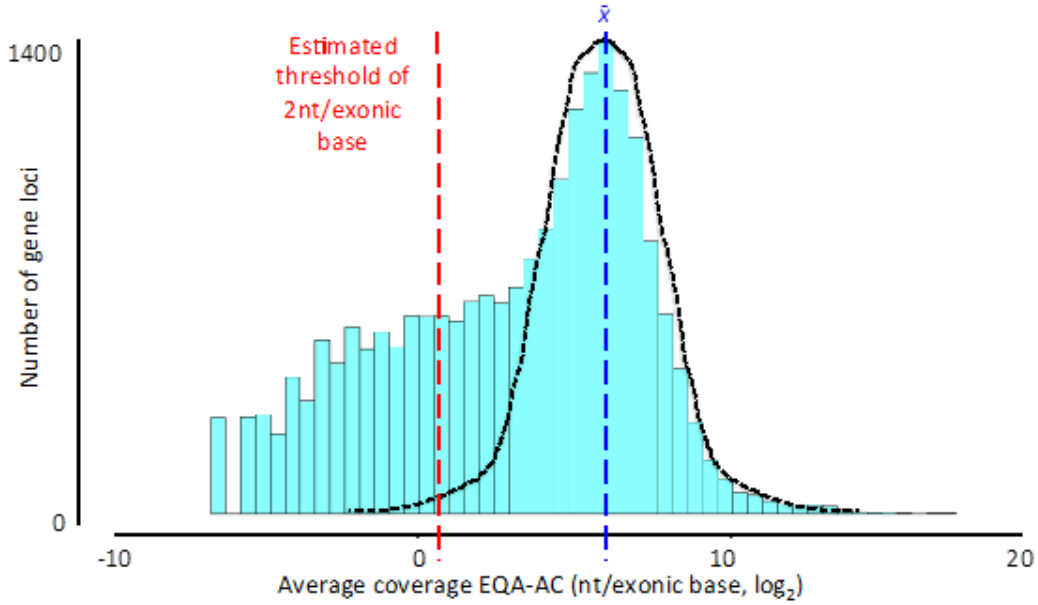

Figure 2.9. *Expanded coverage histogram of EQA-AC. The distribution of protein coding genes was largely considered to be a Normal Distribution. To determine a rational threshold for expression depth protein coding gene expression depth was estimated to be a roughly Normal distribution (outlined by the dashed black line). Estimating a cut-off value that would capture 95% of expressed genes suggested the threshold to be approximately 2nt/exonic base (dashed red line).*

Differentially Expressed Genes Compared to Adult Articular Cartilage

Using the thresholds of $p<0.05$, average group expression ≥ 2 in both comparison groups, and a fold change ≥ 2, five DEG lists were generated. The number of differentially expressed gene loci in each comparison is shown in Table 2.3 below. The greatest number of expression differences were found between EQA-AC and EQF-IZ and the least number between EQA-AC and EQN-AC.

Comparison Tissue Group	DEG with increased expression in EQA-AC	DEG with decreased expression in EQA-AC	Total DEG
EQA-NA	1100	1091	2191
EQN-AC	356	1261	1617
EQN-EPI	1053	1301	2354
EQF-IZ	1058	2905	3963
EQF-ANL	2028	1756	3784

***Table 2.3**. Numbers of differentially expressed gene loci (DEG) for comparison with EQA-AC.*

Histograms of p*-values for differential gene expression comparisons*

For each tissue comparison to EQA-AC, a *p*-value histogram was generated. These are shown in Figures 2.10 a-e. These graphs give an immediate impression of how different two samples may be in terms of their gene expression (i.e., a random flat distribution across all of the *p*-value bins versus increased percentages of loci in the low *p*-value bins). High bars at $p<0.05$ with a steep slope to baseline *p*-value levels are also a function of either uniformity of the data or a large sample size or both. The *p*-value histograms from sample sizes of 5 or 7 biological replicates per tissue type, indicates that there are substantial gene expression differences between the majority of the compared groups. The comparison between EQA-AC and EQN-AC has the least steep slope incline and lowest relative low p-value columns. This may represent the analysis being underpowered with just 5 biological replicates in the EQA-AC sample set, or it may

represent lesser difference between these two tissue types as compared to other tissue type comparisons.

There is some artifact in the *p*-value histograms that are evident as higher bars in bins with *p*-values of 0.35-0.375 and between 0.4 and 0.425. This results from expression data where all but one biological replicate in a group has zero coverage and one sample has an expression coverage of <1.

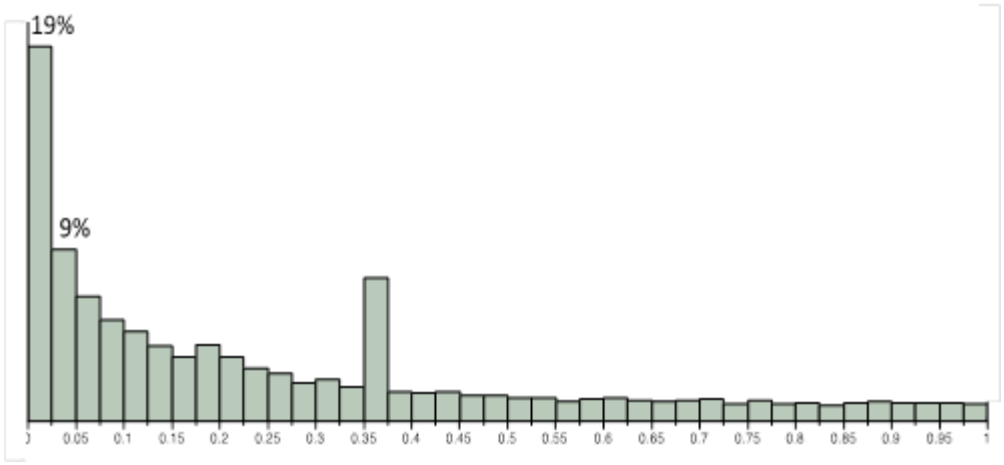

***Figure 2.10a**. p-value histogram of differential gene expression between EQA-AC and EQA-NA*

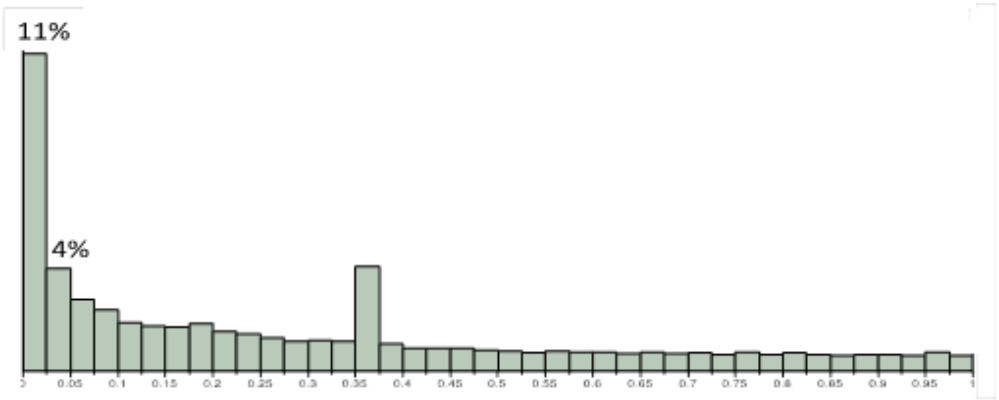

***Figure 2.10b**. p-value histogram of differential gene expression between EQA-AC and EQN-AC*

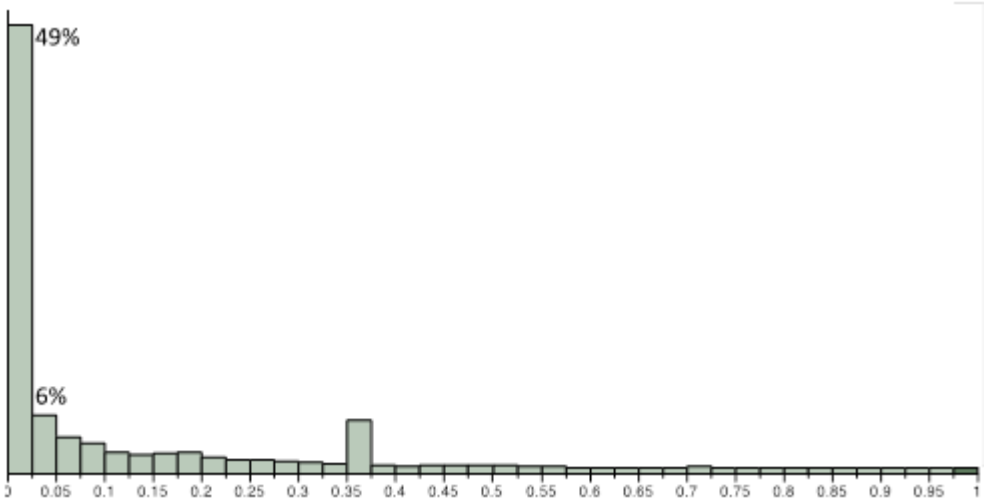

***Figure 2.10c**. p-value histogram of differential gene expression between EQA-AC and EQF-IZ*

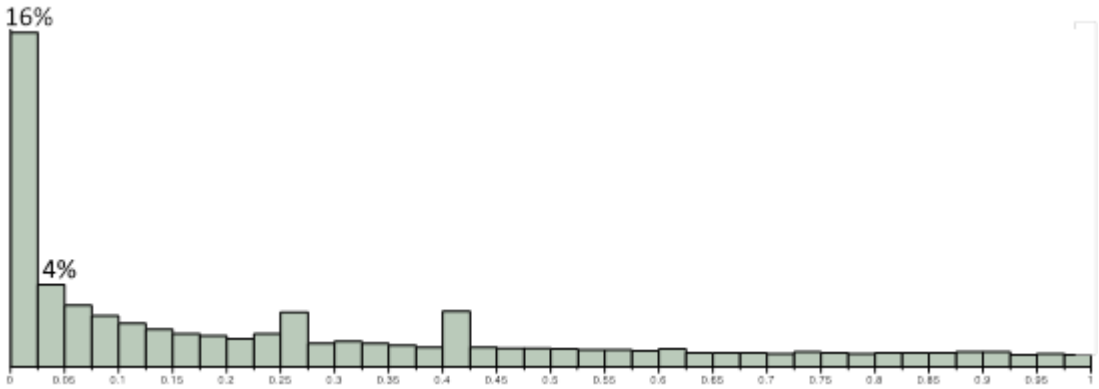

***Figure 2.10d**. p-value histogram of differential gene expression between EQA-AC and EQN-EPI*

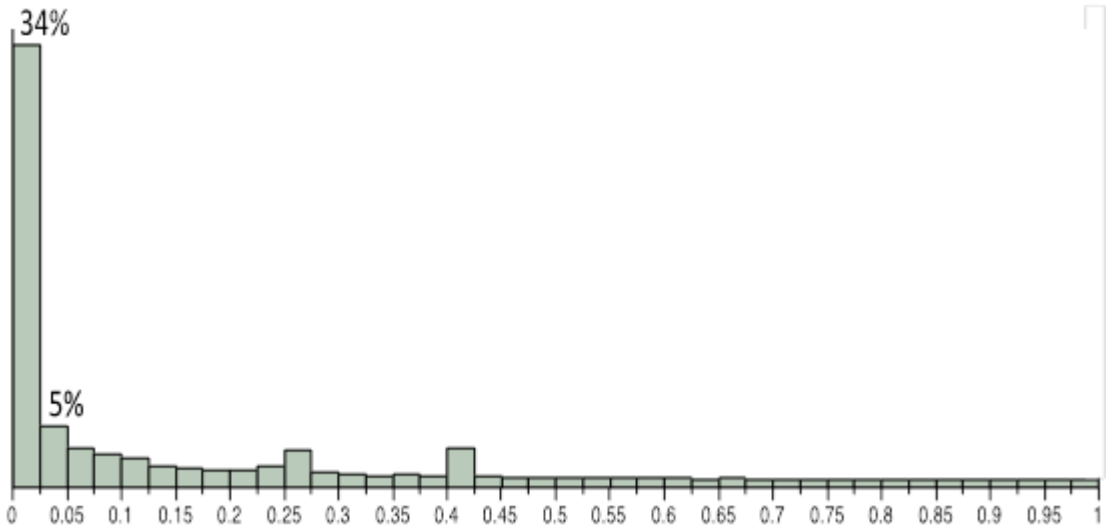

***Figure 2.10e**. p-value histogram of differential gene expression between EQA-AC and EQF-ANL*

Volcano plots

Volcano plots provide a global view of gene expression differences between two experimental groups. Each dot on the plot represents a gene locus plotted as a function of its fold change and *p*-value. To overcome small and large number distortions, values are Log transformed for better visualization. Expression fold changes of genes (Log_2 transformed) are plotted on the *x*-axis. As such, a two-fold change in gene expression represents one Log_2 unit on the *x*-axis. On the *y*-axis, the *p*-values corresponding to each gene expression comparison between the two tissue types are plotted as their negative Log_{10} value. Thus, for example, the *y*-axis value of a gene expression difference with a *p*-value = 0.001, becomes 3. The farther the gene loci points are from zero in either positive or negative direction on the *x*-axis, or on the *y*-axis, the greater the fold change and the smaller the *p*-value respectively. Thus, the furthest points have low p-values and high fold changes differences. Figure 2.11 illustrates the volcano plot of EQA-AC expression compared to EQA-NA. The red and green highlighted areas represent genes with 2 fold changes in either direction and corresponding *p*-values <0.01. This provides an example of how these plots are often used to filter large transcriptome level datasets. One important note about the generation of these volcano plots: in the Materials and Methods section it was described how expression values where per group average were <1, were changed to '1' for the fold change calculation. This was done to reduce fold change distortion. As previously mentioned, we considered these not to be biologically relevant to our experiment at this time. This resulted in many fold changes becoming 1. Since $Log_2(1) = 0$, there is an artifact vertical line at the zero point on the *x*-axis. Figures 2.12 a-e illustrates the volcano plots from the 5 different comparisons performed between each tissue and adult articular cartilage. The *x*- and *y*-axes are depicted with the same scale for ease of comparison. Adult articular cartilage and nasal septum

have significantly different expression of gene loci as can be seen by values on the *y*-axis over 4 (this would equate to *p*-values = 0.0001, for example; Figures 2.11 and 2.12a).

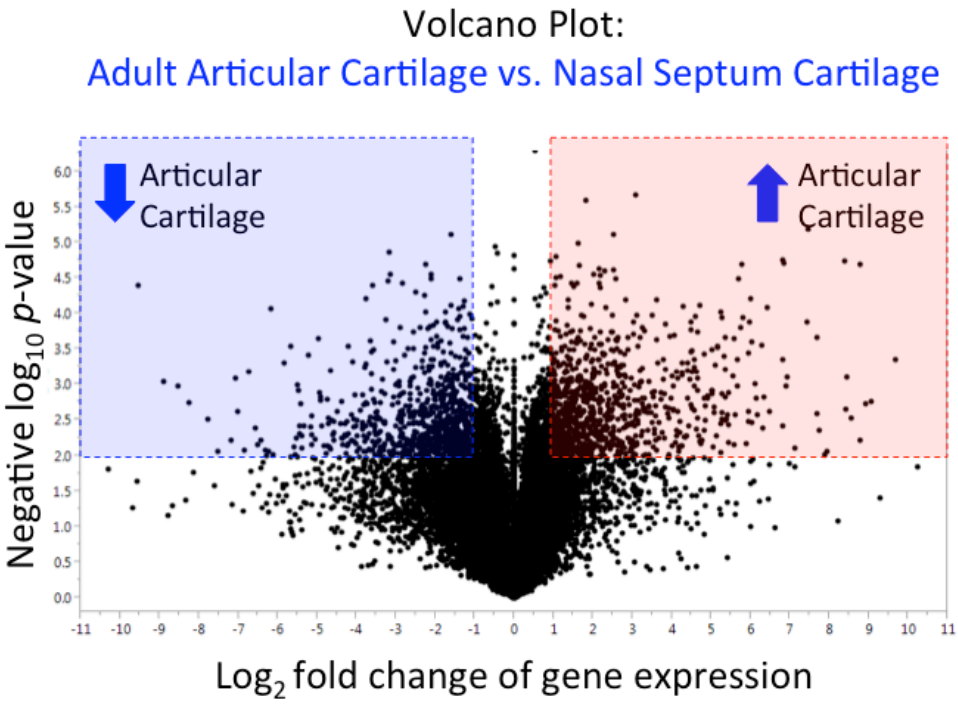

Figure 2.11. *Volcano plot of gene expression on a loci level. Adult articular cartilage (EQA-AC) is being compared with adult nasal septum cartilage (EQA-NA). Negative log_{10} p-value (y-axis) is plotted against log_2 fold change (x-axis). Each gene locus is represented by a dot. The two shaded boxes indicate genes where the fold change between EQA-AC and EQA-NA is ≥2 and the p-value is <0.01. The box shaded in red represents genes where expression is higher adult articular cartilage. The blue shaded area represents genes where the expression is lower in articular cartilage compared to adult nasal septum cartilage.*

The comparison of neonatal articular cartilage with adult articular cartilage (Figure 2.12b) has a narrower spread of points suggesting that gene expression differences are not as large between these two tissues. Gene expression differences between articular cartilage and the interzone-rich fetal carpal tissue (Figure 2.12c) shows an interesting pattern with marked changes in gene expression pattern as evidenced by a large spread of loci dots on the negative side of the *x*-axis. These reflect gene loci where expression in the fetal IZ-rich tissue is greater than in the adult

cartilage. Balanced gene expression differences are noted in the volcano plots comparing adult articular cartilage to nasal septum cartilage (Figure 2.12a) and anlagen tissue (Figure 2.12e).

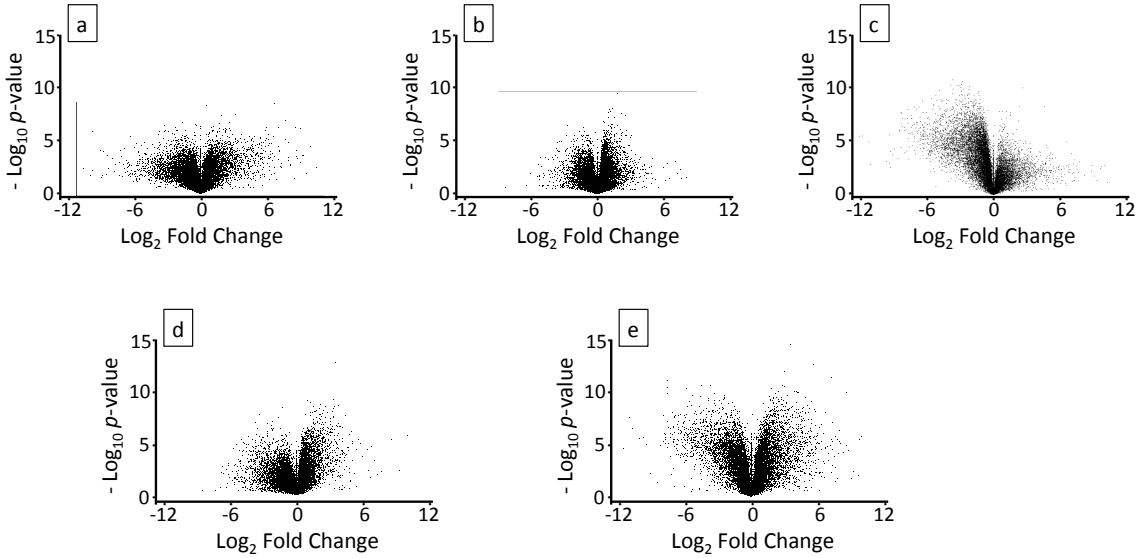

Figures 2.12 a-e. *Volcano plots showing expression differences on a transcriptome level between EQA-AC and the five other groups. Graphs are plotted with Log_2 fold change of gene expression on the* x*-axis and -Log_{10} p-value on the* y*-axis with axes scales consistent. (a) EQA-AC vs. EQA-NA; (b) EQA-AC vs. EQN-AC; (c) EQA-AC vs. EQF-IZ; (d) EQA-AC vs. EQN-EPI; (e) EQA-AC vs. EQF-ANL.*

Analysis 1. Gene Ontology Category Comparison - *CategoryCompare*

This analysis was performed by completing an enrichment analysis on each of the five DEG lists and then looking at the five-way intersection of the enrichment results.

Biological Process Category

The Biologic Process category of GO is the best annotated and thus contains the largest number of genes[109]. It is worth noting at this point that genes will be annotated to more than one GO category and often more than one GO term within each category. Thirteen GO categories were enriched in the five-way comparison as illustrated in the *UpSetR* graph in Figure 2.13. Interestingly, removing the neonatal articular cartilage from the comparison would add 99 GO categories to the list. This is not surprising, given that neonatal articular cartilage is likely the tissue in the comparison set that one would predict to be most similar to adult articular cartilage. As expected, the enriched GO categories in this analysis relate to skeletal development, chondrocyte and cartilage development, and extracellular matrix development and organization (Table 2.4).

Molecular Function Category

Analysis of the genes in the five way category comparisons yielded 9 GO categories that were enriched. These are illustrated in Figure 2.14 along with the description of the categories in Table 2.5. The enriched groups include glycoprotein binding, integrin and collagen binding terms, which center on matrix biology and cell-matrix interactions. Given the inclusion of developing joints and the known importance of the Transforming Growth Factor family and *Wnt* signaling, it is not surprising that these terms would be enriched.

Cellular Component Category

Seven GO categories were enriched in this analysis. Six of the seven categories relate to cellular adhesion and extracellular domains, again consistent with the importance of the extracellular matrix in cartilage biology. These data are shown in Figure 2.15 and Table 2.6, respectively.

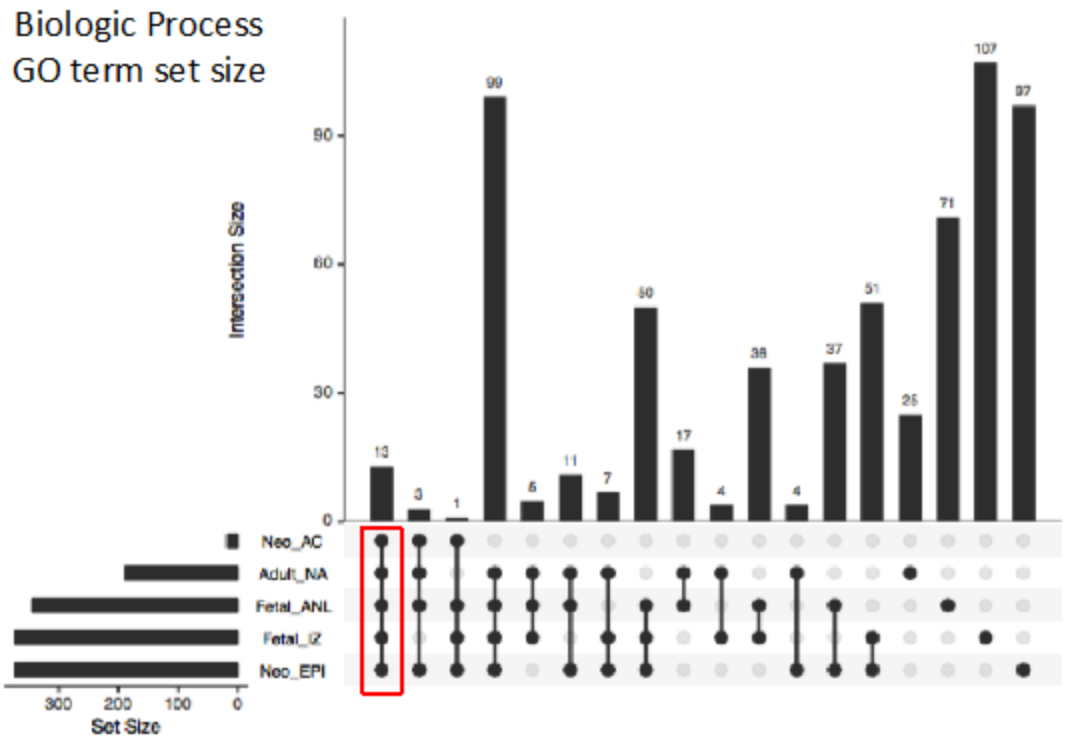

Figure 2.13 CategoryCompare *output represented in an UpSetR plot showing 13 Biologic Process GO categories enriched in the five way comparison (outlined by the red box). The set size graph to the bottom right of the image represents the number of GO categories per DEG list used as input.*

GO Identity	Biological Process GO Description
GO:0001501	skeletal system development
GO:0001503	ossification
GO:0001944	vasculature development
GO:0002062	chondrocyte differentiation
GO:0007162	negative regulation of cell adhesion
GO:0010975	regulation of neuron projection development
GO:0030155	regulation of cell adhesion
GO:0030198	extracellular matrix organization
GO:0031589	cell-substrate adhesion
GO:0043062	extracellular structure organization
GO:0051216	cartilage development
GO:0060348	bone development
GO:0061448	connective tissue development

Table 2.4*. Table listing the 13 enriched Biologic Process domain GO terms.*

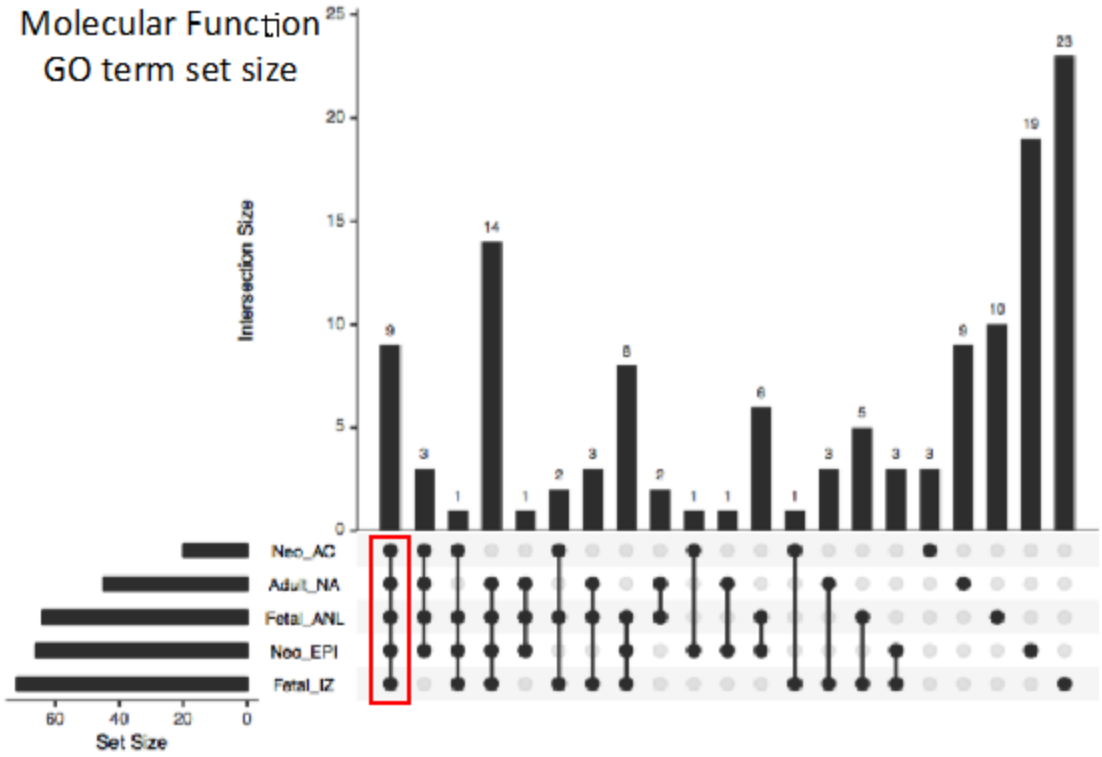

Figure 2.14 CategoryCompare *output represented in an UpSetR plot showing 9 Molecular Function GO categories enriched in the five way comparison (outlined by the red box). The set size graph to the bottom right of the image represents the number of GO categories per DEG list used as input.*

GO Identity	Molecular Function GO term description
GO:0001948	glycoprotein binding
GO:0005178	integrin binding
GO:0005518	collagen binding
GO:0005539	glycosaminoglycan binding
GO:0008201	heparin binding
GO:0017147	Wnt-protein binding
GO:0050431	transforming growth factor beta binding
GO:0050839	cell adhesion molecule binding
GO:1901681	sulfur compound binding

Table 2.5. *Table listing the 9 enriched Molecular Function domain GO terms.*

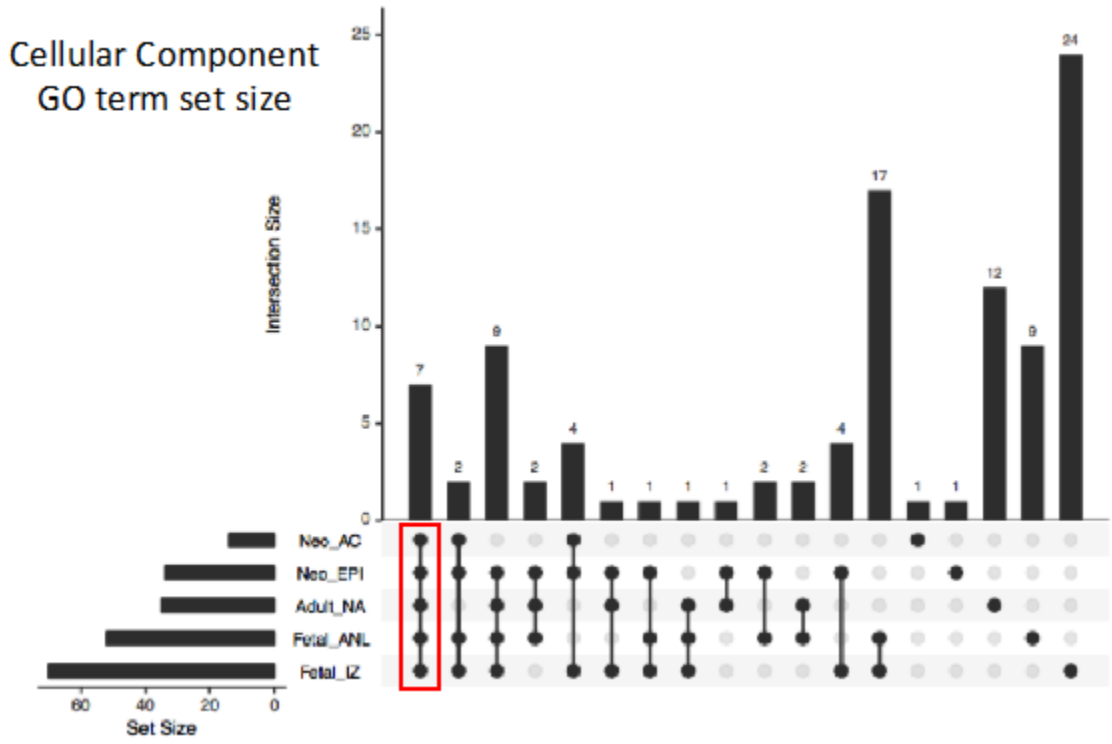

Figure 2.15 CategoryCompare *output represented in an UpSetR plot showing 7 Cellular Component GO categories enriched in the five way comparison (outlined by the red box). The set size graph to the bottom right of the image represents the number of GO categories per DEG list used as input.*

GO Identity	Cellular Component GO Term
GO:0005578	proteinaceous extracellular matrix
GO:0005604	basement membrane
GO:0005924	cell-substrate adherens junction
GO:0005925	focal adhesion
GO:0030055	cell-substrate junction
GO:0031012	extracellular matrix
GO:0044420	extracellular matrix component

Table 2.6. *Table listing the 7 enriched Cellular Component domain GO terms.*

Intersection of categories

The genes that comprised the enriched categories were exported and collated (listed in Table 2.7). Forty-one genes were found in the BP category, 26 genes in the CC category, and 15 in the MF category, making a total of 84 gene names. However, many duplicate listings are present, reflecting genes with a higher level of annotation data available. In Table 2.7, genes represented in two of the three categories are shown in blue and those that are shown in red are represented in all three GO categories. Removal of the replicates leaves 54 gene loci that were found to be differentially expressed from GO enrichment analyses. These are listed along with their respective coverage from the RNA-seq data set in Table 2.8. For each gene, the tissue with the highest or lowest expression value of the six tissues is depicted in bold. Genes shaded in green are upregulated in EQA-AC compared to the other groups (n = 24). One gene in this group, *FRZB*, shows the greatest coverage in EQN-NA not EQA-AC. Genes shaded in red are down regulated in EQA-AC compared to the other tissues (n = 28) with the exception of one gene. This gene, *WHSC1*, has the lowest coverage in EQA-NA not EQA-AC. Both genes are denoted in the table with **. EQA-AC shows the second highest level of expression for *FRZB* and the second lowest level of expression for *WHSC1*.

To visualize these genes and apply some data regarding the fold change in the group-to-group comparisons, a heat map was generated. This map is shown in Figure 2.16. The red – blue key is such that genes with increased expression in adult articular cartilage compared to the comparator tissue are shown in red, and those with decreased expression are shown in blue.

Biologic Process		Cellular Component	Molecular Function
ADGRB2	MERTK	CILP	*COMP*
ANGPTL4	MFAP4	CLU	*CTHRC1*
ANKH	*MMP14*	COL12A1	*DCN*
BCL6	*MMP2*	*COMP*	*FGF1*
COMP	NDFIP1	*DCN*	*FRZB*
CTHRC1	*NDNF*	*EPHA2*	*FZD1*
EPHA2	*NDP*	*FGF1*	*FZD2*
FGF1	PLS3	*FZD1*	*GPC4*
FLI1	PRNP	*FZD2*	*LTBP1*
FRZB	PTK7	*GPC4*	MAP2
FZD1	RUNX2	HSPG2	*NDNF*
IGF2	SEMA3F	*ITGB5*	PCOLCE2
ITGB5	*SEMA7A*	*LTBP1*	*SEMA7A*
JAK3	*SERPINH1*	*LTBP2*	*SERPINH1*
LAG3	SPP1	*MATN1*	*VCAM1*
LECT1	SRCIN1	MATN3	
LOC100059872	SRGN	MFAP2	
LTBP1	*TNFRSF11B*	MFAP4	
LTBP2	*VCAM1*	*MMP14*	
MAF	WHSC1	*MMP2*	
MATN1		*NDNF*	
		NDP	
		PALLD	
		PTK7	
		TIMP2	
		TNFRSF11B	

Table 2.7. *Genes annotated to enriched GO categories in EQA-AC relative to the five other cartilaginous tissues studied are listed. Expression of these individual loci may have been up-regulated or down-regulated. Although 82 genes are listed in total, a number of them have annotation data in more than one GO category. Those annotated to two or three GO categories are shown in blue and red italic letters, respectively. Condensing the duplicated listings results in a total of 54 individual genes.*

Gene	Average Coverage Value (nt/exonic base)					
	EQF-IZ	EQF-ANL	EQN-AC	EQN-EPI	EQA-NA	EQA-AC
CILP	169	20	226	48	33	**17820**
CLU	903	831	20424	11079	35029	**137115**
COMP	2149	9040	55474	52057	29356	**221849**
DCN	2292	2331	14768	11541	7929	**78398**
FGF1	9	9	33	43	63	**525**
ITGB5	658	252	458	375	446	**1344**
LTBP2	83	14	58	40	22	**735**
NDNF	279	81	353	187	7	**2481**
NDP	13	14	19	4	14	**73**
TIMP2	1707	702	6575	2616	2307	**13388**
TNFRSF11B	91	160	741	335	366	**1706**
FRZB **	480	631	631	2360	**10620**	*5206***
PCOLCE2	231	262	262	2219	638	**18437**
VCAM1	174	183	183	99	81	**402**
ANGPTL4	137	6	139	82	62	**429**
ANKH	223	45	493	239	291	**1686**
BCL6	52	56	174	165	174	**788**
LAG3	7	3	11	6	9	**208**
LOC100059872	21	16	64	27	62	**129**
MAF	61	41	110	52	47	**360**
NDFIP1	1191	548	1513	1017	1099	**2908**
PLS3	374	168	360	280	317	**1250**
PRNP	404	158	823	312	269	**1651**
SPP1	72	112	152	272	42	**1843**
SRGN	29	2	338	180	17	**860**

Gene	Average Coverage Value (nt/exonic base)					
	EQF-IZ	EQF-ANL	EQN-AC	EQN-EPI	EQA-NA	EQA-AC
COL12A1	2060	1862	292	509	189	**48**
EPHA2	70	70	17	35	12	**6**
FZD1	218	108	44	142	303	**26**
FZD2	265	156	23	34	37	**8**
GPC4	182	217	51	85	109	**27**
HSPG2	468	638	284	427	358	**111**
LTBP1	876	259	92	101	111	**37**
MATN1	6184	27072	621	1987	8901	**32**
MATN3	1407	8004	1301	4644	4065	**61**
MFAP2	2436	1240	707	1081	1060	**201**
MFAP4	2076	570	837	936	7868	**222**
MMP14	1470	835	423	680	594	**166**
MMP2	2371	2056	923	1404	3239	**231**
PALLD	233	57	78	184	168	**17**
PTK7	234	381	94	156	227	**38**
CTHRC1	1497	2574	2574	399	1243	**15**
MAP2	19	17	17	8	21	**4**
SEMA7A	21	81	81	61	26	**5**
SERPINH1	4199	5383	5383	4450	3163	**1353**
ADGRB2	80	32	11	8	6	**2**
FLI1	101	47	70	60	61	**21**
IGF2	3822	1914	57	47	27	**6**
JAK3	54	28	33	43	34	**13**
LECT1	3332	13341	2990	9006	21210	**199**
MERTK	43	27	11	22	26	**5**
RUNX2	21	400	49	190	26	**7**
SEMA3F	104	14	6	33	7	**3**
SRCIN1	41	27	25	35	67	**3**
WHSC1 **	109	63	12	16	**3**	*7***

Table 2.8. *List of the 54 genes derived from the GO category enrichment analyses showing average groups coverage (nt/exonic base; values rounded to a whole number). Genes highlighted in red are upregulated in EQA-AC compared to the other groups and those in blue are down regulated compared to the other tissues. There are two exceptions in the list. FRZB and WHSC1. Both genes are denoted in the table with **. In the case of FRZB EQA-NA shows the highest expression of all the 6 tissues. In the case of WHSC1, EQA-NA shows the lowest expression among the six tissues.*

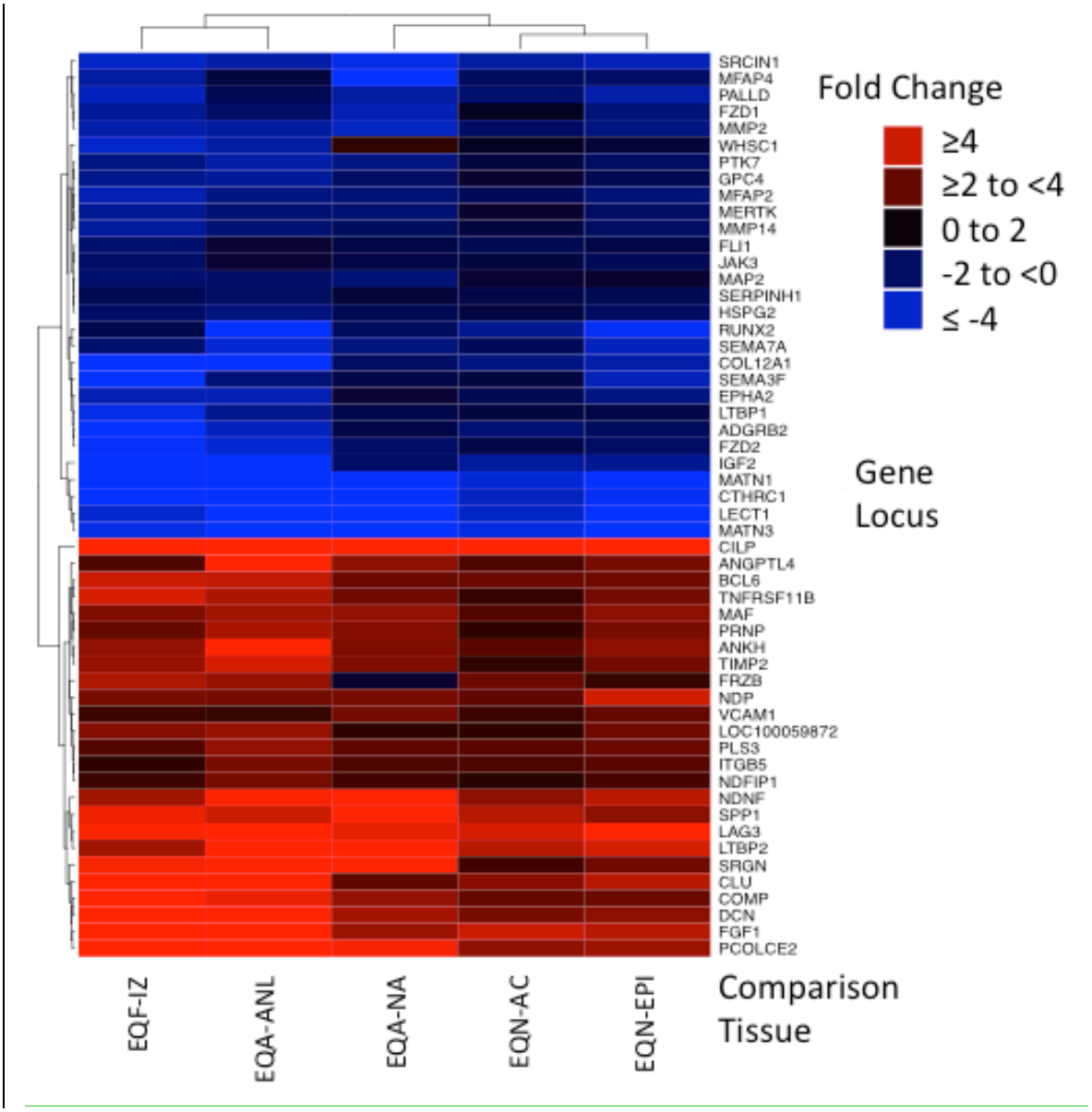

Figure 2.16 *A heatmap showing the fold change by color between average coverage in EQA-AC and each tissue group. Increased or decreased gene expression in EQA-AC relative to the comparator tissue is illustrated by the red or blue color shades, respectively.*

Analysis 2: Intersection of Differentially Expressed Genes Lists

Differentially expressed genes identified in the 5 DEG analyses were captured as gene names. The common genes between these lists, therefore, represent loci that were differentially expressed between each tissue and adult articular cartilage, i.e., all 5 comparisons. Using both an online Venn diagram tool and R code, the exact same combined list of 215 genes was generated. One gene, *TF*, was mapped ambiguously. This gene (*TF*) was maintained in the data analysis set since its coverage between the different tissue types at both loci was of interest when interrogated. The list of 215 genes (based on p-value <0.05, fold change ≥2, expression depth ≥2 on group average level) is given in Appendix 2.1. Of note, there are only a few classic articular cartilage biomarkers of amongst them: COMP, BOC and CILP. The comparisons can be visualized in the UpSetR graph shown in Figure 2.17

A principal component analysis using coverage data for these 215 loci was performed to verify if *en masse* they could segregate EQA-AC from the other tissues. As is clearly seen (Figure 2.18), PCA analysis based on these loci do indeed segregate the biological replicates of adult articular cartilage into a tight cluster that is distinct from the five other experimental groups. This analysis also segregates EQF-IZ, EQF-ANL ad EQA-NA into distinct tissue type clusters. Of high interest, the list of 54 genes identified from GO analyses (Analysis 1, above) is a complete subset of the 215 loci list.

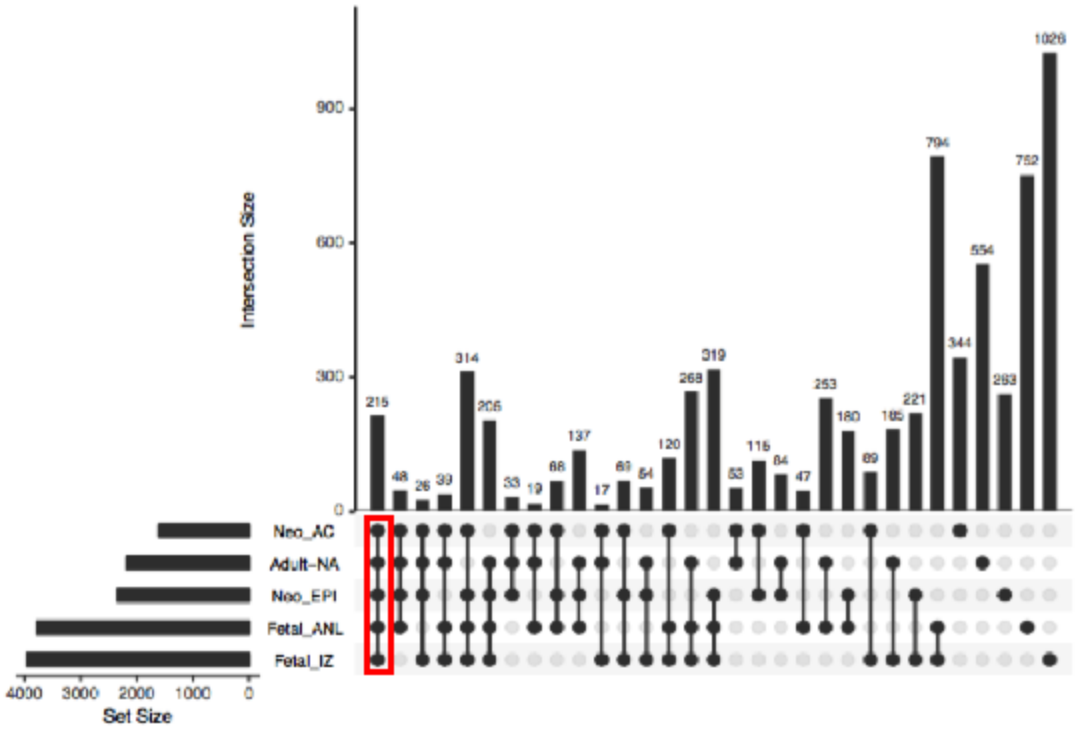

Figure 2.17. *UpSetR graph showing the intersection of genes relative to tissue group in which they are differentially expressed when compared to EQA-AC. The group with 5 connected nodes (outlined in red) represents gene loci that are differentially expressed between EQA-AC and all the other 5 tissue types. The set size graph to the left of the image indicates the number of DEG in each list.*

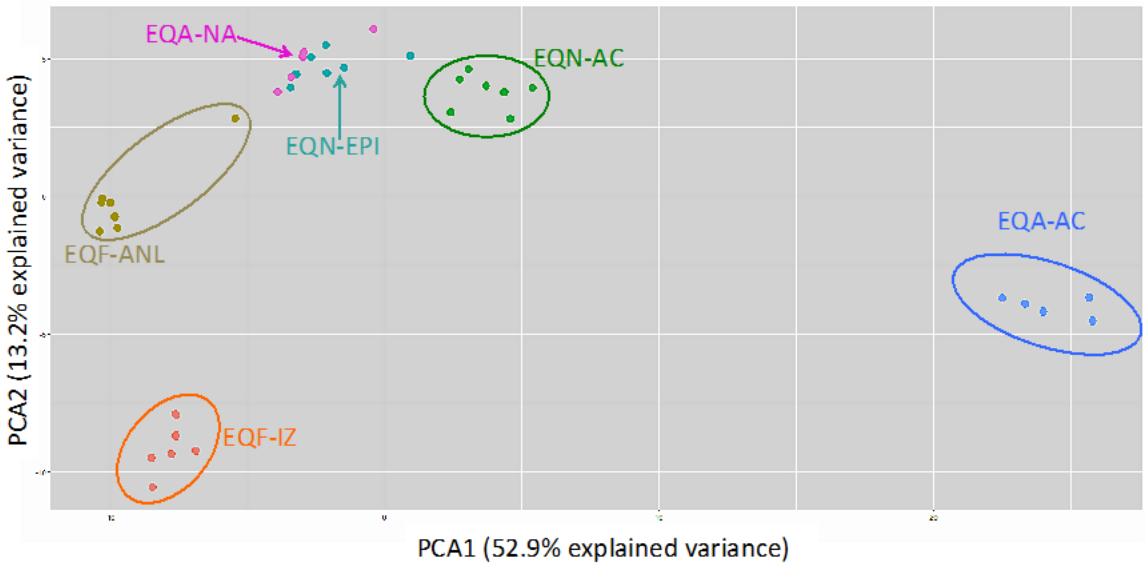

Figure 2.18. *Principal component analysis of the 215 intersection genes derived from the 5 DEG lists. Each point represents a biological replicate in the indicated experimental group. EQA-AC clearly segregates spatially from the other tissue types and clusters by itself on the right side of the graph. Of interest is that this PCA on these 215 loci also segregate EQF-IZ and EQA-NA as tight clusters, although in a position well separated from EQA-AC.*

Analysis 3: Principal Component Analysis Differentially Expressed Genes.

Previous principal component analyses have focused on differences between paired sample sets from the individuals in the same age group, i.e. the comparison of EQA-AC to EQA-NA, EQN-AC to EQN-EPI, and EQF-IZ to EQF-ANL. The criterion for gene loci inclusion was statistically significant differential expression in more than one of these analyses, but without any fold change or coverage depth thresholds. The objective was to determine if a principal component analysis would segregate the different tissue types, and to explore whether plotting different principal components would segregate the groups in novel spatial ways. Just over 6000 loci fulfilled the criteria for inclusion in the PC analysis. A set of 135 gene loci were derived that could segregate the tissue types. These genes are listed in Table 2.9 with their group average

expression. One version of the spatial segregation of these tissue types is shown in Figure 2.19a. Interestingly, different PC's plotted against each other separated the tissue types in an alternative spatial arrangement graphically (Figure 2.19b). This was very encouraging as a previous study performed in our lab using microarray technology on the neonatal samples (EQN-AC and EQN-EPI) was able to detect only modest gene expression differences between the two tissues[72]. Figure 2.19a and 2.19b are two dimensional plots. However, PC analyses can be plotted with a third dimension as is illustrated in Figure 2.20. This graph further separates the experimental groups, but is shown for illustration purposes only.

Gene	EQF-IZ	EQF-ANL	EQN-AC	EQN-EPI	EQA-NA	EQA-AC
ABLIM3	**9.1**	1.1	0.6	3.7	1.7	1.4
ACSL5	9.8	3.5	1.4	9.4	**26.9**	3.4
ADAMTS16	**21.5**	0.7	0.3	0.6	0.3	0.4
ADAMTS19	**73.4**	53.0	2.9	2.5	4.8	0.6
ADAP2	9.4	0.8	1.3	**10.1**	3.7	2.7
ADGRG2	84.9	12.9	69.5	18.8	29.8	**341.9**
ALX4	0.3	0.2	0.0	0.0	**99.4**	0.1
ANGPTL6	**608.3**	95.9	24.6	14.3	36.4	15.4
ARHGEF9	33.7	53.8	16.3	10.9	29.3	**42.0**
ARL4A	**11.9**	7.3	3.1	10.0	6.0	7.2
ARSK	7.3	11.3	9.4	6.7	**86.3**	40.5
AURKB	**93.9**	76.5	0.9	4.5	0.3	0.2
BAIAP3	5.9	5.2	2.2	2.2	**22.1**	9.7
BLVRB	30.5	30.8	19.7	16.1	88.6	**114.0**
CAMKV	**121.2**	31.2	2.8	2.0	13.1	6.5
CAND2	25.5	**31.4**	13.9	9.8	25.9	24.6
CASP4	**7.4**	1.4	0.7	**7.4**	3.5	3.2
CCNF	**35.7**	26.7	0.6	1.8	0.9	0.8
CDCA8	**58.4**	49.7	1.8	4.5	2.3	2.6
CENPP	**29.1**	22.7	11.0	8.5	21.3	23.6
CEP85	25.5	32.6	15.1	10.7	17.1	**33.7**
CKB	12.9	3.1	1.9	**18.3**	8.0	7.1
CLIP4	3.6	0.8	2.7	0.5	**88.2**	2.5
CNDP1	6.8	1.1	26.8	3.1	0.2	**69.7**
CNGB1	1.2	0.8	0.2	0.4	**5.6**	0.1
COL5A3	**188.5**	16.2	23.9	46.2	39.4	41.5
CPVL	6.1	16.5	2.4	12.0	59.0	**111.2**
CSNK1G3	28.9	26.9	**29.9**	18.6	22.5	27.7
DCN	1026.2	1280.4	7175.1	4464.7	5866.9	**61279.2**
DKK3	**356.6**	27.5	30.8	20.5	59.3	60.4
DMPK	70.3	**87.4**	28.5	22.6	62.7	44.5
DNASE1L1	53.8	35.0	29.3	26.0	55.3	**106.1**
DPYSL3	**264.3**	61.9	6.1	16.6	31.7	18.0
ECM2	75.4	24.1	466.8	129.1	18.7	**885.4**
ELMO1	28.3	4.6	11.0	7.1	11.3	**45.4**
EXOC3L1	**5.8**	0.8	0.6	4.7	1.6	0.5
FANCD2	**60.8**	52.6	1.1	3.9	1.4	0.5
FRMD1	17.0	**54.4**	1.0	0.9	21.2	1.2
GINS4	**35.2**	28.2	5.6	7.4	9.1	8.9
GOT1L1	0.2	0.2	0.6	0.6	**12.3**	0.2
GPM6A	4.9	1.2	1.0	8.9	2.1	**10.0**
GRK5	39.6	10.9	262.0	90.7	14.3	**497.3**
GSTA3	0.1	0.8	0.1	0.9	5.8	**15.1**
GYLTL1B	28.2	19.5	15.9	12.6	**66.6**	28.6
HFM1	21.8	**31.1**	9.1	6.5	14.8	22.1
HSPA12B	**219.5**	137.7	8.9	15.5	54.2	17.7
IGSF10	40.6	7.8	41.1	7.7	6.9	**211.5**
IL4I1	0.6	0.5	0.4	0.5	**6.8**	1.8
INCENP	**67.5**	66.1	4.6	6.7	7.8	9.8
ITGB4	5.8	1.9	2.3	**11.1**	7.5	5.2
KIF15	47.0	**47.9**	2.9	4.6	3.9	2.8
KIF23	**109.8**	100.5	1.8	6.6	3.1	0.6
KIFC1	**119.8**	101.0	2.5	6.7	3.2	1.8
LAMA5	**10.8**	6.4	1.5	7.9	9.8	2.3
LAPTM5	**52.4**	12.0	5.9	42.2	17.7	10.9
LOC100054455	0.9	0.2	0.7	**10.8**	0.7	0.5
LOC100055936	42.9	42.7	33.7	26.2	**218.5**	92.6
LOC100063854	**40.5**	2.7	6.7	17.6	4.8	11.5
LOC100271875	0.1	0.1	0.1	0.5	3.6	**11.0**
LOC102147959	**183.2**	33.5	8.0	5.7	2.9	4.3
LOC102149409	**1.1**	1.0	0.8	0.3	0.4	0.4
LOC106781549	0.4	**3.2**	0.2	0.2	1.0	1.0
LOC106782061	6.6	5.4	1.4	0.2	**96.6**	7.9
LOC106782621	0.9	1.6	0.6	**4.6**	2.9	1.2
LTBP4	334.1	124.6	120.5	35.8	78.4	**755.0**
MAFB	40.1	10.7	7.5	42.1	14.0	**46.0**
MAPK7	**48.1**	34.9	16.3	16.4	44.6	29.0
MBD6	58.2	58.3	37.7	31.0	87.4	**139.4**

Table 2.9. *Expression data for gene loci derived from the Principal Component Analysis of genes as described in Analysis 3. The values are group average expression depths in nt/exonic base. Numbers in bold font represent the hughest expression of the 6 groups.*

Gene	EQF-IZ	EQF-ANL	EQN-AC	EQN-EPI	EQA-NA	EQA-AC
MCM10	**11.9**	8.3	0.5	1.2	0.4	0.1
MCM3	**138.6**	86.5	15.4	19.7	29.3	28.6
MCM5	**152.7**	111.7	9.1	13.5	19.2	17.3
MFAP4	920.2	305.7	421.7	377.0	**5611.5**	181.1
MFNG	4.8	0.5	0.5	**6.4**	2.4	0.9
MIR139	0.0	0.0	0.0	0.0	0.0	0.0
MIR8976	28.0	26.5	18.8	12.3	**99.8**	80.9
MMP15	**48.1**	3.4	1.4	4.1	3.2	1.1
MTTP	0.1	**6.8**	0.0	0.1	0.4	0.0
MXD3	**111.2**	102.1	1.4	3.9	0.6	0.6
MYBL2	**113.5**	100.0	1.3	5.4	0.6	0.2
MYH9	**194.3**	58.2	64.3	84.7	88.7	100.0
MYO10	40.4	44.4	24.7	19.0	46.8	**153.1**
MYOM2	1.9	2.3	1.4	2.9	**56.7**	0.5
NALCN	6.9	2.0	9.0	1.8	9.4	**10.3**
NAT14	**74.3**	15.6	10.2	7.2	17.1	18.4
NAV1	24.7	25.5	15.1	33.1	**183.5**	80.2
NDNF	123.4	44.0	184.0	76.5	5.6	**2008.1**
NECAB3	43.3	46.8	23.4	17.5	**126.8**	64.0
NES	**81.8**	19.3	1.0	5.8	3.4	1.8
NFIB	**218.6**	27.7	81.1	53.9	48.7	126.7
NLN	8.9	9.9	10.4	9.2	18.2	**27.6**
PANX3	1.5	**248.5**	6.8	13.5	5.5	3.6
PDE1A	0.8	0.1	0.2	0.3	0.6	**19.7**
PDE2A	**11.9**	1.3	2.6	11.3	2.8	2.0
PDE6B	6.5	4.2	18.6	18.3	12.2	**26.1**
PDLIM1	**190.9**	11.3	14.4	30.1	13.8	28.6
PGM5	**46.8**	2.5	1.3	7.1	4.5	3.8
PITX1	0.9	0.6	38.2	17.0	0.0	**137.1**
PLCE1	62.2	33.9	**74.9**	32.1	54.4	34.9
PLEKHA7	2.2	1.0	1.6	1.0	6.7	**20.7**
PLEKHG1	10.7	11.5	**23.4**	12.3	5.2	5.3
POLA2	**59.5**	52.8	10.3	8.8	13.3	14.0
PPP1R16B	**7.7**	5.3	0.7	5.5	2.5	1.0
PRSS38	3.0	1.8	0.7	0.5	**22.0**	1.5
PTGS1	34.2	9.7	13.5	3.4	**516.9**	38.7
PTPRD	**76.8**	30.4	1.5	3.4	6.9	4.3
PTPRZ1	2.0	**11.2**	0.2	0.1	0.5	2.4
RET	**27.9**	1.6	3.9	1.9	3.8	3.7
RET	**18.5**	0.3	0.2	1.6	2.0	0.9
RNF144B	33.7	62.6	**125.5**	79.4	49.8	16.6
RWDD3	22.5	15.9	13.7	9.4	**56.2**	38.3
S1PR1	22.3	2.4	3.4	**25.3**	6.5	7.2
SCNN1B	0.1	0.3	0.2	0.5	**25.5**	0.8
SETD3	55.1	62.8	59.4	45.8	**152.1**	99.7
SNCAIP	**74.7**	18.1	2.7	2.9	3.8	4.9
STAB1	**34.2**	9.4	4.3	19.3	19.8	13.2
STK33	21.5	**51.9**	8.4	6.7	33.0	15.4
SULF1	**151.9**	37.6	11.5	13.4	22.6	101.9
SUSD4	25.7	3.6	25.3	9.0	3.3	**228.7**
SVEP1	**69.6**	5.4	2.2	10.7	2.0	17.6
TCF19	**119.0**	94.6	6.2	10.9	7.9	10.7
TDRD1	0.0	0.0	1.4	0.3	1.0	**18.3**
TFAP2A	0.3	0.2	0.2	0.2	**59.7**	0.4
TIMELESS	**29.2**	19.9	1.3	2.7	1.0	2.2
TMEM126B	40.3	31.1	24.3	19.8	62.6	**77.5**
TMEM253	0.6	0.5	0.5	0.3	**1.7**	1.0
TMIE	0.4	**10.6**	0.5	0.5	2.1	1.8
TP53I11	24.8	20.8	3.4	18.6	**54.0**	6.7
TPPP	**20.0**	1.4	1.4	6.1	3.2	1.7
TRIM2	41.2	11.5	51.8	15.1	20.3	**59.1**
TUBB2A	**106.5**	11.9	27.5	9.6	75.1	54.4
UBALD2	11.3	10.4	8.6	7.8	12.1	**33.6**
UNC13C	0.7	0.5	0.3	0.1	**22.1**	0.1
VWF	**61.1**	6.7	10.3	59.3	35.9	29.0
ZEB1	**161.4**	35.3	52.6	40.1	51.1	48.7
ZNF219	14.4	10.2	7.7	6.7	**35.1**	18.3

Table 2.9. *Expression data for gene loci derived from the Principal Component Analysis of genes as described in Analysis 3. The values are group average expression depths in nt/exonic base. Numbers in bold font represent the hughest expression of the 6 groups.*

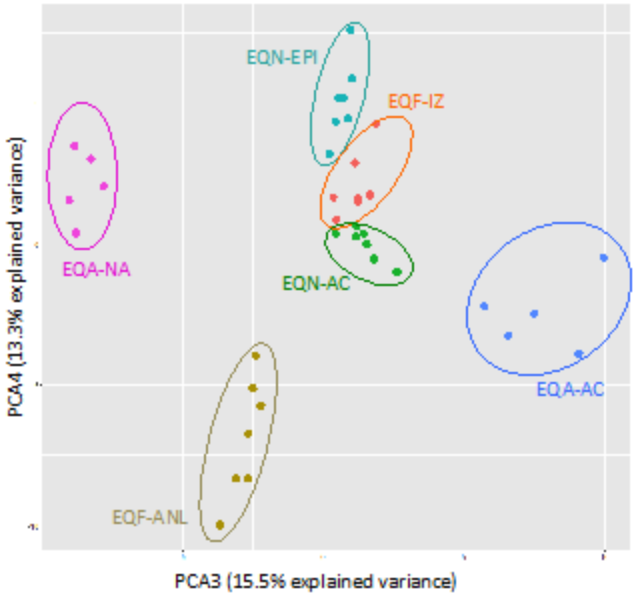

Figure 2.19a. *Principal component analysis of PCA3 plotted against PCA4. All tissue types are clearly segregated into groups that cluster tightly.*

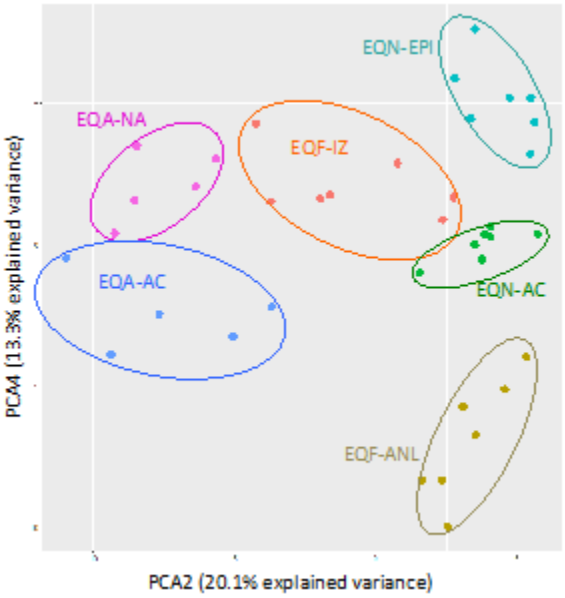

Figure 2.19b. *Principal component analysis of PCA2 plotted against PCA4. All tissue types are segregated, but with less tight clustering that would be difficult to distinguish without color designations.*

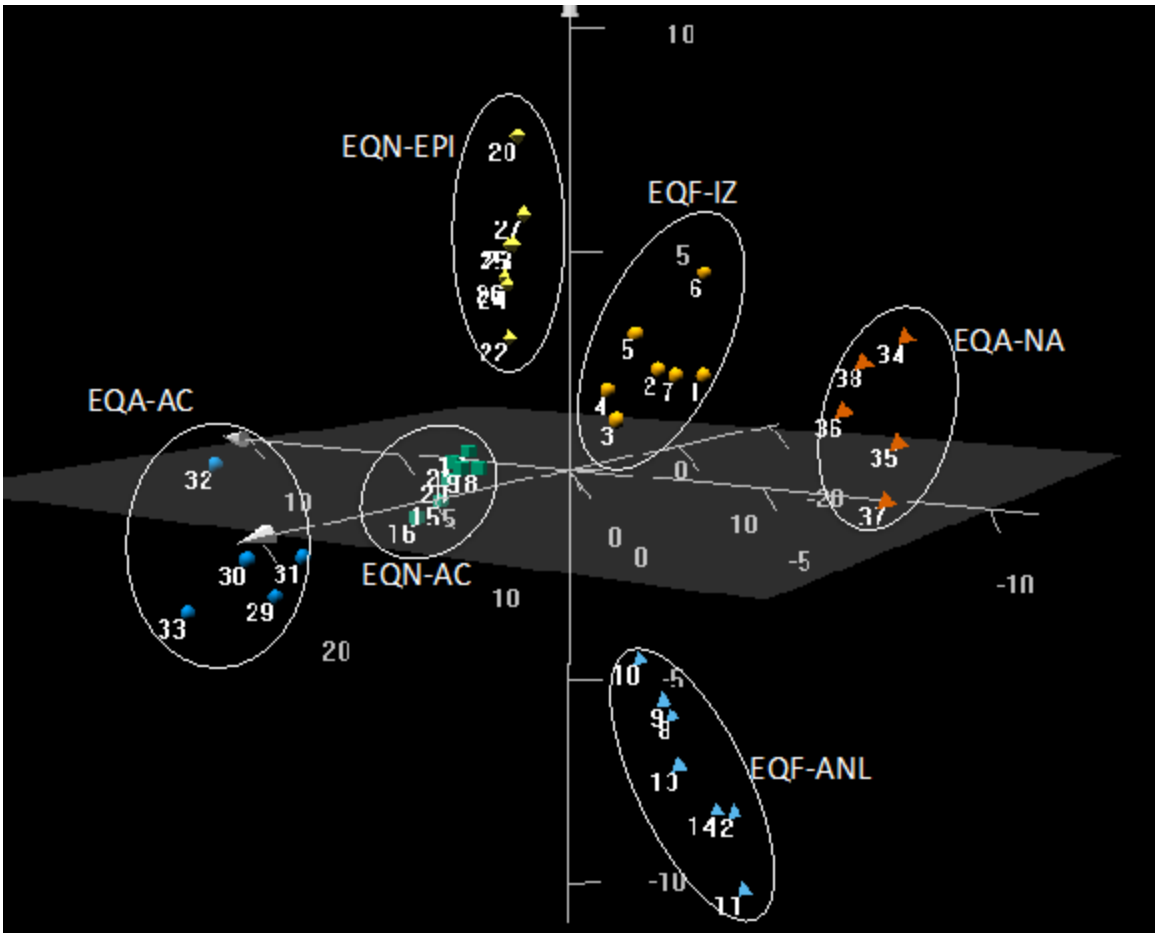

Figure 2.20. *Three dimensional PCA of the 135 gene loci. With the addition of the z-axis the segregation of all of the tissue groups is quite evident.*

Differential Expression of Traditional Articular Cartilage Biomarker Genes

A selection of the classically recognized biomarker genes for hyaline articular cartilage was scrutinized in the RNA-seq data set. Of these gene loci, *COL2A1* was highly expressed in EQA-AC but was not statistically different in pairwise comparisons of EQA-AC with the other five tissues. Comparative expression graphs are shown in Figures 2.21a-g. The average coverage per group for these genes is shown in Table 2.10. Also depicted in that table are the pair wise comparisons with EQA-AC that were statistically significant (shown shaded in pink; $p<0.05$). These ten genes were all statistically significant when EQA-AC and EQF-ANL were compared. *COL2A1* is known to be a biomarker gene for cartilage broadly, compared to non-cartilaginous tissues. However, it provides less resolution to differentiate different types of cartilaginous tissues, and based on these data, fails to distinguish neonatal cartilage from adult cartilage. It is interesting to note that only three gene loci from this small selection of biomarkers are present in the 215 or 54 gene lists from our previous analyses. None of these biomarkers appear in the 135 genes derived by PCA.

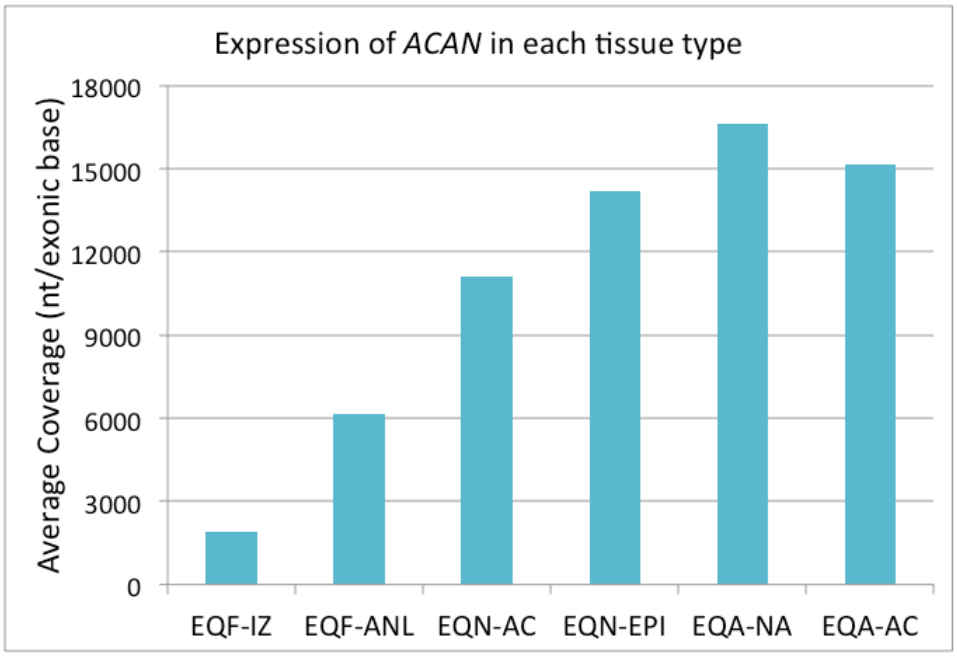

Figure 2.21a. Average expression of ACAN in each tissue type.

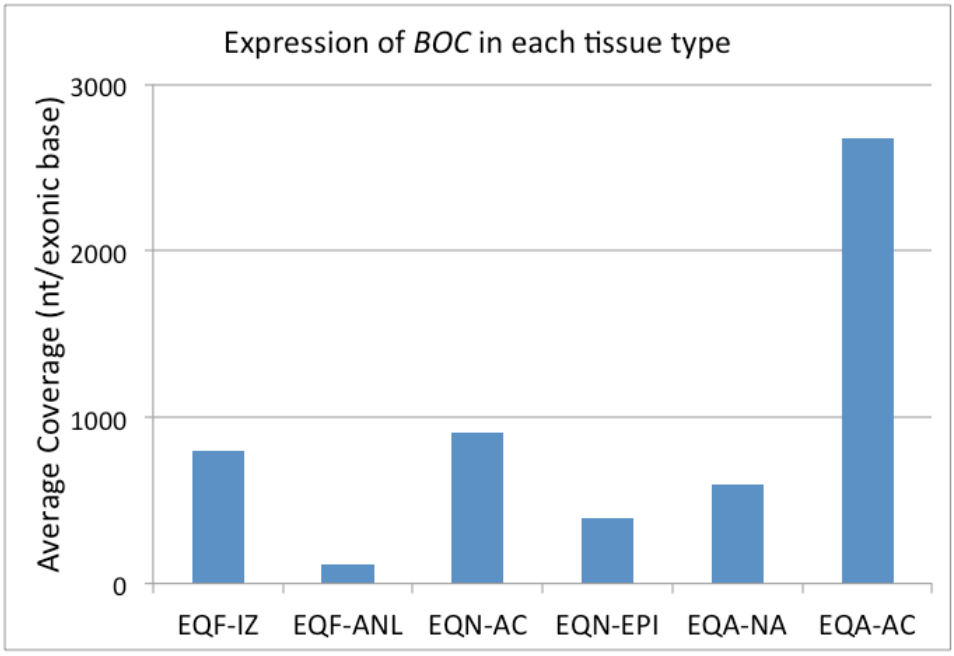

Figure 2.21b. Average expression of BOC in each tissue type.

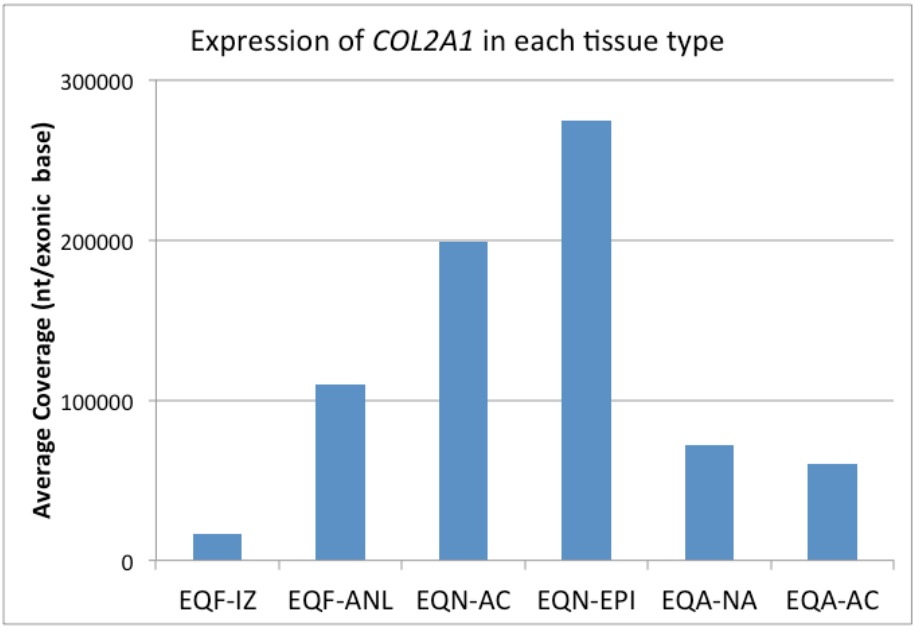

Figure 2.21c. Average expression of COL2A1 in each tissue type.

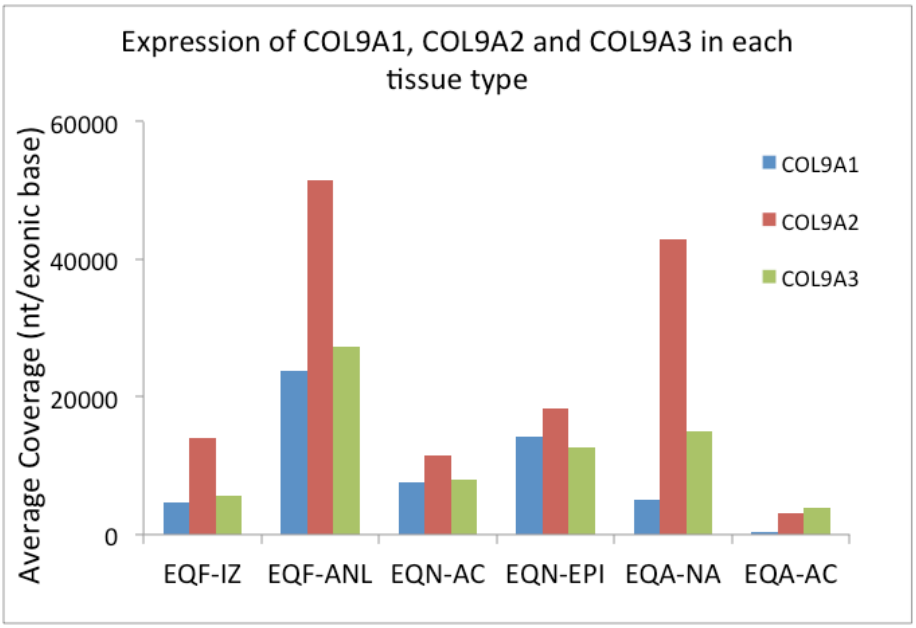

Figure 2.21d. Average expression of COL9A1, COL9A2 and COL9A3 in each tissue type.

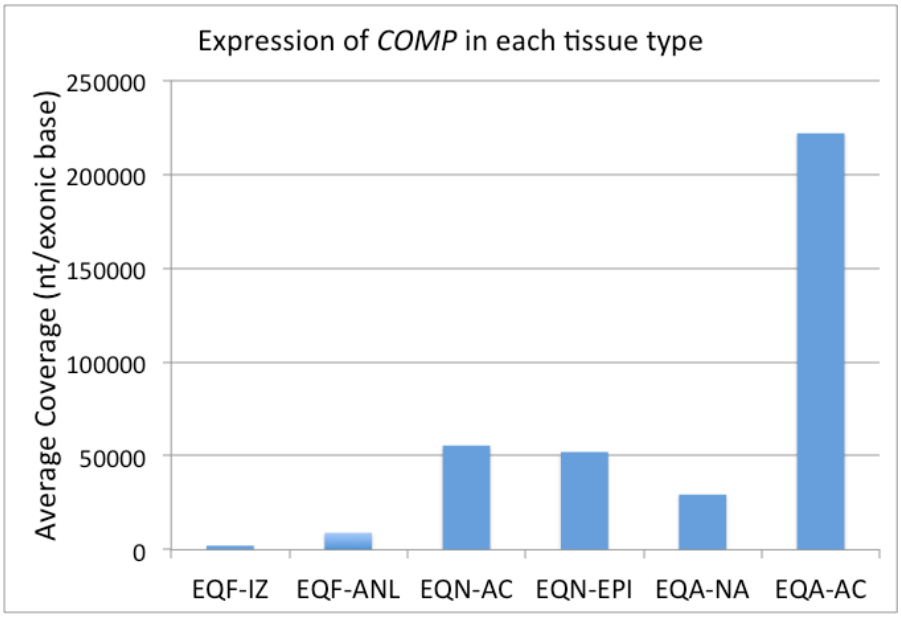

Figure 2.21e. Average expression of COMP in each tissue type.

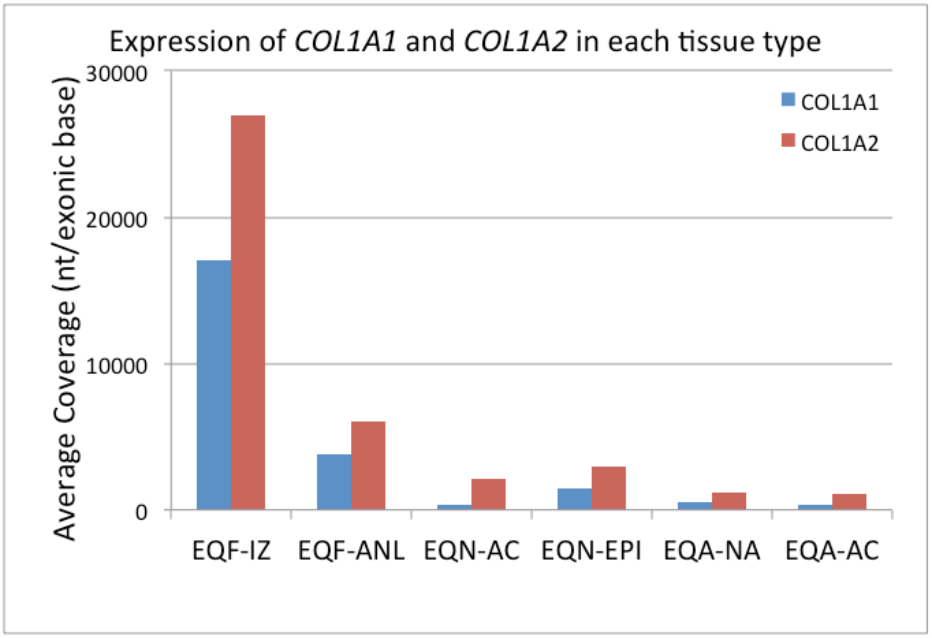

Figure 2.21f. Average expression of COL1A1 and COLA2 in each tissue type.

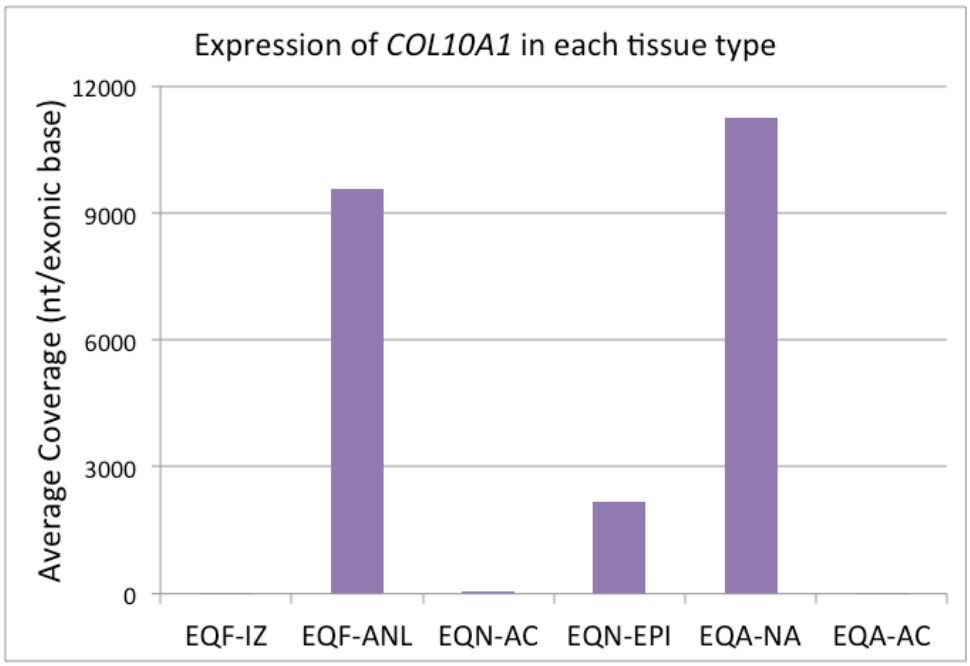

Figure 2.21g. Average expression of COL10A1 in each tissue type.

	Group Average Coverage (nt/exonic base)					
Gene Name	**EQF-IZ**	**EQF-ANL**	**EQN-AC**	**EQN-EPI**	**EQA-NA**	**EQA-AC**
ACAN	1895	6154	11121	14210	**16645**	15181
BOC	798	114	909	396	596	**2675**
COL2A1	16149	110176	198869	**274685**	72279	60261
COL9A1	4762	**23832**	7668	14219	5061	445
COL9A2	13985	**51449**	11418	18314	42936	3190
COL9A3	5561	**27367**	7910	12617	14949	3873
COMP	2149	9040	55474	52057	29356	**221849**
COL1A1	**17070**	3817	321	1464	498	341
COL1A2	**26916**	6013	2093	2944	1210	1080
COL10A1	13	9581	42	2159	**11253**	27

Table 2.10. *Average coverage (nt/exonic base) for each tissue group. In each gene row the highest expression is highlighted in bold font. The values shaded in pink represent genes that are significantly differentially expressed when compare pairwise with EQA-AC (p-value <0.05). Only COMP COL9A1 and COL9A2 are significantly differentially expressed between EQA-AC and each of the other tissues. Fetal anlagen (EQF-ANL) is the only tissue in which all 10 loci are differentially expressed relative to EQA-AC*

Differential Expression of mRNA Transcript Variants

Significant alternative splicing events between samples were identified by pairwise comparison with EQA-AC as described in the Materials and Methods. Table 2.11 illustrates the data from these comparisons.

Tissue Compared to EQA-AC	Number of Significant ASM's Identified		Alternative Splicing Event									
			Alternative Splice Site		Alternative Transcription Start /Stop Site		Exon Skipping		Intron Retention		Combination Event	
	Total	Annotated	*Total*	Annotated	*Total*	Annotated	*Total*	Annotated	*Total*	Annotated	*Total*	Annotated
EQF-IZ	*70*	64	*19*	17	*12*	9	*25*	23	*13*	12	*2*	2
EQF-ANL	*68*	58	*19*	18	*14*	8	*25*	22	*8*	8	*2*	2
EQN-AC	*22*	17	*7*	7	*6*	4	*8*	5	*1*	1	*0*	0
EQF-EPI	*38*	31	*10*	9	*9*	7	*17*	13	*1*	1	*1*	1
EQA-NA	*63*	58	*16*	16	*9*	4	*26*	24	*11*	9	*3*	3

Table 2.11. *Summary of ASM's identified in comparisons made between EQA-AC and the other five cartilaginous tissues. The total number of ASM's discovered in different splice variant categories are given, as well as the number that are annotated in EquCab2.0 AR102.*

In total, 261 significant ASMs were documented with 87.4% being annotated with gene names. The wiggle tracts and schematic diagrams in Figures 2.22 and 2.23 illustrate representative data. In Figure 2.1, an alternative start site is visualized in the gene *RTKN*. This gene encodes for Rhotekin, a scaffold protein that interacts with GTP-bound Rho proteins. Isoforms have been documented in some cancers (http://www.genecards.org/cgi-bin/carddisp.pl?gene=RTKN). Collagen type XVI is a FACIT collagen (a fibril-associated collagen with interrupted triple helices). Members of this collagen family help to maintain the integrity of the extracellular matrix by their association with fibril-forming collagens such as Collagen type I and type II.

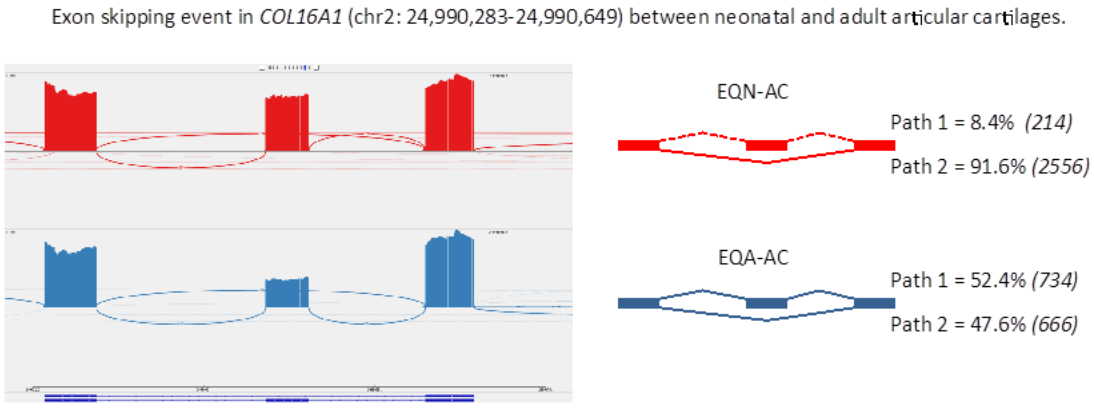

Figure 2.23. *An example of an exon skipping event in the* COL16A1 *locus. The wiggle tract image on the left illustrates RNA-seq data for two samples from EQN-AC (red) and EQA-AC (blue). This gene is expressed at a higher level in the neonatal tissue, but also almost exclusively uses the path depicted as Path 2 that skips the exon. With maturation into adult articular cartilage, splicing at this locus changes to express both isoforms almost equally. The diagrammatic representation to the right provides relative percentages of path utilization. Total level of coverage for each path based on the mapping of splice junctions reads is noted in parentheses.*

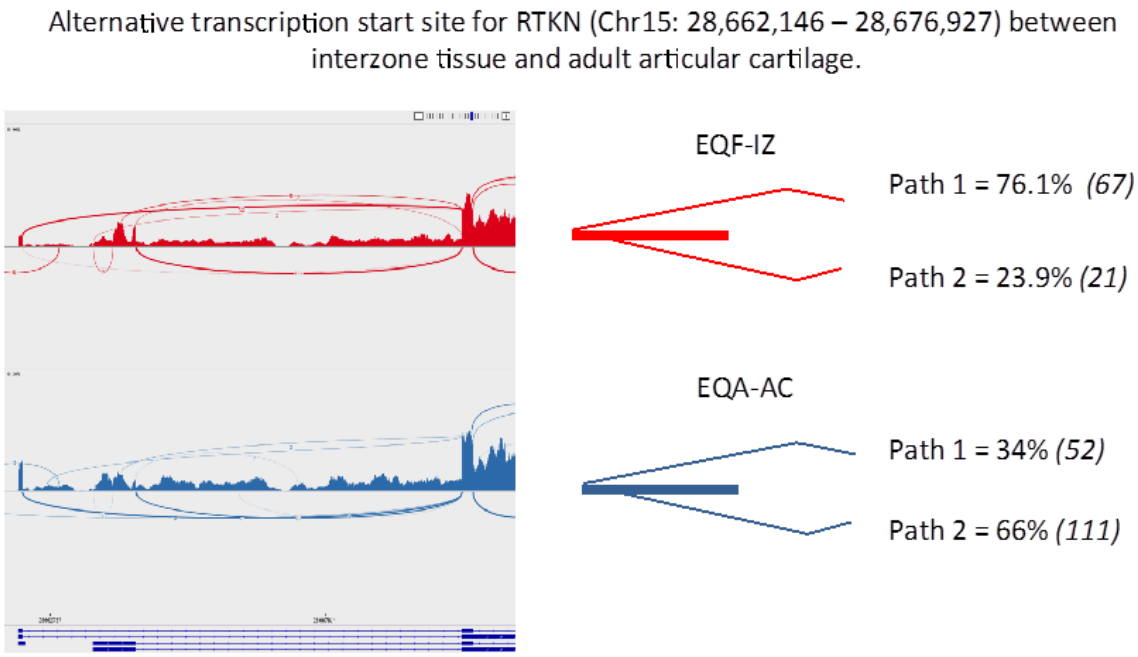

Figure 2.22. *An example of an alternative transcription start site in the* RTKN *locus. The wiggle tract image on the left illustrates RNA-seq data for two samples from EQF-IZ (red) and EQA-AC (blue). There is a switch to a predominance of the downstream transcription start site in adult articular cartilage tissue over the Interzone-rich sample. The diagrammatic representation to the right provides relative percentages of path utilization. Total level of coverage for each transcriptional start site is noted in parentheses.*

Discussion

The sample set assembled, quality of the RNA isolated, and both the number and quality of RNA-seq reads generated allowed a much more comprehensive analysis of the mRNA transcriptome from equine articular cartilage than previous analyses. The data support the hypothesis that adult articular cartilage has an unique tissue-restricted pattern of gene expression compared to other cartilaginous tissues. Based on the number of gene loci found to be differentially expressed for the five comparisons in this study (Table 2.3), adult articular cartilage has the largest difference with interzone (EQF-IZ) and most similarity with neonatal articular cartilage (EQN-AC). This is not necessarily surprising given that the comparison to interzone represents a wide developmental difference[110] and a tissue that is not yet cartilaginous.

In an earlier study from our laboratory, the comparison between adult and neonatal articular cartilage was performed on a microarray platform[73]. In that analysis, the array profiled 9,367 probe sets, of which 6.9% (642 probe sets) were found to be differentially expressed between the two tissues. Increased expression of *COL2A1, COL9A1, COL9A2*, and *COL9A3* in neonatal cartilage relative to adult cartilage was observed. This was confirmed in the current data with a total of 15% of gene loci differentially expressed between these two tissues (thresholds: coverage ≥2 nt/exonic base in both samples, fold change ≥2, uncorrected p-value <0.05).

The microarray did not include probes for every gene loci in the equine genome. However, as an overall observation, both studies identified a number of growth factors from the Insulin-like Growth Factor family and Fibroblast Growth Factor family that were expressed in greater quantities in neonatal cartilage. As has been similarly documented in human studies, aging

cartilage expresses lower amounts of growth factors that, furthermore are less available to chondrocytes by virtue of binding protein affinity[10,11,91]. In an independent equine study performed by Peffers *et al,* RNA-seq data was compared between adult articular cartilage (4 years old horses) and aged articular cartilage (horses >15 years old)[75]. Their data support a finding in aging human cartilage showing that aged cartilage gene expression represented reduced ECM anabolic activity, as well as reduced cytokine and growth factors expression[11]. In that study it was reported that gene expression regarding *Wnt* signaling-related loci was reduced in the aged tissue. The oldest individual in our adult horse sample set was 51 months of age. Thus, the age distributions in the two studies are different. However, we also found that *Wnt* signaling-related genes, as well as cartilage ECM synthesis- and organization-related genes to be significantly enriched GO categories and signature features in adult articular cartilage. Conclusions that can be drawn from these studies are that genes in GO categories related to growth and anabolism are expressed at progressively lower levels in cartilage during the transition from neonate to aged horse.

Importantly, another study done previously in our laboratory compared articular cartilage repair tissue with normal articular cartilage on the equine cDNA microarray[72]. In that study, inferior cartilage repair tissue was characterized by a depletion of ECM matrix gene expression and appropriate collagen expression. Therapeutic improvements will need to address the amount, type, and structural organization of matrix molecules synthesized by repair tissue.

One of the goals in the current study was to define a gene expression profile that distinguishes normal adult articular cartilage from other cartilaginous tissues. All three analytical approaches identified differentially expressed gene loci. The list of 54 genes generated by CategoryCompare was a subset of the 215 genes identified by intersection of the 5 DEG's. While significant

differential expression in the individual pairwise comparisons was defined at $p<0.05$ and not corrected for multiple comparisons, identification of loci with an expression profile that truly distinguishes articular cartilage (Appendix 2.1) was achieved by the experimental design requiring significant differential expression in all five comparisons (Figure 2.5). Random false positives in any one pairwise comparison would be unlikely to be repeated in all five pairwise comparisons. The success of this analytical approach is evident in the PCA analysis (Figure 2.18). Articular cartilage samples both tightly clustered and clearly separated from the other experimental groups, with the two principal components selected accounting for over 63% of the variance between the samples. Interestingly, the expression of these gene loci also cluster and segregate the fetal interzone and neonatal articular cartilage samples, consistent with a close developmental and maturation relationship to adult articular cartilage.

Additional PCA performed in this study using gene loci derived from intra-group (by age) comparisons derived a different set of gene loci that segregate the experimental groups with reasonably tight clustering (Figures 2.19a, 2.19b, 2.20). This analysis, however, was not keyed on adult articular cartilage. Interestingly, but perhaps not surprisingly, the 135 loci used for these PCAs share only 5 genes with the 215-gene set generated from the five DEG lists (Appendix 2.1).

Traditional gene biomarkers that have been used to characterize articular cartilage include, but are not limited to, high expression of *COL2A1, ACAN, COMP, BOC,* and low expression of *COL1A1* and *COL10A1*. Comparative expression of these markers was interrogated in the six cartilaginous-related tissues in the current study. While expression at these loci can distinguish a cartilaginous tissue from a non-cartilaginous tissue, the results demonstrate that they will not

distinguish adult articular cartilage from other cartilages. Only 3 of these 10 loci were included in the analyses keying on articular cartilage (54 and 215 gene lists) and none were present in the PCA analysis based on sample age (135 gene list). These gene loci are very important in cartilage biology, but as biomarkers, should be used primarily to distinguish cartilage from non-cartilaginous tissues.

Differential analyses of mRNA transcript variants from the same gene loci shows a great deal of promise and a number of tissue restricted isoforms and isoform switching events were identified in the current study (Table 2.11). We confirmed two important and previously reported articular cartilage transcript isoforms (data not shown). The *COL2A1* locus has previously been reported to produce two mRNA isoforms: Type IIA procollagen and Type IIB procollagen[69]. In the Fibronectin gene (*FN1*) we also identified the exon skipping event previously described[68]. The analysis, however, also identified many novel splice variants. As depicted in Figure 2.22, interzone tissue and adult articular cartilage exhibit differential use of transcriptional start sites for the gene *RTKN*. This particular gene encodes for Rhotekin – a scaffold protein that interacts with GTP-Rho in the Rho signal transduction pathway. Another example is shown in Figure 2.23, an exon-skipping event in COL16A1 for which no current support in the literature can be found. This splicing event is one that is significantly different between neonatal articular and adult articular cartilage. The identification of transcriptional refinements such as these will provide new insight into the biology of chondrocytes in different cartilaginous tissues, or as a function of development, maturation, and tissue repair.

In conclusion, the data presented in this chapter have provided support on both a loci level and transcript isoform level for a discrete articular cartilage transcriptome signature. It is an

important area for further study, such as additional RNA-seq data analysis and validation by RT-qPCR, especially for tissue-restricted splice variants[70]. Further analyses and experimentation are required to mature these data for benchtop use in determining whether any given chondrocyte possesses an 'articular phenotype', or a specific stem cell type with the potential to differentiate into chondrocytes with an 'articular phenotype.' The study also illustrates analyses made possible by transcriptome profiling and the power of RNA-sequencing technology. This breakthrough technology offers enormous opportunity to better understand cartilage biology and assist in the translation of these data to more robust clinical practices.

Appendix 2.1

215 Genes Derived From the 5-way intersection of Siginificantly Differentially Expressed Genes Beteween EQA-AC and the other 5 Cartilaginous Tissues

ADAM12
ADGRB2
ADGRG2
ADGRL2
ADIRF
ADSSL1
ANGPTL4
ANGPTL5
ANKH
ARHGAP26
ATP10A
B3GALT1
BCL6
BOC
C15H2orf40
C24H14orf132
C2H1orf167
CAMKK1
CDKN3
CDO1
CFAP44
CFH
CHRNA3
CHRNB4
CHST1
CILP
CILP2
CKS2
CLMP
CLU
CMTM7
CNKSR3
COL12A1
COL9A1
COL9A2
COLEC12
COMP
CP
CPLX3
CRABP1
CREG1
CTHRC1
CTTNBP2
DCN
DDHD1
DOK5
DUSP14
E2F3
EPHA2
FAM132A
FAM212B
FGF1
FIBIN
FLI1
FRMD4A
FRZB
FZD1
FZD2
GAS2
GATM
GDF9
GNAI1
GNB4
GNG2
GPC4
GRIN2D
GUCY2C
GXYLT2
HECW2
HLF
HOMER2
HSD3B7
HSPG2
IER3
IGF2
IGLON5
IGSF10
ITGB5
ITIH4
IVNS1ABP
JAK3
JPH1
KCNC4
KCNJ8
LAG3
LARP6
LECT1
LMAN1L
LNX1
LOC100052601
LOC100054601
LOC100057155
LOC100057500
LOC100058594
LOC100059872
LOC100060639
LOC100061358
LOC100065202
LOC100065912
LOC100072916
LOC100146620
LOC100629745
LOC100630794
LOC102147420
LOC102147836
LOC102148436
LOC102149855
LOC102150094
LOC102150130
LOC102150994
LOC106780831
LOC106780907
LOC106780993
LOC106781011
LOC106781665
LOC106782077
LOC106782173
LOC106782190
LOC106782351
LOC106782455
LOC106782976
LOC106783227
LTBP1
LTBP2
MAF
MAGEL2
MAOB
MAP2
MAPK12
MATN1
MATN3
MERTK
MFAP2
MFAP4
MIR8995
MMP14
MMP2
MRGPRF
MTHFR
MYO10
NDRP1
NDNF
NDP
NELL2
NIPAL2
NPW
NR6A1
NXPH3
OCIAD2
OLFML3
PALLD
PARP8
PCOLCE2
PER3
PKIG
PKMYT1
PLCB1
PLS3
PPL
PPM1E
PRNP
PROS1
PRSS8
PTK7
PTP4A3
RANBP17
RBPJL
RMDN2
RUNX2
SAMD11
SCUBE1
SEMA3F
SEMA7A
SERPINH1
SGCG
SHROOM1
SIK2
SLC19A1
SLC1A4
SLC23A2
SLC35F2
SLC7A3
SPATS2L
SPP1
SRCIN1
SRGN
STK17B
STK39
STOM
SUPT3H
SUSD4
SYBU
SYDE2
TASP1
TCEAL2
TCEAL6
TCF7L1
TCP11
TF
THSD1
TIMP2
TK1
TM4SF1
TMEM47
TMLHE
TNFRSF11B
TRNAD-GUC
TSPAN7
VCAM1
WHSC1
ZMPSTE24
ZNF385B
ZNF385C
ZNF385D
ZWILCH

Chapter 3 Comparative Chondrogenic Potential of Equine Fetal Progenitor Cells and Adult Adipose- and Bone Barrow Derived Cells.

Introduction

The central tenant of regenerative medicine is the restoration of a tissue to its fully functional original form. For this to occur, it is recognized that three variables must be in place and interact appropriately[20]. These include the appropriate cells, proper intracellular signals, and a suitable extracellular matrix scaffold[111]. With the advent of joint surgery and early intervention using minimally invasive arthroscopic techniques, it has been observed that surgical debridement of diseased articular cartilage tissue helps to limit the rate and extent of further cartilage degradation by reducing ongoing inflammation[5]. Furthermore, reducing the time taken to 'cover' any exposed subchondral bone with some kind of repair tissue decreases patient morbidity and hastens a return of joint function[26]. With these observations, techniques that deliberately introduce or deliver cells to the lesion site have become routine in clinical practice. One such technique is microfracture[19]. This method involves making small fractures in the exposed subchondral bone plate at the site where diseased cartilage has been debrided. In doing this, bone marrow-derived blood forms a clot within the lesion site. This facilitates development of a fibrocartilage repair tissue and reduces post-operative morbidity[88]. However, whilst the repair tissue is laid down over a shorter time course, it is still biomechanically inferior relative to normal articular cartilage and poorly integrated into the native tissue at the lesion margins[19,26]. As such, lifespan and functionality of fibrocartilage repair tissue are limited and long term outcomes are disappointing[22].

The pursuit of more 'suitable' cells or an increased number of 'therapeutic' cells to augment articular cartilage repair has led to the exploration, both anecdotal and experimental, of many cells types and donor tissue sources. Logically, there has been much interest in the use of

autologous chondrocytes harvested during a preceding surgery from the same patient – a method called ACT – Autologous Chondrocyte Transplantation. This technique is still used by orthopedic surgeons worldwide [19,23,26]. Adult articular chondrocytes are normally in the G_0 stage of the cell cycle – that is fully differentiated and mitotically quiescent. Removed from the cartilage matrix and expanded in number by *in vitro* culture, however, they de-differentiate to varying degrees which leads to the formation of fibrocartilage when placed back into a cartilage defect[22,23,112]. Various techniques have been studied to enhance the "re-differentiation" of *in vitro* expanded chondrocytes. These include hypoxic culture conditions[113], non-adherent culture conditions, stimulation with chondrogenic factors such as TGFβ[114-116], transfection to achieve overexpression of genes shown to be important for a chondrogenic phenotype such as *SOX9* and *IGF-1*[112,117,118], and the addition of substances thought to facilitate chondrogenesis or stabilize the chondrogenic phenotype[119-121], including hyaluronic acid[122].

Early on in the process of ACT, engineered matrices were employed with the goals of improving retention of cells in the defect and enhancing chondrogenic traits in the contained cells. The technique is referred to as MACT - Matrix Assisted Chondrocyte Transplantation[24,123]. The addition of a matrix, that is a refinement on the original thrombin activated fibrin glue for ACT, may offer better physical and enzymatic protection for transplanted cells. The use and evaluation of structurally complex or biochemically modified matrices is an extensive subject; a review of which is beyond the scope of this chapter. Suffice to say that the physicochemical properties, materials used and factors retained within matrices are all under investigation.

Limitations of *in vitro* expanded chondrocytes together with donor site associated morbidity has necessitated a wider search and evaluation of cell types useful for joint therapy. Understandably, the exploration of adult multipotent stem cells and embryonic associated stem

cells (embryonic cells[124,125] or umbilical blood derived cells[32,126-128]) has received significant attention. Mesenchymal stem cells have the cellular potential to be induced to differentiate into mesodermal lineages such as osteoblasts and adipocytes, in addition to chondrocytes[9,32,35,36,39,129-132]. After induction in specialized medium *in vitro,* the phenotype of these cell are often assessed by the expression of a few key marker genes. Examples of such marker genes includes Collagen type II (*COL2*) and Aggrecan (*ACAN*) in chondrocytes, Ostepontin (*SPP1*) and Osteocalcin (*BGLAP*) in osteocytes, and Fatty Acid Binding Protein 4 (*FABP4*) in adipocytes[133,134].

Whether markers of chondrogenesis in adult derived cells are studied via gene expression or via the synthesis of biomarker proteins, induced chondrocytes in clinical and laboratory studies have failed to meet therapeutic expectations. This may be due to the limited assessment possible with small gene or protein lists to define a cells' entire phenotype, the progenitor cells not being appropriate starting points to achieve the desired differentiated cell type, or conditions in the joint being suboptimal pre- and/or post-delivery. Of the many variables that are likely to be involved, the chondrogenic potential of selected cell types is the focus of the current study.

Developmentally, interzone cells have received attention as joint progenitor cells[49,59,135]. Through lineage tracing, they have been shown to develop into articular cartilage, intrasynovial structures such as menisci, and the synovial membrane[136]. Their ability to differentiate into cartilage under chondrogenic induction conditions is unknown, but based on their normal cell fate, interzone cells may have a high chondrogenic potential. In this chapter, the hypothesis tested was that interzone cells have a chondrogenic potential that exceeds that of adult bone

marrow derived and adipose derived mesenchymal stem cells. Specific aims were to (i) assess and compare histological architecture, cell morphology, and proteoglycan matrix staining in chondrogenic pellets generated from equine adult mesenchymal stem cells and fetal musculoskeletal progenitor cells in culture, and (ii) compare steady state mRNA levels encoding *ACAN* (Aggrecan core protein), *COL2A1* (Collagen type II), and *COL1A1* (Collagen type I). The outline of these experiments is schematically shown in Figure 3.1.

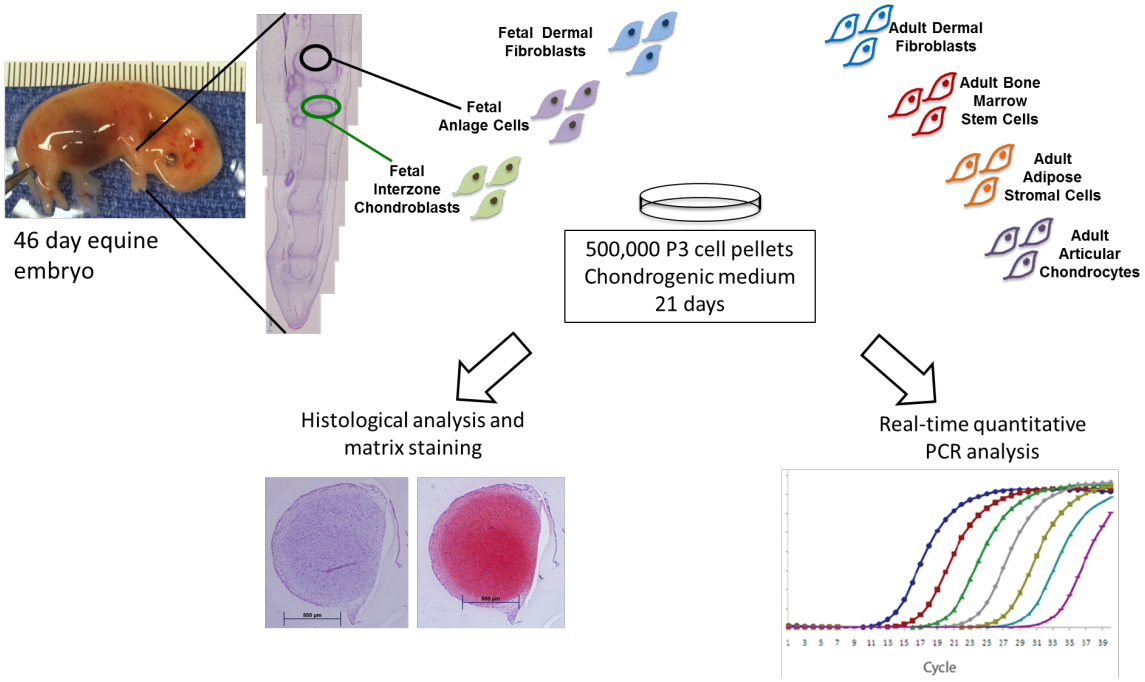

Figure 3.1. *Schematic outline of the experimental design in this chapter. The 46-day-old fetus in the top left corner is shown against a millimeter scale. The adjacent composite photomicrograph is a forelimb from this embryo showing the limb from mid-radius to third phalanx. The portion of limb shown in the image is 3mm in length.*

Materials and Methods

Experimental Samples

Seven equine fetuses aged 45-46 days of gestation were harvested from mixed light breed mares (IACUC 2014-1215). Briefly, mares' estrus cycles were synchronized to facilitate accuracy of pasture breeding using two doses of intramuscular synthetic prostaglandin F2α (500 μg of cloprostenol sodium, Estrumate©). The mares were pasture bred with the stallion remaining with the mares for 10 days. Daily serum progesterone levels were used to confirm the approximate date of ovulation, which was called day 0 of gestation if the mare was confirmed pregnant. Six days after the stallions were separated from the mares (16 days after the mares were programmed to ovulate), a *per rectum* ultrasound examination was performed to determine embryonic vesicle size as an additional technique to confirm gestational age[137]. Appropriate serum progesterone levels and ultrasonographic evaluation pre rectum were used to confirm pregnancy.

On days 45 or 46 of gestation, the fetus was recovered from the standing sedated mare using a non-surgical uterine lavage technique. On the day of collection, pregnancy status was confirmed by transrectal ultrasonography. The mare's vulva was cleaned aseptically, and using a sterile pipette, 2 mg of synthetic prostaglandin E_2 paste (in 2.5ml triacetin and 125mg silicon dioxide gelling agent) was instilled along the length of the cervical ostium after gentle and minimal digital dilation. After one hour, mares were returned to the stocks and sedated with detomidine (10 - 16 μg/kg IV) and butporphanol (6 - 16 μg/kg IV). Once sedated, the cervical ostium was digitally dilated *per vagina* using aseptic technique to allow positioning of a 28mm OD endotracheal tube to the level of the internal ostium of the cervix. Following the introduction of 2 - 3L of warmed sterile lactated Ringers' solution, the uterus was to-and-fro lavaged. This action readily displaced the embryo within its vesicle, which then passed out

through the tube into an attached sterile fluid bag. A progressive improvement on the technique was developed which involved balloting the fluid filled uterus *per rectum* as the tube was held in place in the cervical ostium. In all cases, the passage of the fetal membranes was assured. Fetuses were immediately and copiously rinsed in ice cold sterile Dulbecco's phosphate buffered saline (PBS; Gibco, cat# 14190144) with 2% (v/v) amphotericin B (anti-mycotic, Gibco, cat# 15290026), and 2% (v/v) penicillin/streptomycin (antibiotic; Gibco, cat# 15070063). Each fetus was catalogued and placed in a sterile container on ice for immediate tissue processing. After the lavage procedure, each mare was given 500 μg of cloprostenol sodium (Estrumate©) by intramuscular injection q 24h for 2 days (synthetic prostaglandin F2α) to promote uterine clearance of any residual flush fluid. Mares also received a single dose of flunixine meglumine (1mg/kg IV, non-steroidal anti-inflammatory). None of the mares from which fetuses were flushed suffered any ill effects of the procedure as evidenced by post-harvest urogenital infections, colic, or other complications. They have remained apparently healthy to date.

Fetal cell lines:

One forelimb and one hind limb from each fetus were used to obtain interzone cells and anlage chondrocytes. Meticulous dissection of soft tissues over the limbs was performed using a dissecting microscope and sterile microscopic instruments. Developing carpal and tarsal joints were then isolated and placed in sterile 1.5 ml microcentrifuge tubes. Interzone cells were liberated from early cuboidal bone anlage by digestion in 500 μl of commercial 0.25% trypsin EDTA solution (Gibco, cat# 25200056) for 5-10 minutes with gentile agitation using a micropipette. The enzymatic activity was then quenched with 1 ml Dulbeccos Modified Eagles Medium (DMEM, Gibco, cat# 10569044) supplemented with 10% (v/v) Fetal Bovine Serum (FBS), 1% (v/v) P/S, and 1% amphotericin B (complete medium). Cuboidal bone anlage and undigested

tissue fragments were allowed to settle by gravity for 3 minutes. Suspended cells in the supernatant were then transferred to a sterile 15 ml polypropylene tube, pelleted by centrifugation at 1000 rpm for 3 minutes, re-suspended in 5 ml of complete medium, and plated in six well cell culture plates (Bio-Star, VWR cat# 10062-892). Importantly, no collagenase was used in the isolation of interzone cells.

Anlage chondrocytes were isolated from dissected internal cubes of distal metaphyseal anlage of the developing humerus and femur. Great care was taken during dissection to stay clear of the epiphysis, diaphysis, and anlage surface. The potential for any contaminating cells was further minimized by digestion in 500 μl of the commercial 0.25% trypsin EDTA solution for 5-10 minutes, followed by gravitational settling of the anlage cubes and two rinses in sterile Dulbecco's phosphate buffered saline supplemented with 2% (v/v) P/S, and 2% (v/v) amphotericin B. The chondrocytes were then liberated from the anlage matrix by digestion in 1 ml of 0.5% collagense D (Worthington, cat# CLS4; http://www.worthington-biochem.com/cls/pl.html) for 10-20 minutes with gentile agitation using a micropipette. Quenching of the collagenase activity, cell pelleting, and plating of primary anlage chondrocytes were similar to the procedures described above for interzone cells.

Fibroblasts were isolated from sections of truncal dermis dissected from a region of skin far removed from any skeletal structures. Care was taken during dissection to avoid both the epidermis and hypodermis. The subcutaneous dermal tissue was minced and then digested in 1 ml of the commercial 0.25% trypsin EDTA solution for 10-20 minutes with gentile agitation using a micropipette. Gravitational settling of undigested tissues, quenching of the trypsin activity,

cell pelleting, and plating of primary fibroblasts were similar to the procedures described above for interzone and chondroblast cells.

Adult cell lines:

Tissue samples were collected immediately post-mortem from six young adult mixed light breed horses at 15-17 months of age euthanized for reasons unrelated to the current study (IACUC 00843A2005). Bone marrow aspirates were obtained using an 8 FrG Jamshidi needle and heparinized syringes [47]. The samples were maintained at 4^{o}C until direct plating in 1:1 complete medium into T-75 tissue culture flasks (Bio-Star, VWR cat# 82050-856), which was performed within one hour of euthanasia. Red blood cells were removed by serial rinsing with PBS over the course of the first few days of culture to yield adherent cells. Subcutaneous adipose tissue was harvested from fat at the base of the tail head. After rinsing, it was minced, lightly digested and plated as previously described[37,121]. Dermal fibroblasts were obtained from dermis taken from skin reflected at the tail base during adipose collection. Dermal tissue was minced and placed in tissue culture plates in complete medium allowing adherent fibroblast cells to grow out onto the plastic. The processing and plating of adipose and dermal tissue samples were completed within three hours of euthanasia. Articular chondrocytes were obtained as previously described[138]. Briefly, articular cartilage from the femoro-tibial joint was shaved down to the calcified layer. After washing several times in PBS with 2% antimycotic and antibiotics supplements as above, the cartilage was either snap frozen in liquid nitrogen for RNA extraction or processed to harvest primary chondrocytes. For the isolation of primary articular chondrocytes, the cartilage shavings were minced, weighed, and digested for 22 hours in medium (OptiMEM [Gibco Cat # 51985091, 5% FBS, 1% antimycotic/antibiotic) containing bacterial collagenase (Worthington) at 7.5mg collagenase/g of cartilage. Primary chondrocytes released from the cartilage matrix were

spun, rinsed, counted, and plated into tissue culture flasks. Dermis was harvested and snap frozen from an age matched control horse to serve as a control sample in the quantitative PCR assay for type I collagen.

Fetal and Adult Cell Lines Obtained:

A total of 3 cells lines were obtained from each of the 7 equine fetuses. A total of 4 cells lines and articular cartilage tissue were obtained as complete sample sets from each of 6 young adult horses. Taken together, the following paired primary cells lines were generated:

1) Adult articular chondrocytes
2) Adults adipose derived stromal cells
3) Adult bone marrow derived cells
4) Adult dermal fibroblasts

n = 6 biological replicates

5) Fetal anlage chondrocytes
6) Fetal interzone derived cells
7) Fetal dermal fibroblasts.

n = 7 biological replicates

Cell Expansion and Cell Pelleting.

Due to the number of primary fetal anlage and interzone cells isolated, serial passage was necessary to obtain sufficient cells for generating 24 pellets. To control for this variable of *in vitro* expansion and to maintain consistency between experimental groups, the other cell types were also cultured as monolayers to Passage 3 (P3) prior to pelleting. Cells were passaged at 65-70% confluence and seeded at 500,000 cells per T75 flask (6,667 cells/cm^2). The cells were fed three times per week with 10ml of complete medium (Dulbecco's Modified Eagles Medium + Glutamax®(DMEM), 1% penicillin/streptomycin, 10% heat inactivated fetal bovine serum). To

generate P3 cell pellets, P2 cells were trypsinized and washed twice in serum free medium. Cells were then resuspended in chondrogenic medium at 500,000 cells per ml as previously described[121]. One milliliter of cell suspension was centrifuged at 500*g* for 3 minutes in a 1.5 ml polypropylene microcentrifuge tube to generate a cell pellet. Chondrogenic induction medium consisted of DMEM, 1% penicillin/streptomycin, 12.5 mg/ml bovine serum albumin, 1 x ITS-A growth supplement (Thermo Fisher Scientific, Cat# 51300044), 1x non-essential amino acids, 100 nM dexamethasone, 50 μg/ml ascorbate-2-phosphate, 10 ng/ml rhTGFβ1 (EMD Milipore, cat# GF111) [42,121,139,140]. After 24 hours, each individual pellet was transferred from the microcentrifuge tube to a single well of a 1% polyHEMA coated 24-well plate. The polyHEMA coating facilitated suspension culture of the pellets, by preventing adhesion to the plastic surface of the culture well. As a control, one T75 flask of passage 3 cells was seeded in complete medium with 500,000 cells, maintained in monolayer culture, and harvested for RNA extraction at 75-80% confluence.

Histological Assessment:

Twelve pellets from each cell line were fixed in 4% paraformaldehyde for 24 hours. They were pre-embedded in 2% agar/2.5% gelatin blocks[141], 2-3 pellets per block. Blocks were then fixed in 4% paraformaldehyde prior to placement in 70% ethanol for batched histological processing. Sections were cut at 5 μm and stained with either hematoxylin and eosin for cell morphology and pellet architecture or Safranin-O to assess proteoglycan content and distribution as described below.

Proteoglycan Staining:

Safranin-O is a stoichiometric orthochromatic dye that binds to sulfate groups in proteoglycan molecules in a 1:1 fashion, making it semi-quantitative[142]. Thus, the 'redness' of the stained section is approximately proportional to the proteoglycan content under the assumption that the overall relative negative charge density of the matrix proteoglycan is similar between samples. The 'redness' values of stained sections were calibrated by three articular cartilage control samples randomly placed in the 30-slide rack. All sections were stained with 0.05% Safranin-O and a Fast Green counterstain in two batches to reduce intra-batch technical variation. Stain uptake of the articular cartilage control sections was analyzed for intra- and inter-batch variation. Mounted sections were imaged with a Nikon Eclipse Ti microscope at 4x in a darkened room to minimize ambient light, and with microscope exposure and brightness uniform for all measurements. ImageJ Fiji software (https://imagej.nih.gov/ij/download.html) was used to analyze all images. Red balancing of the white microscope source light was performed. The contrast level for each pellet after red balancing was fixed and background red, green, and blue components determined. After background assessment, the mean red, green, and blue components of the image itself were measured for each slide and the redness value calculated as shown below.

$$Green_{modified} = \left(Green_{mean} - Green_{background}\right)$$

$$Blue_{modified} = \left(Blue_{mean} - Blue_{background}\right)$$

$$'Redness\ value' = Red_{mean} - \left(\frac{Green_{modified} + Blue_{modified}}{2}\right)$$

This redness value represents the red color of just the Safranin-O stained molecules making comparison between sections possible. The greatest, least, and overall average redness value of a each pellet section were recorded and normalized to articular cartilage control sections.

Neocartilage Assessment:

The Bern Score (Figure 3.1) was employed to semi-quantitatively assess pellet neocartilage [143]. Representative sections of all pellets stained with Safranin-O/Fast Green were assigned coded identifiers and then assessed independently by three observers.

The Bern Score. Grogan *et al* 2006

A	**Uniformity and darkness of Saf-O-Fast Green**	**Score**
	No stain	0
	Weak staining of poorly formed matrix	1
	Moderate even staining	2
	Even dark stain	3
B	**Distance between cells/amount of matrix accumulated**	
	High cell densities with no matrix in between (no spacing between cells)	0
	High cell densities with little matrix in between (cells < 1 cell-size apart)	1
	Moderate cell density with moderate distance between (cells approx 1 cell-size apart)	2
	Low cell density with matrix distance between cells (>1 cell) and an extensive matrix	3
C	**Cell Morphologies represented**	
	Condensed nucleus/pyknotic bodies	0
	Spindle/fibrous morphology	1
	Mixed spindle/fibrous with rounded 'chondrogenic' morphology	2
	Majority rounded /'chondrogenic' (rounded to include presence of lacunae)	3
	Maximum Score	**9**

Table 3.1. *Bern Score guidelines. These guidelines were developed to score cell morphology and matrix staining features of neocartilage grown in vitro. The maximum score, for neocartilage with the most 'cartilage-like' characteristics, is 9.*

Statistical Analysis of redness values and Bern Scores.

Redness values and Bern scores were independently evaluated by one-way analysis of variance with Tukey's *post hoc* corrections for multiple comparisons. Differences were considered statistically significant if the corrected *p*-value was $p<0.05$. The intra-observer differences for Bern score analysis was evaluated by ANOVA.

RNA isolation and quantitative real-time PCR.

Passage 3 cells in monolayer culture were lysed with QIAzol® (Qiagen, cat# 79306), a guanidinium thiocyanate-phenol-chloroform extraction reagent, at 75-80% cell confluence and snap frozen in liquid nitrogen. After 21 days of culture, twelve pellets from each cell type were rinsed with nuclease-free PBS, and snap frozen in aliquots (3 pellets per aliquots). The samples were then transferred to a freezer and stored in at -80^{o}C for subsequent total RNA extraction.

Total RNA was isolated using a column-based kit with modifications as previously described (Qiagen RNeasy Micro Kit, cat# 74004)[73]. Frozen pellets were homogenized in 2 ml of Qiazol® (3 pellets/2ml). Processing contaminants were then removed from RNA samples by ethanol precipitation. Purified RNA was quantified using the Qubit BR Assay or Qubit HS Assay (Life Technologies®, cat#s Q10210, Q32852) and NanoDrop ND 1000 spectrophotometer. Qualitative parameters of the RNA preparations were assessed using a Bioanalyzer 2100 (Agilent Technologies, Eukaryotic Total RNA Nano & Pico Series II). All RNA samples met quality thresholds, 260/280 ratios of 1.7-2.0, 260/230 ratios of 1.8-2.1, and an Agilent RNA integrity number (RIN) of ≥ 7.0.

The removal of any genomic DNA contamination and the reverse transcription of total RNA to yield cDNA was performed with a commercially available kit (Maxima First Strand cDNA

Synthesis Kit® for RT-qPCR with dsDNase, Life Technologies, cat# K1672). Complementary DNA was uniformly diluted to 5 ng/μL and stored at -20°C in 100 μL aliquots. Commercially available, validated equine-specific TaqMan® primer probe sets were used to quantitate steady state mRNA levels of *ACAN*, *COL1A1* and *COL2A1* genes. (See Table 3.2 for details of the primer-probe sets). Appropriate negative, positive and random DNA controls were performed in triplicate on each PCR reaction plate. These included water cDNA as the negative control, and mixed cDNA that included genomic DNA from several tissues as a positive control. Each sample was assigned a randomly generated number for randomization of plate loading to control for any plate effects. After comparing five commercially available equine-specific endogenous control gene primer-probe sets, β 2 microglobulin (*B2M*) was selected for its uniform performance across cell types and culture conditions in consideration of MIQE guidelines[144] (data not shown).

Real-time quantitative PCR (qPCR) reactions were performed in 284 well plates with a total reaction volume of 10 μL, using 22.5 ng of cDNA template per reaction. Reactions were performed on a robotic ViiA™ 7 Real-Time PCR System (Thermo Fisher Scientific). Reaction amplification efficiencies were measured by LinRegPCR and threshold cycles were calculated[145]. Relative expression (RE; relative quantity, RQ) of gene targets was determined using the $2^{-\Delta\Delta Ct}$ method[146]. Calibrator samples for these calculations were a single dermis sample from an age-matched control horse for the *COL1A1* analysis, and the average articular cartilage tissue DDCt values for *ACAN* and *COL2A1* from all adult horses used in the generation of cell pellets.

Statistical analysis of qPCR data:

Statistical analysis of qPCR results was performed on individual lnRQ values using one-way analysis of variance. Expression was considered significantly different if the *p*-value was <0.05.

Gene Symbol	Gene Name	ThermoFisher Catalog #	ThermoFisher Catalog ID	Predicted Amplicon Length	Exons Spanned	NCBI EquCab 2.0 Coordinates
B2M	Beta-2-microglobulin	4331182	Ec03468699_m1	70 nt	1 - 2	Chr.1: 144492381 - 144497809
COL2A1	Collagen type II alpha 1	4351372	Ec03467416_m1	73 nt	52 - 53	Chr.6: 65629017 - 65660099
COL1A1	Collagen type I alpha 1	4351372	Ec03469680_m1	138 nt	9 - 10	Chr.11: 25913092 - 25929428
ACAN	Aggrecan Core Protein	4351372	Ec03469667_m1	72 nt	1 - 2	Chr.1: 94344146 - 94381944

Table 3.2 *Table listing details of the TaqMan© primer-probe sets employed in the qPCR reactions.*

Results

Cell Expansion & Pelleting

All cell lines proliferated actively once the primary cells had been established. Fetal anlage cells and primary adult articular chondrocytes were the quickest to plate down and were the first to require passage. Adult dermal fibroblasts were grown out from minced tissue and took the longest time to generate primary adherent cells. The fetal dermal tissue had a less fibrous consistency and cells adhered from these samples readily. Subjectively, the fetal cells expanded more rapidly and had a shorter time to passage than the adult cells. Adult adipose derived cells seemed to be the slowest of the adult cell lines in terms of the interval between passage.

Gross Assessment of Pellets

All pellets increased in size during the culture period regardless of the cell type. No pellets disintegrated. Pellets varied in size from less than 1 mm to over 2 mm in diameter, with characteristic cell type size relationships conserved across biological replicates. For fetal cells, pellet size relationships were: anlage cell > interzone cell > dermal fibroblast. In adult samples, the relative sizes were: articular chondrocyte > bone marrow derived cell > adipose derived cell > dermal fibroblast. Figure 3.2 shows their relative size with a 1 mm increment scale.

Key to abbreviations for cell types in graphs and table in this chapter.

ACT: Adult Articular Cartilage Tissue
AAC: Adult Articular Chondrocyte
ADC: Adult Adipose Derived Cell
BMC: Adult Bone Marrow Derived Cell
ADF: Adult Dermal Fibroblast
ANL: Fetal Anlage Cells
IZ: Fetal Interzone Cells
FDF: Fetal Dermal Fibroblast

- M : denoted monolayer culture
- P : denotes pellet culture

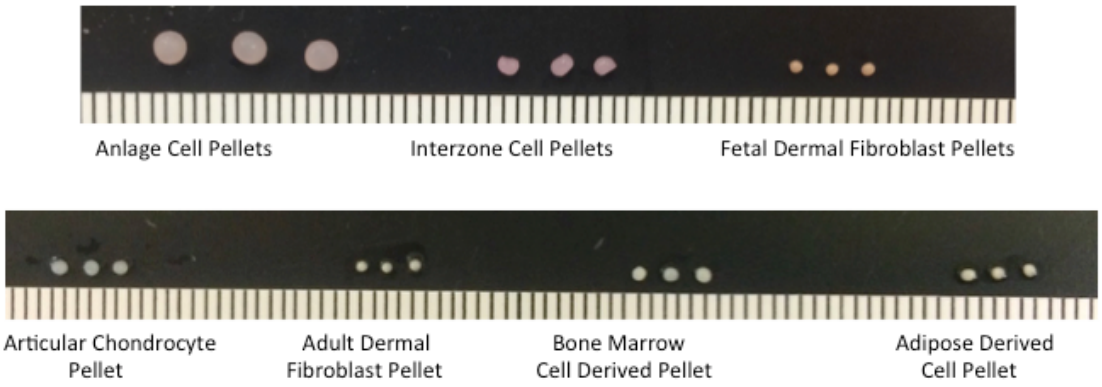

***Figure 3.2**. Pellet size relationships representative of different cell types. All pellets for generated from 5x10^5 cells and grown for 21 days in chondrogenic medium. The upper panel depicts fetus-derived cell pellets and the lower panel depicts adult-derived cell pellets. The scale in both panels is shown in millimeters.*

Morphological Description of Cell Pellets.

Figure 3.3 shows representative images of all the pellets described in this section over a range of magnifications. All adults derived cells and all fetal derived cells are from the same adult and fetus, respectively. All images are sized identically making direct size comparisons possible.

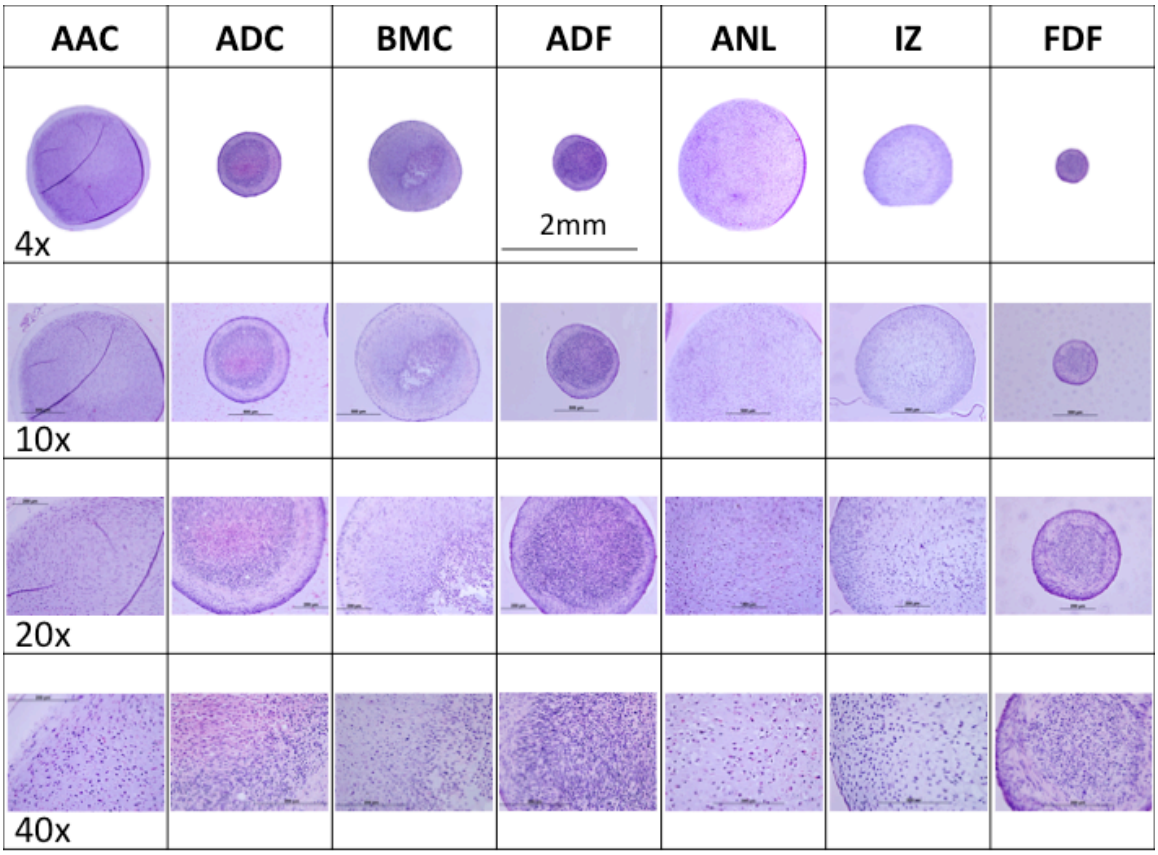

Figure 3.3. *Panel showing hematoxylin and eosin stained sections of pellets under different magnifications. All adult derived cells were from the same animal and all fetal derived cells from were the same animal. AAC – Adult Articular Chondrocytes, ADC – Adipose derived cells, BMC- Bone Marrow Derived Cells, ADF – Adult Dermal Fibroblasts, ANL- Fetal Anlagen Cells, IZ- Interzone Derived Cells, FDF – Fetal Dermal Fibroblasts. In the whole pellet image (4x) panels, the background pre-embedding matrix has been removed for image clarity.*

Adult Articular Chondrocyte Pellets (AAC): Pellets were composed of polygonal cells with minimal acidophilic cytoplasm and round to oval nuclei often within lacunae separated by moderate to marked amounts of lightly basophilic matrix. Cells along the outer rim were at a higher density with less matrix. Some pellets were composed of streams, 3-5 cell layers thick, of spindle cells along the outer rim. Variably sized, streaming tails of matrix with the previously described cells extended from the periphery of a few pellets. In addition, a thick rim of homogenous, acellular matrix circumferentially bordered some pellets of this cell type.

Adult Adipose Derived Cell Pellets (ADC): Pellets were composed of an outer, densely cellular rim of spindle cells approximately 3-6 cell layers thick. Spindle cells had minimal amounts of basophilic cytoplasm. Nuclei were round to oval and normochromic. A less dense proliferation of similar spindle cells continued to the center with acidophilic cytoplasm. Variably sized cores of necrotic cells and debris occupied pellet centers.

Adult Bone Marrow Derived Cell Pellets (BMC): Pellets were typically composed of an outer, moderately cellular rim of spindle and polygonal cells approximately 6-10 cell layers thick within a lightly eosinophilic to acidophilic matrix. Nuclei were round to oval and normochromic. Low to moderate numbers of cells exhibited lacuna. Pellets exhibited continued streams of spindle to polygonal cells throughout the pellet or contained central necrotic debris with admixed polygonal cells. A higher cell density characterized the center of most pellets.

Adult Dermal Fibroblast Pellets (ADF): Pellets were composed of an outer, densely cellular rim of spindle cells approximately 3-6 cell layers thick. The spindle cells had minimal amounts of basophilic cytoplasm. Nuclei were round to oval and normochromic. A less dense proliferation

of similar spindle cells continued to the center with acidophilic, sometimes fibrillar cytoplasm. Variably sized cores of necrotic cells and debris occupied the center of the pellet.

Fetal Anlage Chondroblast Pellets (ANL): Pellets were composed of polygonal cells with minimal acidophilic cytoplasm and round to oval nuclei often within lacunae separated by moderate to marked amounts of lightly basophilic matrix. Most often, cells were arranged in singlets or pairs. There was mild variation in cell size. Cells along the outer rim were at a higher density with less matrix. A few pellets had streams (2-4 cell layers thick) of spindle cells along the outer rim.

Fetal Interzone Cell Pellets (IZ): Pellets were composed of polygonal to spindle cells with minimal acidophilic cytoplasm and round to oval nuclei often within lacunae separated by low to marked amounts of lightly basophilic matrix. Cells along the outer rim were at a higher density with less matrix (3-7 cell layers thick). Variably sized cores of necrotic cells and debris occupied the center of the pellet.

Fetal Dermal Fibroblast Pellets (FDF): Pellets were composed of an outer, densely cellular rim of spindle cells approximately 1-3 cell layers thick. The spindle cells had minimal amounts of basophilic cytoplasm, with round to oval and normochromic nuclei. A less dense proliferation of similar spindle cells arranged more haphazardly continued to the center, with an acidophilic, sometimes fibrillar cytoplasm. Variably sized cores of what appears to be necrotic cells and debris occupied the center of the pellets.

Proteoglycan Staining:

All sections were accommodated in two sequential staining batches performed on the same day using aliquots of the same stain solutions. Control cartilage samples analyzed using ImageJ© from these two staining batches did not identify any significant differences or any effect of slide position within the 30-slide staining rack. Slide redness intensities were normalized to mean redness values from same-batch control sections. No significant inter-observer variation was found.

Figure 3.4 shows representative images of all the pellets stained with Safranin-O with a Fast Green background stain. These are sections from the same pellets depicted in Figure 3.3. Safranin-O stains proteoglycan a deep red color and displayed some variation between biological replicates, but also clear and consistent experimental group features. Absence of proteoglycan in a section results in a turquoise color from the Fast Green background stain.

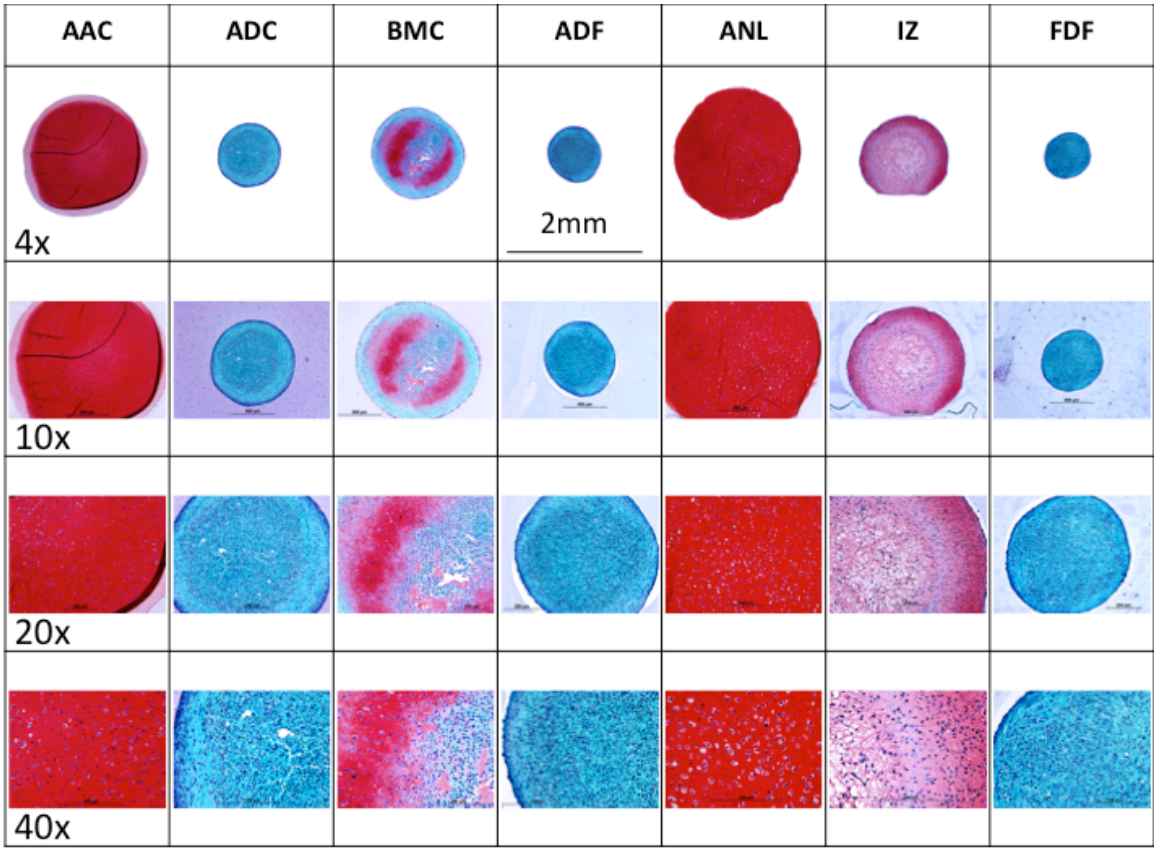

Figure 3.4. *Panel showing Safranin-O/Fast Green stained sections of the same set of pellets seen in Figure 3.3 pellets under different magnifications. AAC – Adult Articular Chondrocytes, ADC – Adipose derived cells, BMC- Bone Marrow Derived Cells, ADF – Adult Dermal Fibroblasts, ANL- Fetal Anlagen Cells, IZ- Interzone Derived Cells, FDF – Fetal Dermal Fibroblasts. In the whole pellet images (4x) panels the background pre-embedding matrix has been removed for image clarity.*

Neocartilage Assessment:

Pellets were evaluated histologically using the Bern scoring system previously developed for this purpose[143]. The semi-quantitative nature of the assessment allows for a maximum score of 9, which would indicate cell morphology and proteoglycan rich matrix elaboration similar to articular cartilage. The redness values calculated for the cross-sectional area of the pellet in each cell type as a pellet culture are shown in Figure 3.5. Table 3.3 shows the mean and standard deviation of the Bern scores generated for pellets of each cell type as assessed by three independent and blinded evaluators. Figure 3.6 displays the mean score of each individual pellet (mean of the three reviewer scores) as a single dot, reflecting variation between biological replicates.

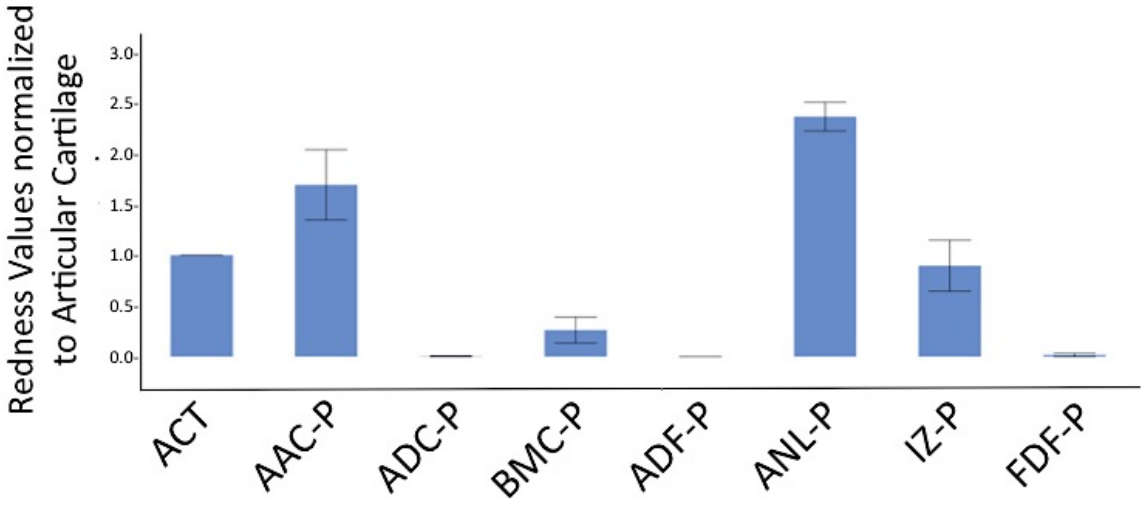

Figure 3.5 *Bar chart showing the redness value for the whole pellet section area normalized to articular cartilage sections cut from the same block and stained in the same batch. Standard error bars are shown.*

Cell Pellet Type	Average Group Bern Score ± SD
Articular Chondrocyte	7.26 ± 1.19
Adipose Derived Cell	1.69 ± 0.47
Bone Marrow Derived Cell	3.69 ± 2.01
Adult Dermal Fibroblast	1.24 ± 0.15
Anlage Chondroblast	8.60 ± 0.27
Interzone Cell	5.54 ± 1.21
Fetal Dermal Fibroblast	1.51 ± 0.66

Table 3.3. *Mean Bern scores for each experimental group. Data reflect the average score +/- the standard deviation from three independent and blinded assessments.*

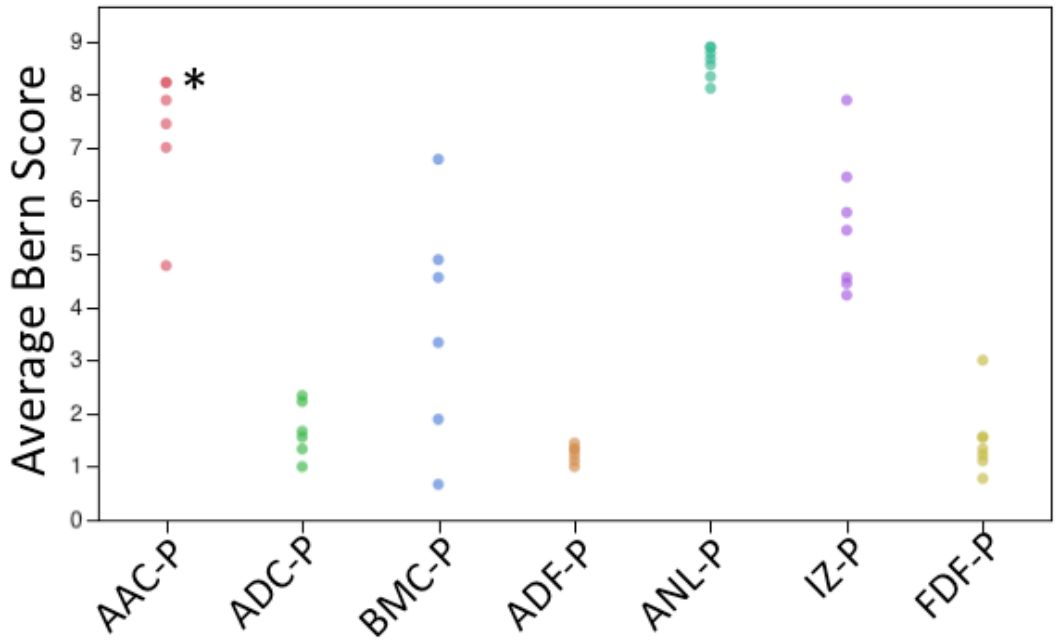

Figure 3.6. *Dot plots displaying the mean Bern scores for the biological replicates within each cell type. The asterisk* indicates two samples with identical Bern Scores, resulting in the dots being superimposed.*

Anlage chondroblast pellets generated the highest Bern scores with a range between 7.67 and 8.67 and a mean score of 8.60, reflecting a high level of consistency between biological replicates. Pellets generated from articular chondrocytes had a range of mean scores from 5 to 7.67 with an overall mean of 7.26 and similar consistency between biological replicates. In contrast, bone marrow and interzone derived cell pellets exhibited greater heterogeneity between individual pellets. Adipose derived cells, adult dermal cells, and fetal dermal cells generated consistently low scoring pellets under the chondrogenic induction protocol used in this study.

Gene Expression Analysis

All three TaqMan® primer probe sets generated high quality qPCR data with reaction efficiencies of 2.0 ± 0.2. The adult articular cartilage samples (n = 6) demonstrated some variation in Aggrecan core protein (*ACAN*) and Collagen type 2 (*COL2A1*) gene expression (reported below, Figures 3.8 and 3.9). An age matched control cartilage tissue sample was harvested and initially used as the calibrator gene for *COL2A1* and *ACAN* expression. However, the range of expression of the experimental articular cartilage samples was substantial and after consultation with a statistician the decision was made to use the average expression values of the experimental samples as the calibrator value (DCt) in the DDCt calculations of relative expression or relative quantitation (RQ). RQ values are depicted as box and whisker plots as these logarithmic values should be mathematically represented as bar graphs (no zero value) and calculating averages is inappropriate.

Aggrecan Core Protein Expression

Messenger RNA transcripts encoding aggrecan core protein (*ACAN*) were detected in all experimental samples, but in different amounts (Figures 3.7, 3.8 and Table 3.4). All monolayer cultures had significantly less relative quantities than pellets cultures ($p<0.001$; Table 3.5). Adult articular chondrocytes grown as a monolayer demonstrated significantly higher expression than other monolayer cultured cells, but relative steady state levels were not significantly different from ADF, FDF or ADC pellet cultures. These three cell types are no better than monolayer P3 chondrocytes in their expression of aggrecan core protein. Interestingly, in pellet culture, articular chondrocytes and anlage chondroblast cells consistently expressed *ACAN* at levels similar to or greater than articular cartilage calibrator samples. Bone marrow derived cell pellets and interzone cell pellets expressed *ACAN* at levels lower than articular cartilage tissue, but substantially higher than the monolayer cells.

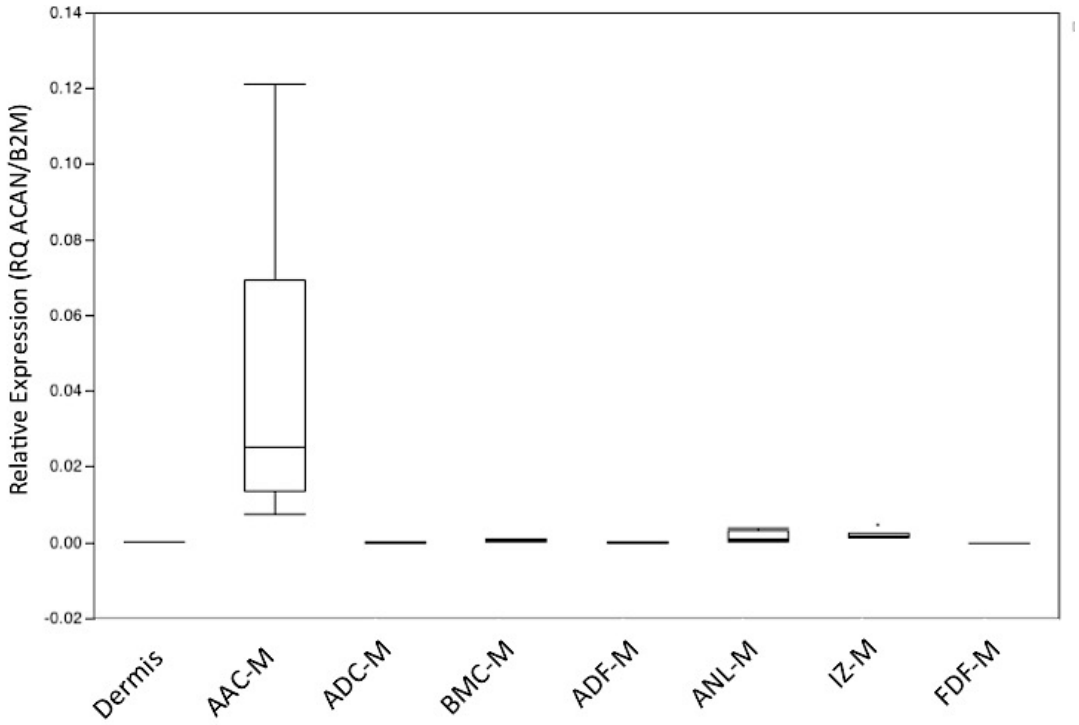

Figure 3.7. *Box and Whisker plot illustrating expression of ACAN mRNA in monolayer cell cultures relative to expression in adult articular cartilage (mean equal to 1.0, but not shown due to confines of the y-axis scale). Note the substantially lower steady state level of expression relative to pellet values reported in Figure 3.8).*

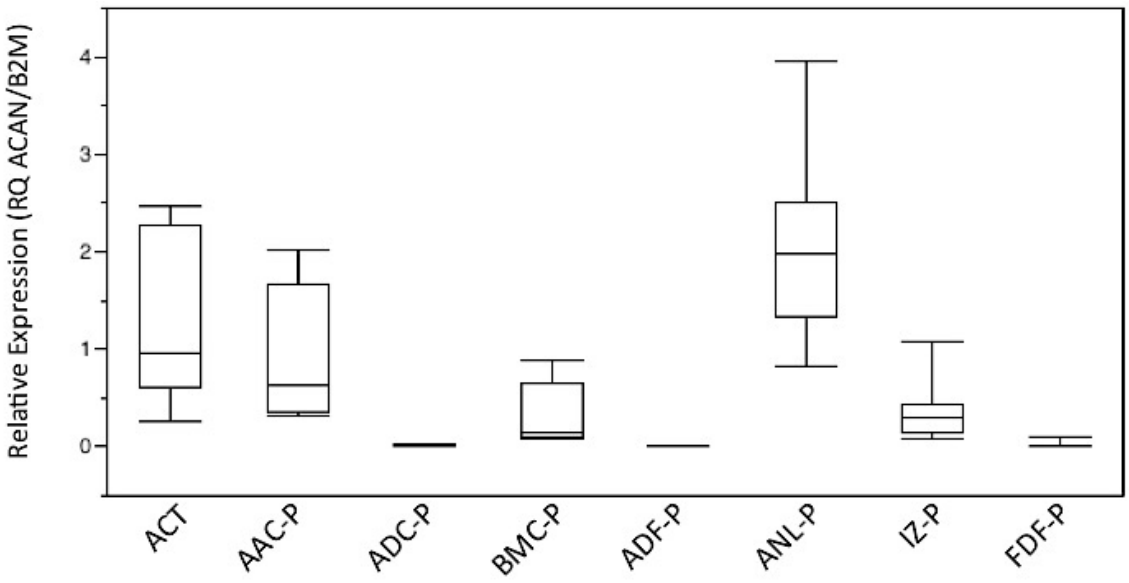

Figure 3.8. *Box and Whisker plot illustrating expression of ACAN in cell pellet cultures relative adult articular cartilage (ACT). Mean expression in ACT samples was set at 1.0. The average ΔCt of these samples was used for calibration of the other samples.*

Range of *ACAN* Relative Expression (RQ: *ACAN/B2M*)		
Tissue	**Lowest Relative Expression**	**Highest Relative Expression**
Dermis	0.00003	0.00003
ACT	0.26858	2.47662
AAC-M	0.00214	0.03378
ADC-M	0.00000	0.00004
BMC-M	0.00003	0.00027
ADF-M	0.00000	0.00006
ANL-M	0.00011	0.00105
IZ-M	0.00036	0.00127
FDF-M	0.00000	0.00000
AAC-P	0.32281	2.02092
ADC-P	0.00148	0.02398
BMC-P	0.07771	0.88282
ADF-P	0.00044	0.00396
ANL-P	0.82946	3.96198
IZ-P	0.09423	1.08863
FDF-P	0.00163	0.11392

***Table 3.4**. Table showing the range of ACAN Relative Expression values for each cell and tissue type tested.*

Cell type/culture conditions.	FDF-M	ADC-M	ADF-M	Dermis	BMC-M	ANL-M	IZ-M	ADF-P	FDF-P	ADC-P	AAC-M	BMC-P	IZ-P	AAC-P	ACT
ANL-P	3.34E-10	3.34E-10	3.34E-10	3.34E-10	3.34E-10	3.34E-10	3.34E-10	3.34E-10	3.34E-10	3.34E-10	3.34E-10	0.007095	0.033145	0.900966	0.997109
ACT	3.34E-10	3.34E-10	3.34E-10	3.34E-10	3.34E-10	3.34E-10	3.34E-10	3.34E-10	3.34E-10	3.37E-10	3.49E-10	0.275727	0.623428	1	
AAC-P	3.34E-10	3.34E-10	3.34E-10	3.34E-10	3.34E-10	3.34E-10	3.34E-10	3.34E-10	3.34E-10	3.79E-10	5.34E-10	0.655547	0.938043		
IZ-P	3.34E-10	3.34E-10	3.34E-10	3.34E-10	3.34E-10	3.34E-10	3.34E-10	3.34E-10	4.29E-10	2.44E-08	1.1E-07	0.999999			
BMC-P	3.34E-10	3.34E-10	3.34E-10	3.34E-10	3.34E-10	3.34E-10	3.34E-10	3.35E-10	7.93E-09	1.13E-06	4.63E-06				
AAC-M	3.34E-10	3.34E-10	3.34E-10	5.51E-10	4.01E-10	3.54E-06	0.000268	0.071377	0.997197	1					
ADC-P	3.34E-10	3.34E-10	3.34E-10	1.07E-09	6.31E-10	1.49E-05	0.000979	0.161597	0.999938						
FDF-P	3.34E-10	3.34E-10	3.34E-10	8E-09	4.43E-09	0.00024	0.012513	0.620252							
ADF-P	3.34E-10	3.74E-10	3.18E-08	4.42E-05	0.000192	0.423015	0.975674								
IZ-M	3.34E-10	8.04E-09	7.59E-06	0.00295	0.021944	0.999172									
ANL-M	3.34E-10	6.69E-07	0.000536	0.045699	0.31449										
BMC-M	3.37E-10	0.026081	0.790846	0.994404											
Dermis	3.54E-06	0.891707	1												
ADF-M	4.25E-08	0.907723													
ADC-M	0.000484														

***Table 3.5** – p-values of differences in ACAN gene expression as assessed by relative steady-state mRNA levels among different cell type and culture conditions. Significant differences are depicted by pink shading (p<0.05 – Tukey's post hoc correction).*

***COL2A1* expression**

Expression of *COL2A1* was observed in all experimental reaction wells, but the relative quantities of steady state mRNA varied enormously (Table 3.6). All cells in monolayer culture showed negligible expression of *COL2A1* as expected (Figure 3.9). Anlage cell pellets synthesized significantly more *COL2A1* than pellet or monolayer cultures from any other cells type ($p<0.05$; Table 3.7, Figures 3.9 and 3.10). However, pellet cultures from anlage, adult articular cartilage, bone marrow, and interzone cells were not different from native articular cartilage tissue (ACT).

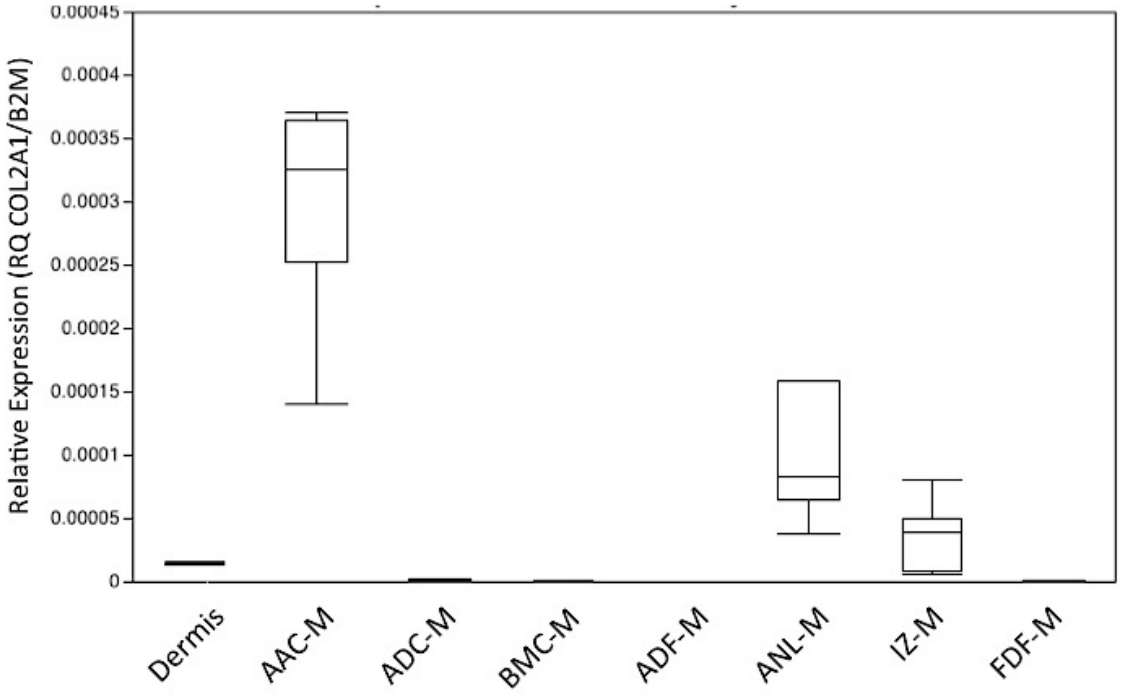

***Figure 3.9**. Box and Whisker plot illustrating expression of COL2A1 mRNA in dermis and monolayer cell cultures relative to expression in adult articular cartilage (mean equal to 1.0, but not shown due to confines of the y-axis scale) and dermis. Note the substantially lower steady state level of expression relative to pellet values reported in Figure 3.10).*

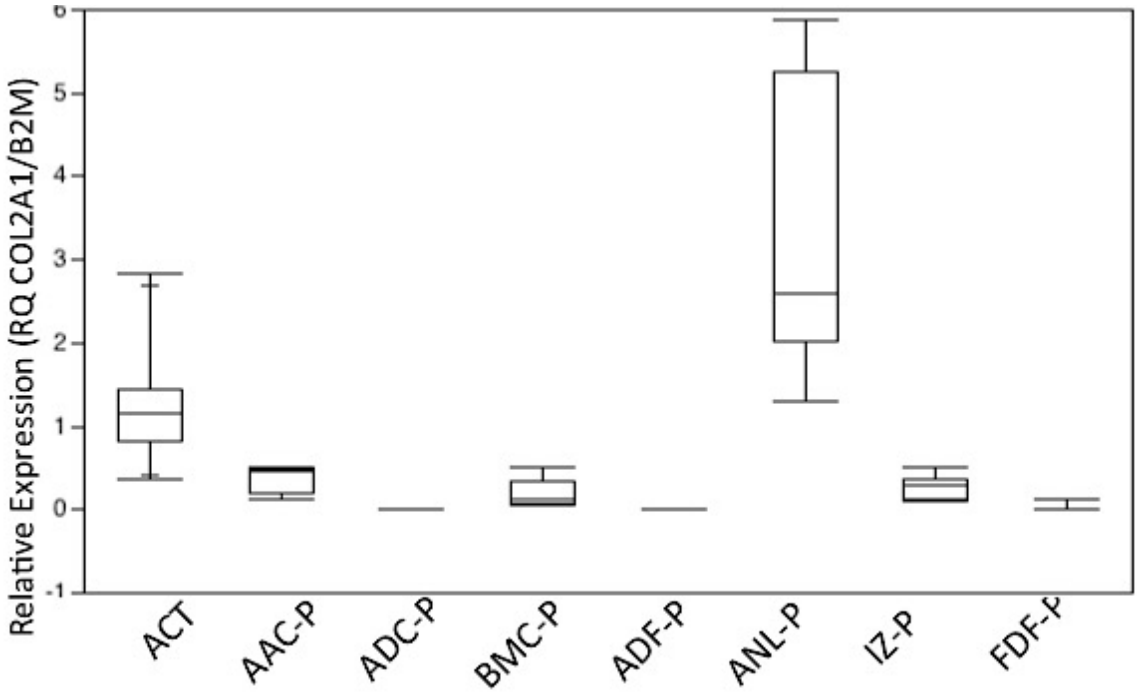

Figure 3.10. *Box and whisker plot of relative expression of COL2A1 in cell pellet cultures relative to adult articular cartilage (ACT) and dermis. COL2A1 relative expression was calibrated to average expression in the articular cartilage samples from the 6 experimental adult horses.*

Range of *COL2A1* Expression (RQ *COL2A1/B2M*)		
Tissue	**Lowest Relative Expression**	**Highest Relative Expression**
Dermis	0.00001	0.00002
ACT	0.37372	2.82778
AAC-M	0.00014	0.00037
ADC-M	0.00000	0.00000
BMC-M	0.00000	0.00000
ADF-M	0.00000	0.00000
ANL-M	0.00004	0.00040
IZ-M	0.00001	0.00008
FDF-M	0.00000	0.00000
AAC-P	0.13723	0.51002
ADC-P	0.00002	0.00401
BMC-P	0.04924	0.51763
ADF-P	0.00000	0.00028
ANL-P	1.30426	5.87503
IZ-P	0.09910	0.50106
FDF-P	0.00003	0.13764

Table 3.6. *Table showing the range of COL2A1 Relative Expression values for each cell and tissue type tested.*

Cell type/culture conditions col2a1	ADF-M	ADC-M	BMC-M	FDF-M	Dermis	IZ-M	ADF-P	ANL-M	AAC-M	ADC-P	FDF-P	BMC-P	IZ-P	AAC-P	ACT
ANL-P	3.34E-10	3.34E-10	3.34E-10	3.34E-10	3.34E-10	3.34E-10	3.34E-10	3.34E-10	3.34E-10	3.34E-10	3.34E-10	0.004149	0.028185	0.14696	0.970108
ACT	3.34E-10	3.34E-10	3.34E-10	3.34E-10	3.34E-10	3.34E-10	3.34E-10	3.34E-10	3.34E-10	3.34E-10	3.34E-10	0.376794	0.807031	0.979889	
AAC-P	3.34E-10	3.34E-10	3.34E-10	3.34E-10	3.34E-10	3.34E-10	3.34E-10	3.34E-10	3.35E-10	3.35E-10	4.52E-10	0.998504	1		
IZ-P	3.34E-10	3.34E-10	3.34E-10	3.34E-10	3.34E-10	3.34E-10	3.34E-10	3.34E-10	3.35E-10	3.35E-10	5.59E-10	0.999995			
BMC-P	3.34E-10	3.34E-10	3.34E-10	3.34E-10	3.34E-10	3.34E-10	3.34E-10	3.34E-10	4.27E-10	4.71E-10	2.79E-08				
FDF-P	3.34E-10	3.34E-10	3.34E-10	3.34E-10	0.001027	9.21E-05	0.005992	0.135724	0.968537	0.981046					
ADC-P	3.34E-10	3.46E-10	5.45E-10	9.09E-10	0.067504	0.037303	0.394846	0.973856	1						
AAC-M	3.34E-10	3.52E-10	6.43E-10	1.19E-09	0.081094	0.047965	0.451602	0.984613							
ANL-M	3.34E-10	2.79E-09	5.48E-08	1.78E-07	0.647456	0.707117	0.998075								
ADF-P	3.34E-10	9.86E-07	2.3E-05	8.47E-05	0.995617	0.999915									
IZ-M	3.34E-10	1.54E-05	0.000372	0.001399	1										
Dermis	1.99E-08	0.009378	0.082219	0.190374											
FDF-M	3.77E-05	0.972845	1												
BMC-M	0.000635	0.999706													
ADC-M	0.040813														

Table 3.7. *Table showing* p*-values of differences in COL2A1 gene expression as assessed by relative steady-state mRNA levels among different cell type and culture conditions. Significant differences are depicted by pink shading (p<0.05 – Tukey's post hoc correction).*

COL1A1 expression

Expression of *COL1A1* was variable across the samples tested (Figure 3.11, Table 3.8), but with relatively high levels in both monolayer and pellet cultures. Native articular cartilage normally expresses very low levels of *COL1A1* and, as expected, steady state *COL1A1* mRNA levels were consistently negligible in these experiments. Bone marrow cells in monolayer and pellet cultures displayed variable levels of *COL1A1* mRNA across biological replicates, as did adipose derived cell pellets and interzone pellets. In comparison, anlage pellets expressed more consistent and lower levels of *COL1A1,* exhibiting significant differences with several groups (Table 3.9). Interzone pellets exhibited a wide range of relative expression values. This can be an important metric as *COL1A1* expression is considered an indicator of fibrocartilage deposition.

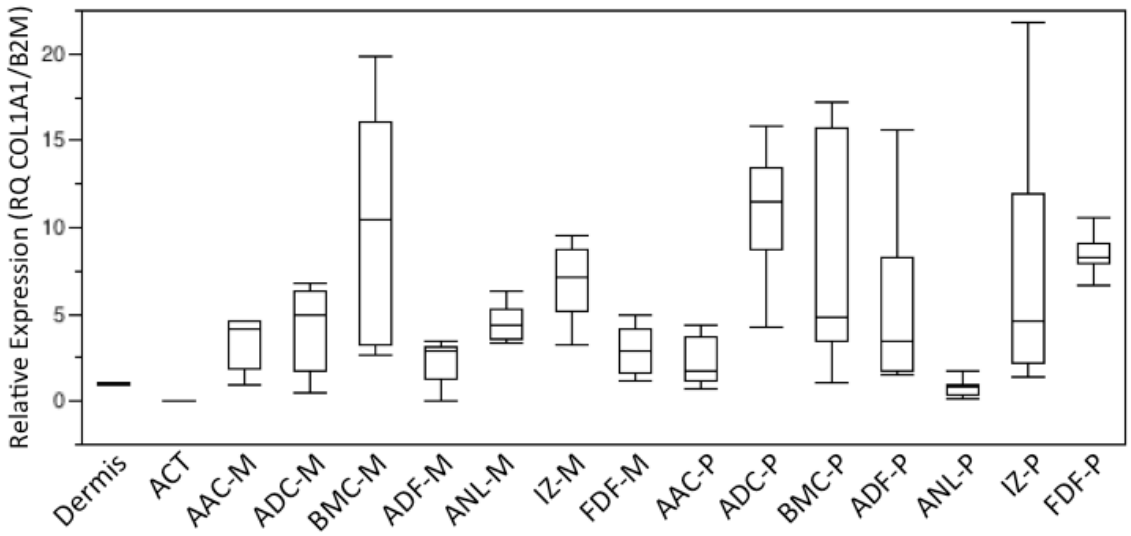

Figure 3.11. *Box and Whisker plot illustrating expression of COL1A1 in monolayer and pellet cell cultures relative to dermal tissue. Mean expression in dermis is set at 1.0, which was used as the calibrator gene for COL1A1.*

Range of *COL1A1* Expression (RQ: *COL1A1/B2M*)		
Tissue	**Lowest Relative Expression**	**Highest Relative Expression**
Dermis	0.67609	0.80730
ACT	0.00294	0.04577
AAC-M	0.96042	4.62356
ADC-M	0.43137	6.79531
BMC-M	2.64256	19.87737
ADF-M	0.05067	3.41272
ANL-M	3.37476	6.36278
IZ-M	3.25671	9.54588
FDF-M	1.22528	4.94411
AAC-P	0.65760	4.34085
ADC-P	4.21812	15.82401
BMC-P	1.04023	17.27484
ADF-P	1.48322	15.61235
ANL-P	0.10219	1.77019
IZ-P	1.40046	21.77171
FDF-P	6.72414	10.55242

Table 3.8. *Table showing the range of COL1A1 Relative Expression values fro each cell and tissue type tested. P*

Cell type/culture conditions.	ACT	ANL-P	Dermis	ADF-M	AAC-P	FDF-P	AAC-M	ADC-M	ADF-P	ANL-M	IZ-P	BMC-P	IZ-M	BMC-M	FDF-P
ADC-P	3.3416E-10	3.96E-06	0.01322	0.007028	0.045881	0.221603	0.433064	0.531118	0.753133	0.899992	0.966825	0.995202	0.999812	1	1
FDF-P	3.3416E-10	9.75E-06	0.029601	0.01784	0.105188	0.418569	0.678135	0.764467	0.927432	0.986156	0.998048	0.999929	1	1	
BMC-M	3.3416E-10	4.05E-05	0.049693	0.037998	0.180374	0.569314	0.798899	0.85926	0.968599	0.996029	0.999624	0.999992	1		
IZ-M	3.3416E-10	9.26E-05	0.096297	0.081758	0.330775	0.793204	0.941612	0.965409	0.997374	0.999936	0.999999	1			
BMC-P	3.3416E-10	0.000876	0.228137	0.250224	0.643608	0.965137	0.995675	0.997821	0.999978	1	1				
IZ-P	3.3416E-10	0.001093	0.292562	0.324729	0.749923	0.988892	0.999304	0.9997	1	1					
ANL-M	3.3416E-10	0.002712	0.412099	0.482449	0.879539	0.998567	0.999968	0.999988	1						
ADF-P	3.3416E-10	0.016629	0.658869	0.786002	0.984523	0.999994	1	1							
ADC-M	3.3446E-10	0.100191	0.89679	0.973728	0.999816	1	1								
AAC-M	3.3419E-10	0.067655	0.87905	0.964625	0.999746	1									
FDF-M	3.3418E-10	0.097068	0.938902	0.989969	0.999991										
AAC-P	3.3777E-10	0.558154	0.999436	1											
ADF-M	3.9098E-10	0.920219	1												
Dermis	8.9174E-07	0.999969													
ANL-P	4.0233E-08														

Table 3.9. *p-values of differences in COL1A1 gene expression as assessed by relative steady-state mRNA levels among different cell type and culture conditions. Significant differences are depicted by pink shading (p<0.05 – Tukey's post hoc correction).*

Discussion

The data presented in this chapter support the hypothesis that the interzone cell is a superior cell type for generating cartilage under these standard chondrogenic induction conditions, than either adult bone marrow derived cells or adipose derived cells. As such, the hypothesis is not rejected. The interzone cell pellets had a zonal appearance to their cross section. The peripheral zone showed moderate staining for a proteoglycan-laden matrix, but was not as densely stained as that in the anlage pellets or many of the adult articular chondrocyte pellets. The central area of interzone pellets exhibited a reticular pattern without any proteoglycan stain uptake and limited cellularity. The possible reasons for this could be that the center of the pellet is undergoing necrosis and the nuclei were lost in processing, or that the area has altered cell function and some kind of fluid or loose matrix that was lost during processing. The reticulate pattern could therefore be an artifact. A zonal architecture to neocartilage pellets has been previously documented in the literature for chondrocytes, but to our knowledge, this is the first report of neocartilage generated from interzone cells[121]. The interzone pellets did, however, demonstrate significant *COL1A1* expression. This has been documented in neocartilage derived from many different cell types including articular chondrocytes, bone marrow derived cells, and adipose derived cells[121,138,147]. In all cases it has been considered highly undesirable as the presence of type I collagen is a hallmark of biomechanically inferior fibrocartilage and not articular cartilage. A recent study comparing human bone marrow derived cells, adipose derived cell, articular chondrocytes and nasal septum chondrocytes reports interesting findings regarding collagen type I and type II expression among these tissues[28]. Their study used a polyspun nanofiber matrix for cell culture so direct comparison to the current data should be made with caution. However, they found that both mesenchymal cell types (bone marrow

derived and adipose derived cells) showed similar expression levels of collagens type I and type II, and that the proportions relative to one another changed little over the culture period. They reported that over the culture period (21 days) both types of induced chondrocyte expressed relatively more collagen type II to collagen type I. The neocartilage was not evaluated histologically for regional localization of gene expression in the study, other than a qualitative assessment of glycosaminoglycan (GAG) synthesis using Alcian Blue. However, there appeared to be a visual difference between the amount of Alcian blue staining in the images shown between the chondrocyte origin pellets and the mesenchymal cell origin pellets, with the former showing more GAG staining.

For the evaluation of neocartilage in the current experiments, we found both the semi-quantitative Safranin-O staining technique (redness value) and the Bern scoring system to be useful. Anlage chondroblast pellets consistently achieved high Bern Scores. Morphological characteristics and gross matrix architecture displayed similarities to native cartilage such as lacunae occupied by single cells, cells being spaced apart with proteoglycan rich matrix between them, and the pellet being quite homogeneous and devoid of a 'necrotic' center. The absence of a necrotic center is of particular interest as it suggests that the central cells in these large pellets may be adapted to a lower oxygen tension[9,148]. This characteristic is considered an important feature of chondrocytes that typically exist in low oxygen tensions, between 1% and 10% depending on the distance from the articular surface[8]. Chondrocytes exist in a physiologic hypoxia, a condition that has been termed *physoxia*[9,148].

Bone marrow derived stem cells displayed an interesting range of chondrogenic potential, as evidenced by variable proteoglycan deposition leading to a wide range of Bern Scores. Figure 3.13 shows representative images from all of the bone marrow derived cell pellets generated.

There are interesting zonal and regional areas of intense proteoglycan deposition and cell morphology akin to articular cartilage, but other regions in the same pellets ` where chondrogenesis did not occur. These findings have not been reported in the literature. In the panels for pellets *BMC EQA1502* and *BMC EQA5107* there is an edge effect where the pellet developed a flat edge presumably upon which it rested during culture. Near this flattened side an area of proteoglycan synthesis can be seen. This could be a result of coincidence, a result of hydrostatic forces, and/or a function of oxygen tension in that region of the pellet against. Culture in normal ambient oxygen concentrations (~21%) represents extreme hyperoxia for chondrocytes [2,9,89,148-151] and may not be optimal for chondrogenic induction.

Recent work by Cote, *et al*. discusses the variation in cells derived from bone marrow aspirates[152]. Indeed, this study demonstrated marked differences in chondrogenic ability among clonal colonies from the same donors. Their goal was to pre-select suitable clones for more efficacious chondrogenesis from bone marrow aspirates. The authors demonstrated significant variation in the ability of different cells obtained from the same bone marrow aspirate to generate neocartilage under pellet culture in chondrogenic induction medium. It is possible that my current results reflect this phenomenon. It has also been reported that cell pellets from mixed animal sources do not survive well in pellet culture, but the reason for this is unknown[121]. As such there may be more cell-cell interactions influencing cellular differentiation pathways in bone marrow derived cells than generally realized. Given the current interest in and use of bone marrow derived cells clinically, these would be valuable hypotheses to test.

Our data indicate that adipose derived cells have very limited chondrogenic differentiation potential under the conditions of this study. These findings differ from other reports in the literature[33,37,42,44,153], which may be related to culture conditions differences. For example, many studies cultured cells in a hydrogel or collagen matrix. Additionally, the chondrogenic induction

medium recipes are not uniform. Some groups used varying amounts of FBS in the medium. At the onset of this project, medium with FBS supplementation was evaluated. Compared to FBS-free medium, which is also well represented in the literature, pellets grown in the presence of FBS were friable and did not generate as much matrix (data not shown). These variables must be taken into consideration when comparing the results from multiple studies.

During the collection of tissue for the development of primary adipose cell lines, we experienced a situation that may also represent an important source of variation. The technique employed to process the adipose tissue is commonly used and has been reported multiple times[33,42,44,132,154]. In earlier adipose tissue collections from donors not used in the current study, colonies of morphologically diverse cells adhering to the culture flask were observed. The majority of cells were spindle shaped, but the cells in a few colonies displayed a more cuboidal shape. The concern was the potential for fibroblast contamination resulting from the admixed fibrous tissue in the adipose sample. During the next adipose tissue collection, all the visible connective tissue from the adipose samples was meticulously trimmed. However, this culture failed to yield any adherent cells and was discarded after 14 days. For the current sample set, we carefully trimmed only moderate to large connective tissue planes from the adipose tissue that had been collected. This yielded mixed cell populations where the majority of cells were spindle shaped, consistent with what has been reported by others[33,42,132,153]. Taken together, it is possible that so-called adipose derived stem cell preparations often include at least some contribution of cells derived from fibrous tissue. Interestingly, these cell preparations were initially termed the "adipose derived stromal fraction" [37]

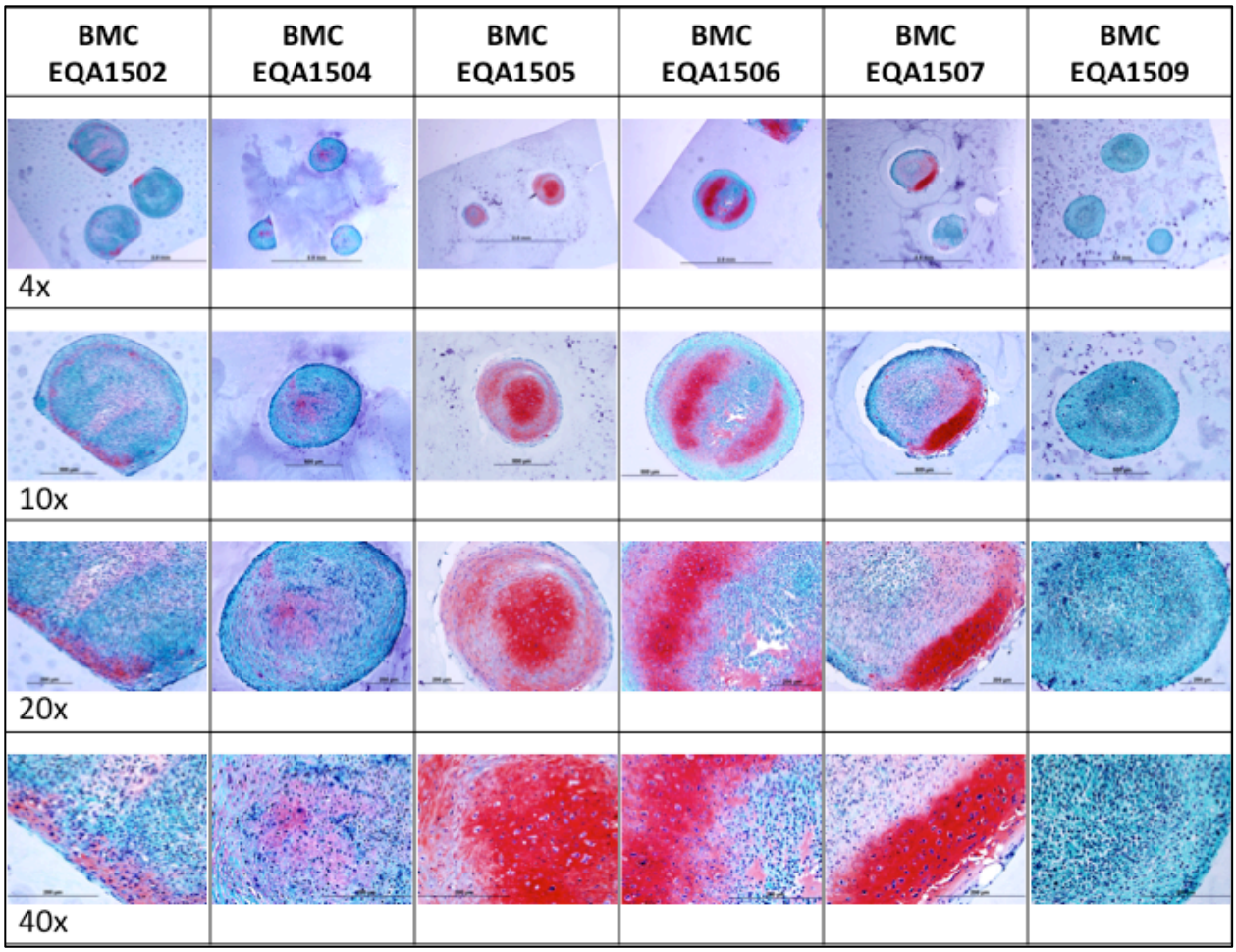

***Figure 3.12**. Panel showing photomicrographs of cell pellets from all six bone biological replicates at various magnifications. All of the images shown are from sections stained with Safranin-O. The images are taken to enable direct comparison across different samples.*

Bone marrow- and adipose-derived cells were harvested using well documented techniques currently used in research and clinical applications[47,121,153]. Typically these cells are considered to be mesenchymal stems cells and termed bone marrow stem cells and adipose derived stem cells respectively. Mesenchymal stem cells are defined as multipotent adult stem cells capable of differentiating into mesodermal tissue such as cartilage, bone and fat, so-called tri-lineage differentiation potential. In humans, the presence or absence of specific surface markers, adherence to plastic in culture, and tri-lineage differentiation potential are used as criteria for

'stem-ness'[9]. Presently, there is a lack of complete uniformity between equine and human mesenchymal stem cell surface markers[39,40].

In earlier studies using equine bone marrow derived and adipose derived cells, tri-lineage differentiation was performed. Basically cells were grown in relevant induction medium and osteoblastic, chondrogenic and adipogenic characteristics were assessed. These studies are based on limited output metrics that are not standardized, including the deposition of alkaline phosphatase rich substrate for osteogenesis, synthesis of proteoglycan rich matrix for chondrogenesis, and the accumulation of intracytoplasmic lipid droplets for adipogenesis. From a gene expression perspective, demonstrating expression of Ostepontin (*SPP1*) and Osteocalcin (*BGLAP*) in induced osteocytes, *COL2A1* and *ACAN* in induced chondrocytes, and Fatty Acid Binding Protein 4 (*FABP4*) in adipocytes have been used[39,133]. Tri-lineage differentiation potential was not assessed in this study. The cell isolation methods used, however, are consistent with techniques used in equine clinical practice for orthopedic disease.

Of the cell types compared in the current study, the data suggest that anlage chondrocytes may have the highest chondrogenic potential. In normal development, anlage chondrocytes can be termed 'transient chondrocytes', since they progress through hypertrophic differentiation and apoptosis to be replaced by bone in the process of endochondral ossification[155]. The process of hypertrophic differentiation must be considered when evaluating chondrogenesis *in vitro*. The relative contributions and importance of such variables as oxygen tension, growth *milieu,* and/or intrinsic (biological) programming of the cell are not well defined. Obviously characteristics of hypertrophic differentiation are both qualitative and quantitative in terms of gene expression. Hypertrophic chondrocytes express little ACAN, significant collagen type X and undergo morphologic changes including cellular hypertrophy. Anlage chondrocytes in the current study

expressed large amounts of *ACAN*, but on histologic examination revealed themselves as large cells in large lacunae, with occasional stacking of cell lacunae. An assessment of *COL10* expression or evidence of extracellular matrix mineralization represents an opportunity for further investigation of these very interesting cells.

Our qPCR data showed significant differences in ACAN expression between cartilage shavings taken from similarly bred and age-matched young adult horses that were managed under the same conditions. Cartilage was only shaved from the femoro-tibial joint and the edges of the joint surfaces were avoided. A limitation of the protocol used, however, is that the articular cartilage shavings should have been pooled from each individual horse, and then randomly divide it into the storage containers. Instead shavings from one part of the joint were harvested, stored and used for either isolation of RNA or chondrocytes. We believe this is potential source of the variation may have contributed to baseline articular cartilage gene expression levels between biological replicates. Heterogeneity of articular chondrocytes both in terms of depth within the cartilage[8] and across the articular surface may be areas to consider in optimizing cell selection for ACT.

Further studies on a transcriptome level, as well as an assessment of regional localization of gene expression patterns will extend these cell type comparisons and help determine their capacity to achieve the cellular phenotype of normal articular chondrocytes.

Chapter 4

Reflections and Looking Ahead to Future Studies

Reflections.

Research efforts in this dissertation were aimed at examining the unique tissue-restricted pattern of gene expression of articular cartilage. The specific objectives were to compare the mRNA transcriptome of adult articular cartilage with five other cartilage tissues (adult nasal septum, neonatal articular cartilage, neonatal epiphyseal cartilage, fetal interzone-rich tissue, and the adjacent fetal anlage tissue). The second objective was to identify unique tissue-restricted mRNA transcripts and splice junctions that are unique to adult articular cartilage.

My data has a great deal more depth to be explored. The progress of analyzing this data set was certainly hampered by my initial lack of computational skills and limitations related to annotation of the equine genome. Both of these components are steadily improving. With hind sight and the ever-present mindset of a clinician, I would have preferred cartilage repair tissue as one of our comparison groups. Since this tissue is hard to obtain and usually present in such tiny quantities analysis is challenging and often requires linear amplification of the isolated RNA. That said, data presented here are a substantial resource for us and other research groups in the field of articular cartilage and those interested in computational biology.

The tissues that made up this study set are the envy of many research institutes. We are incredibly fortunate here at the University of Kentucky to be able to obtain such sample sets in relatively short time frames from horses on our university farm or by local donations. The expense, effort and horses' lives that contributed to these data will be shared by researchers world-wide.

A portion of this study was discovery science. However, the unique nature and scope of RNA-seq data is so vast that it can be accessed and mined remotely for future hypothesis driven projects by us and other groups. As such, RNA-seq data can make an impactful contribution to science. The ability to share datasets also addresses important ethical considerations when conducting research involving experimental animals – the three R's of animal research – replace, reduce, and refine. By accessing quality data with reliably reported metadata the redundant use of more animals can be avoided.

The work presented in Chapter 3 is an interesting exploration of techniques currently used in veterinary medicine and utilizes concepts from basic science research. Adult mesenchymal cells are used frequently in clinical applications and sometimes promoted as a panacea for musculoskeletal disease. With emerging interest in tissues from synovial joint development, I wanted to challenge these cells types under chondrogenic conditions. The standard chondrogenic conditions that were used are well represented in the literature. In this study they were employed to compare the chondrogenic differentiation potential of adult and fetal cell types. In performing this study, I observed that cells currently being used in clinical practice, under these conditions, are little better than dermal fibroblasts in their chondrogenic ability. This kind of science is important to convey to veterinary and human medical colleagues. As a group of medical professionals and scientists we must strive to use the best medicine, and in this arena the 'one medicine' concept applies and can help to avoid unnecessary patient morbidity and false hope. The private enterprise nature of clinical veterinary medicine and 'off label use' of medications lends itself to cognitive dissonance and eschewing evidence based medicine. Hypothesis driven research is a critically important factor in both human and

veterinary health science progress. Honoring the rigor of scientific study before clinical application must be a priority.

Future Directons

The wealth of data that exists in the RNA-seq data from Chapter 2 has many possibilities to follow. Firstly, we recognize that the lists of gene sets are uncorrected and as yet not challenged in the lab as a 'cartilage signature'. Within reach, an immediate goal to assist bench top research would be to generate an expression cassette with a technology such as NanoString®. This technology can generate custom designed bar-coded probes that will interrogate an RNA sample at both a qualitative and quantitative level. In designing such a cassette, the hypothesis that these genes will reliably distinguish normal adult articular cartilage from other cartilages could be tested. This may seem redundant given the ever-decreasing cost of sequencing. However, it may result in a rapid lab-based platform that is more accessible for some researchers.

An additional aspect that requires work is to further examine the ASM data. These data have the capability to revolutionize the design of tissue-specific biomarker probes, making them both sensitive and specific. The ASM list generated here had conservative thresholds, but it is possible to uncover and test even more ASM possibilities if we relaxed the thresholds.

Finally, the elephant in the room is the difficulty we have with these huge data sets. My mentor eloquently describes as a problem of 'reductionism'. Our scientific training and molecular biology capabilities so far have driven us to reduce, reduce, reduce. Without the need to reduce, we would be released from the slavery of processing the data so intensely. If we could see global gene expression patterns as signatures rather than reducing the data down to lists or

loci, we would have a powerful tool indeed. As a horse person, I intuitively perform pattern recognition subconsciously, by thin slicing. I don't have to measure the size of hoof, angle of the neck, position of the eye etc. to distinguish a Warmblood horse from a Thoroughbred, or an Arabian from a Saddlebred. I can look at the horse and be right nearly every time because of years at looking at these beautiful creatures. I recognize the pattern. If this could become a reality in computational biology, we would capture and utilize far more information, hopefully in a more consumer –friendly fashion.

In Chapter 3, it was interesting to see how, under these experimental conditions, adult mesenchymal derived cells showed little chondrogenic potential. The generation of neocartilage is a significant area in the field of cartilage research with much focus on matrix assisted differentiation[2,9,89,148-151]. The conditions used here were designed to be 'state of the art' and a platform for direct comparison of cell lines. However, testing hypotheses relating to oxygen tension and the growth of these cells types will be important to further our understanding of their cell biology.

The two fetal cell lines we examined are of particular interest and warrant further investigation as single cell cultures or possibly as co-mixed cell cultures. The anlagen cells appear to have great chondrogenic potential, but it will important for us to determine if that reflects a hypertrophic phenotype or an articular phenotype. In the near term, a lab colleague is pursuing Collagen type X immunostaining on these pellets. The presence and distribution of this biomarker of hypertrophic cartilage will be valuable and may reflect their intrinsic programing or culture medium signaling, both of which would warrant further investigation. Equally interesting would be to examine the distribution of Collagen type I and II across these pellets sections. The

distribution of either of these collagens would add useful information as to how best to optimize *in vitro* chondrogenesis.

During this project, RNA was extracted from all of the cell monolayers and pellets for RNA-sequencing. Additionally, RNA from interzone rich tissue and anlage tissue from these paired samples was sequenced. One hundred and ten samples were submitted for RNA-sequencing as described in Chapter 3 (Table 4.1). The samples yielded excellent quality RNA, even though quantities were very limited in some cases. One hundred base pair, strand-specific paired end reads have been generated. The entire data set was recently downloaded from the University of Illinois website to that of the University of Kentucky. It consisted of a total of 3,822,948,968 paired reads. The average number of reads per sample was 34,754,082 (range: 23,904,800 - 47,003,966). These data will provide some of the answers that have been asked about what Collagen type is expressed and at what level. Since the starting RNA for the qPCR in Chapter 3 and this sample set (barring the fetal tissue samples) was the same, it will be interesting to compare the performance of the qPCR data with the RNA-sequencing data.

Tissue Description		Number of samples
Fetuses 45- 46 days of gestation. (Derived from 7 biological replicates)	Fetal Interzone Rich Tissue	7
	Fetal Anlage Tissue	6
	Monolayer Interzone Cells	7
	Monolayer Fetal Dermal Fibroblasts	7
	Monolayer Anlage Chondrocytes	7
	Proximal Interzone Cell Pellets	7
	Fetal dermal Fibroblast Pellets	7
	Anlage Chondrocyte Pellets	7
Derived from young adult horses aged 15.5-18 months of old. (7 biological replicates)	Monolayer Adult Articular Chondrocytes	6
	Monolayer Dermal Fibroblasts	6
	Monolayer Bone Marrow Derived Cells	6
	Monolayer Adipose Derived Cells	5
	Adult Articular Chondrocyte Pellets	6
	Dermal Fibroblast Pellets	6
	Bone Marrow Derived Cell Pellets	6
	Adipose Derived Cell Pellets	6
	Native Articular Cartilage Tissue	7
	Dermis Tissue	1
Total Number of Tissues Submitted		**110**

Table 4.1. *Sample set submitted for RNA-sequencing that corresponds to work performed in Chapter 3.*

In summary, this thesis was a segment of the continuum that is the research community's collective journey to understand cartilage biology and augment its repair. Data driven discovery science is revolutionizing our view of gene expression. I sincerely hope that these data help us, and others in this field, to make meaningful progress on that journey and provide translatable science for clinical application.

References

1. Silver I, Maroudis A: Measurement of pH and Ionic Composition of Pericellular Sites. Philosophical Proceedings of the Royal Society, Biological Series- B 271:261-271, 1975.
2. Zhou S, Cui Z, Urban JP: Factors influencing the oxygen concentration gradient from the synovial surface of articular cartilage to the cartilage-bone interface: a modeling study. Arthritis Rheum 50:3915-3924, 2004.
3. Hunziker E, Studer M: Ultrastructure of adult human articular cartilage matrix after cryotechnical processing. Microscopy Research and Technique 37:271-284, 1997.
4. Sophia Fox A, Bedi A, Rodeo S: The basic science of articular cartilage: structure, composition, and function. Sports Health 1:461-468, 2009.
5. McIlwraith CW, Frisbie DD, Kawcak CE: The horse as a model of naturally occurring osteoarthritis. Bone and Joint Research 1:297-309, 2012.
6. Benninghoff A: Form und Bau der Gelenknorpel in ihren Beziehungen zur Funktion [Form and structure of hyaline cartialge in relation to function]. Zeit Zelforsch Mikroscop Anat 2:783-862, 1925.
7. Guilak F, Alexopoulos LG, Upton ML, et al: The Pericellular Matrix as a Transducer of Biomechanical and Biochemical Signals in Articular Cartilage. Annals of the New York Academy of Sciences 1068:498-512, 2006.
8. Jadin KD, Wong BL, Bae WC, et al: Depth-varying Density and Organization of Chondrocytes in Immature and Mature Bovine Articular Cartilage Assessed by 3D Imaging and Analysis. Journal of Histochemistry & Cytochemistry 53:1109-1119, 2005.
9. Demoor M, Ollitrault D, Gomez-Leduc T, et al: Cartilage tissue engineering: Molecular control of chondrocyte differentiation for proper cartilage matrix reconstruction. Biochimica Et Biophysica Acta-General Subjects 1840:2414-2440, 2014.
10. Freyria AM, Mallein-Gerin F: Chondrocytes or adult stem cells for cartilage repair: the indisputable role of growth factors. Injury 43:259-265, 2012.
11. Loeser RF: Aging and osteoarthritis: the role of chondrocyte senescence and aging changes in the cartilage matrix. Osteoarthritis Cartilage 17:971-979, 2009.
12. Helmick CG, Felson DT, Lawrence RC, et al: Estimates of the prevalence of arthritis and other rheumatic conditions in the United States: Part I. Arthritis & Rheumatism 58:15-25, 2008.
13. Lawrence RC, Felson DT, Helmick CG, et al: Estimates of the prevalence of arthritis and other rheumatic conditions in the United States: Part II. Arthritis & Rheumatism 58:26-35, 2008.
14. Goodrich L, Nixon A: Medical treatment of osteoarthritis in the horse – A review. The Veterinary Journal 171:51-69, 2006.
15. Richardson DW DG: Dose-dependent effects of corticosteroids on the expression of matrix-related genes in normal and cytokine-treated articular chondrocytes. Inflamm Res 52:39-49, 2003.
16. Fubini SL, Todhunter RJ, Burton-Wurster N, et al: Corticosteroids alter the differentiated phenotype of articular chondrocytes. Journal of Orthopaedic Research 19:688-695, 2001.
17. Robion FC, Doizé B, Bouré L, et al: Use of synovial fluid markers of cartilage synthesis and turnover to study effects of repeated intra-articular administration of methylprednisolone acetate on articular cartilage in vivo. Journal of Orthopaedic Research 19:250-258, 2001.

18. Mienaltowski M, Huang L, Frisbie D, et al: Transcriptional profiling differences for articular cartilage and repair tissue in equine joint surface lesions. BMC Med Genomics 2:60, 2009.
19. Clar C, Cummins E, McIntyre L, et al: Clinical and cost-effectiveness of autologous chondrocyte implantation for cartilage defects in knee joints: systematic review and economic evaluation. Health Technology Assessment 9:III-+, 2005.
20. Mao AS, Mooney DJ: Regenerative medicine: Current therapies and future directions. Proceedings of the National Academy of Sciences of the United States of America 112:14452-14459, 2015.
21. van Susante JLC, Buma P, Schuman L, et al: Resurfacing potential of heterologous chondrocytes suspended in fibrin glue in large full-thickness defects of femoral articular cartilage: an experimental study in the goat. Biomaterials 20:1167-1175, 1999.
22. Vijayan S, Bartlett W, Bentley G, et al: Autologous chondrocyte implantation for osteochondral lesions in the knee using a bilayer collagen membrane and bone graft: a two- to eight-year follow-up study. Journal of Bone & Joint Surgery, British Volume 94-B:488-492, 2012.
23. Brittberg M, Lindahl A, Nilsson A, et al: Treatment of Deep Cartilage Defects in the Knee with Autologous Chondrocyte Transplantation. New England Journal of Medicine 331:889-895, 1994.
24. Wylie JD, Hartley MK, Kapron AL, et al: Failures and Reoperations After Matrix-Assisted Cartilage Repair of the Knee: A Systematic Review. Arthroscopy 32:386-392, 2016.
25. Schiltz JR, Mayne R, Holtzer H: Synthesis Of Collagen And Glycosaminoglycans By Dedifferentiated Chondrocytes In Culture. Journal of Cell Biology 55:A229, 1972.
26. Minas T: A primer in cartilage repair. Journal of Bone & Joint Surgery, British Volume 94-B:141-146, 2012.
27. do Amaral RJ, Pedrosa Cda S, Kochem MC, et al: Isolation of human nasoseptal chondrogenic cells: a promise for cartilage engineering. Stem Cell Res 8:292-299, 2012.
28. Shafiee A, Kabiri M, Langroudi L, et al: Evaluation and comparison of the in vitro characteristics and chondrogenic capacity of four adult stem/progenitor cells for cartilage cell-based repair. J Biomed Mater Res A, 2015.
29. Lallemand E, Vinatier C, J. G: Use of autologous nasal chondrocytes and a self-crosslinking cellulose hydrogel for repairing articular cartilage in horses. *[Utilisation de chondrocytes nasaux autologues et d'un hydrogel cellulosique autoreticulant pour la reparation de cartilage articulaire chez les chevaux.* 38eme Journee de la Recherche Equine, Actes de Colloque:147-152, 2012.
30. Vinatier C, Gauthier O, Fatimi A, et al: An injectable cellulose-based hydrogel for the transfer of autologous nasal chondrocytes in articular cartilage defects. Biotechnol Bioeng 102:1259-1267, 2009.
31. Aust L, Devlin B, Foster SJ, et al: Yield of human adipose-derived adult stem cells from liposuction aspirates. Cytotherapy (Taylor & Francis Ltd) 6:7-14, 2004.
32. Choudhery MS, Badowski M, Muise A, et al: Comparison of human mesenchymal stem cells derived from adipose and cord tissue. Cytotherapy 15:330-343, 2013.
33. Ahern BJ, Schaer TP, Terkhorn SP, et al: Evaluation of equine peripheral blood apheresis product, bone marrow, and adipose tissue as sources of mesenchymal stem cells and their differentation potential. American Journal of Veterinary Research 72:127-133, 2011.
34. Johnson K, Zhu S, Tremblay MS, et al: A stem cell-based approach to cartilage repair. Science 336:717-721, 2012.

35. Steinert A, Rackwitz L, Gilbert F, et al: Concise Review: The Clinical Application of Mesenchymal Stem Cells for Musculoskeletal Regeneration: Current Status and Perspectives. Stem Cells Translational Medicine 1:237-247, 2012.
36. Veronesi F, Giavaresi G, Tschon M, et al: Clinical Use of Bone Marrow, Bone Marrow Concentrate, and Expanded Bone Marrow Mesenchymal Stem Cells in Cartilage Disease. Stem Cells and Development 22:181-192, 2013.
37. Frisbie DD, Kisiday JD, Kawcak CE, et al: Evaluation of adipose-derived stromal vascular fraction or bone marrow-derived mesenchymal stem cells for treatment of osteoarthritis. Journal of Orthopaedic Research 27:1675-1680, 2009.
38. Nixon AJ, Begum L, Mohammed HO, et al: Autologous Chondrocyte Implantation Drives Early Chondrogenesis and Organized Repair in Extensive Full- and Partial-Thickness Cartilage Defects in an Equine Model. Journal of Orthopaedic Research 29:1121-1130, 2011.
39. Penny J HP, Shakesheff KM, Mobasheri A.: The biology of equine mesenchymal stem cells: phenotypic characterization, cell surface markers and multilineage differentiation. Front Biosci 17:892-908, 2012.
40. Radcliffe CH, Flaminio M, Fortier LA: Temporal Analysis of Equine Bone Marrow Aspirate During Establishment of Putative Mesenchymal Progenitor Cell Populations. Stem Cells and Development 19:269-281, 2010.
41. Radtke CL, Nino-Fong R, Gonzalez BPE, et al: Characterization and osteogenic potential of equine muscle tissue- and periosteal tissue-derived mesenchymal stem cells in comparison with bone marrow- and adipose tissue derived mesenchymal stem cells. American Journal of Veterinary Research 74:790-800, 2013.
42. Barberini DJ, Freitas NPP, Magnoni MS, et al: Equine mesenchymal stem cells from bone marrow, adipose tissue and umbilical cord: immunophenotypic characterization and differentiation potential. Stem Cell Research & Therapy 5, 2014.
43. Maia L, Landim-Alvarenga FC, Da Mota L, et al: Immunophenotypic, immunocytochemistry, ultrastructural, and cytogenetic characterization of mesenchymal stem cells from equine bone marrow. Microscopy Research and Technique 76:618-624, 2013.
44. Braun J, Hack A, Weis-Klemm M, et al: Evaluation of the osteogenic and chondrogenic differentiation capacities of equine adipose tissue-derived mesenchymal stem cells. American Journal of Veterinary Research 71:1228-1236, 2010.
45. Broeckx S, Zimmerman M, Crocetti S, et al: Regenerative Therapies for Equine Degenerative Joint Disease: A Preliminary Study. Plos One 9, 2014.
46. Goodrich LR, Chen AC, Werpy NM, et al: Addition of Mesenchymal Stem Cells to Autologous Platelet-Enhanced Fibrin Scaffolds in Chondral Defects: Does It Enhance Repair? J Bone Joint Surg Am 98:23-34, 2016.
47. Kisiday JD, Goodrich LR, McIlwraith CW, et al: Effects of equine bone marrow aspirate volume on isolation, proliferation, and differentiation potential of mesenchymal stem cells. American Journal of Veterinary Research 74:801-807, 2013.
48. Pitsillides AA, Beier F: Cartilage biology in osteoarthritis - lessons from developmental biology. Nat Rev Rheumatol 7:654-663, 2011.
49. Pacifici M, Koyama E, Shibukawa Y, et al: Cellular and Molecular Mechanisms of Synovial Joint and Articular Cartilage Formation. Annals of the New York Academy of Sciences 1068:74-86, 2006.
50. Jenner F, van Osch, GJVM., Cleary, Mairead., Ribitsch, I., Sauer, U., van Weeren, R., Brama, P.: Laser Capture Microdissection of Murine Interzone Cells: Layer Selection and Prediction of RNA Yield. 4 3, 2014.

51. Lefebvre V, Bhattaram P: Vertebrate Skeletogenesis. 90:291-317, 2010.
52. Umeda K, Zhao J, Simmons P, et al: Human chondrogenic paraxial mesoderm, directed specification and prospective isolation from pluripotent stem cells. Sci Rep 2, 2012.
53. Hall BK M, T.: All for one and one for all: condensations and the initiation of skeletal development. Bioessays 22:138-147, 2000.
54. Fell H: The histogenesis of cartilage and bone in the long bones of the embryonic fowl. Journal of Morphology and Physiology 40:417-459, 1925.
55. Rountree RB, Schoor M, Chen H, et al: BMP receptor signalling is required for postnatal maintenance of articular cartilage. . PLoS Biol 2:1815-1827, 2004.
56. Hyde G, Dover S, Aszodi A, et al: Lineage tracing using matrilin-1 gene expression reveals that articular chondrocytes exist as the joint interzone forms. Developmental Biology 304:825-833, 2007.
57. Iwamoto M, Higuchi Y, Koyama E, et al: Transcription Factor Erg Variants and Functional Diversification of Chondrocytes during Limb Long Bone Development. The Journal of Cell Biology 150:27-40, 2000.
58. Iwamoto M, Tamamura Y, Koyama E, et al: Transcription factor ERG and joint and articular cartilage formation during mouse limb and spine skeletogenesis. Developmental Biology 305:40-51, 2007.
59. Koyama E, Ochiai T, Rountree RB, et al: Synovial Joint Formation during Mouse Limb Skeletogenesis. Annals of the New York Academy of Sciences 1116:100-112, 2007.
60. Koyama E, Yasuda T, Wellik DM, et al: Hox11 paralogous genes are required for formation of wrist and ankle joints and articular surface organization. Annals of the New York Academy of Sciences 1192:307-316, 2010.
61. Yasuhara R, Yuasa T, Williams JA, et al: Wnt/β-Catenin and Retinoic Acid Receptor Signaling Pathways Interact to Regulate Chondrocyte Function and Matrix Turnover. Journal of Biological Chemistry 285:317-327, 2010.
62. Dowthwaite GP, Bishop JC, Redman SN, et al: The surface of articular cartilage contains a progenitor cell population. Journal of Cell Science 117:889-897, 2004.
63. Williams R, Khan I, Richardson K, et al: Identification and clonal characterisation of a progenitor cell sub-population in normal human articular cartilage. PLoS One 2010 Oct 14;5(10):e13246 doi: 101371/journalpone0013246:T - epublish, 2010.
64. McCarthy HE, Bara JJ, Brakspear K, et al: The comparison of equine articular cartilage progenitor cells and bone marrow-derived stromal cells as potential cell sources for cartilage repair in the horse. The Veterinary Journal 192:345-351, 2012.
65. Cosden RS, Lattermann C, Romine S, et al: Intrinsic repair of full-thickness articular cartilage defects in the axolotl. Osteoarthritis Cartilage 200.205, 2011.
66. Cosden-Decker RS, Bickett MM, Lattermann C, et al: Structural and functional analysis of intra-articular interzone tissue in axolotl. Osteoarthritis Cartilage 20:1347-1356, 2012.
67. Wade CM, Giulotto E, Sigurdsson S, et al: Genome sequence, comparative analysis, and population genetics of the domestic horse. Science 326:865-867, 2009.
68. Burton-Wurster N, Chen H, Gendelman R, et al: Specific immunological detection of the (V+C)− fibronectin isoform. Matrix Biology 21:393-398, 2002.
69. Sandell LJ, Morris N, Robbins JR, et al: Alternatively spliced type II procollagen mRNAs define distinct populations of cells during vertebral development: differential expression of the amino-propeptide. The Journal of Cell Biology 114:1307-1319, 1991.
70. Hestand M, Zeng Z, Coleman S, et al: Tissue Restricted Splice Junctions Originate Not Only from Tissue-Specific Gene Loci, but Gene Loci with a Broad Pattern of Expression. PloS one 10:e0144302-e0144302, 2015.

71. Bayliss MT, Venn M, Maroudas A, et al: Structure of proteoglycans from different layers of human articular cartilage. Biochemical Journal 209:387-400, 1983.
72. Mienaltowski M, Huang L, Bathke A, et al: Transcriptional comparisons between equine articular repair tissue, neonatal cartilage, cultured chondrocytes and mesenchymal stromal cells. Briefings in Functional Genomics 9:238-250, 2010.
73. Mienaltowski M, Huang L, Stromberg A, et al: Differential gene expression associated with postnatal equine articular cartilage maturation. BMC Musculoskelet Disord 9:149, 2008.
74. Cameron TL, Belluoccio D, Farlie PG, et al: Global comparative transcriptome analysis of cartilage formation in vivo. BMC Dev Biol 9:20, 2009.
75. Peffers MJ, Liu X, Clegg PD: Transcriptomic signatures in cartilage ageing. Arthritis Res Ther 15:R98, 2013.
76. USDA: Lameness and Laminitis in U.S. Horses. National Animal Health Monitoring System. http://wwwaphisusdagov/animal_health/nahms/equine/downloads/equine98/Equine98_dr_Lamenesspdf, 2000.
77. Busschers E, Holt JP, Richardson DW: Effects of glucocorticoids and interleukin-1β on expression and activity of aggrecanases in equine chondrocytes. American Journal of Veterinary Research 71:176-185, 2010.
78. Hu Y, Huang Y, Du Y, et al: DiffSplice: the genome-wide detection of differential splicing events with RNA-seq. Nucleic Acids Res 41:e39, 2013.
79. Pan Q, Shai O, Lee LJ, et al: Deep surveying of alternative splicing complexity in the human transcriptome by high-throughput sequencing. Nat Genet 40:1413-1415, 2008.
80. Singh DO, CF., Hu, Y., Jones, CD., Liu, Y., Chiang, DY., Liu, J., Prins, JF.: FDM: A Graph-based Statistical Method to Detect Differential Transcription using RNA-seq data. Bioinformatics, 2011.
81. Wang K, Singh D, Zeng Z, et al: MapSplice: Accurate mapping of RNA-seq reads for splice junction discovery. Nucleic Acids Research 38:e178, 2010.
82. Hestand MW, K. Zeng, Z. Coleman, SJ. Schroth, GP. Liu, J. MacLeod, JN.: Expression of human tissue-specific splice junctions. Submitted 2013.
83. Hemphill DD, McIlwraith CW, Slayden RA, et al: Adeno-associated virus gene therapy vector scAAVIGF-I for transduction of equine articular chondrocytes and RNA-seq analysis. Osteoarthritis Cartilage 24:902-911, 2016.
84. Rolfe R, Nowlan R, Kenny N, et al: Identification of mechanosensitive genes during skeletal development: alteration of genes associated with cytoskeletal rearrangement and cell signalling pathways. BMC Genomics 15:48-58, 2014.
85. Bowen ME, Ayturk UM, Kurek KC, et al: SHP2 regulates chondrocyte terminal differentiation, growth plate architecture and skeletal cell fates. PLoS Genet 10:e1004364, 2014.
86. Aksoy F, Yildirim YS, Demirhan H, et al: Structural characteristics of septal cartilage and mucoperichondrium. Journal of Laryngology and Otology 126:38-42, 2012.
87. Cluze C, Blond, L., Fontaine, P., Olive, J., Laverty, S.: Foetal and postnatal equine articular cartilage development: magnetic resonance imaging and polarised light microscopy. European Cells & Materials 26:33-48, 2013.
88. Frisbie DD, Morisset S, Ho CP, et al: Effects of Calcified Cartilage on Healing of Chondral Defects Treated With Microfracture in Horses. The American Journal of Sports Medicine 34:1824-1831, 2006.
89. Hatta T, Kishimoto KN, Okuno H, et al: Oxygen tension affects lubricin expression in chondrocytes. Tissue Eng Part A 20:2720-2727, 2014.

90. Khan IM, Redman SN, Williams R, et al: The Development of Synovial Joints, in Gerald PS (ed): Current Topics in Developmental Biology, Vol Volume 79Academic Press, 2007, pp 1-36.
91. Kim S-H, Turnbull J, Guimond S: Extracellular matrix and cell signalling: the dynamic cooperation of integrin, proteoglycan and growth factor receptor. Journal of Endocrinology 209:139-151, 2011.
92. Kim W, Kawcak CE, McIlwraith CW, et al: Histologic and histomorphometric evaluation of midcarpal joint defects in Thoroughbreds raised with and without early conditioning exercise. American Journal of Veterinary Research 73:498-507, 2012.
93. Holden PK, Liaw LH, Wong BJ: Human nasal cartilage ultrastructure: characteristics and comparison using scanning electron microscopy. Laryngoscope 118:1153-1156, 2008.
94. Neuman MK, Briggs KK, Masuda K, et al: A compositional analysis of cadaveric human nasal septal cartilage. The Laryngoscope:n/a-n/a, 2013.
95. van Weeren PR, Firth EC, Brommer H, et al: Early exercise advances the maturation of glycosaminoglycans and collagen in the extracellular matrix of articular cartilage in the horse. Equine Veterinary Journal 40:128-135, 2008.
96. van Weeren PR, Jeffcott LB: Problems and pointers in osteochondrosis: Twenty years on. Vet J 197:96-102, 2013.
97. Hyde G, Boot-Handford RP, Wallis GA: Col2a1 lineage tracing reveals that the meniscus of the knee joint has a complex cellular origin. J Anat 213:531-538, 2008.
98. Aszodi A, Bateman JF, Hirsch E, et al: Normal skeletal development of mice lacking matrilin 1: redundant function of matrilins in cartilage? . Mol Cell Biol 19:7841–7845, 1999.
99. Bolger A, Lohse M, Usadel B: Trimmomatic: A flexible trimmer for Illumina Sequence Data. . Bioinformatics btu170, 2014.
100. Venkatesh T, Suresh PS, Tsutsumi R: tRFs: miRNAs in disguise. Gene 579:133-138, 2016.
101. Flight RM, Harrison BJ, Mohammad F, et al: CategoryCompare, an analytical tool based on feature annotations. Front Genet 5:98, 2014.
102. Yu G, Wang LG, Han Y, et al: clusterProfiler: an R package for comparing biological themes among gene clusters. OMICS 16:284-287, 2012.
103. Boyle E, Weng S, Gollub J, et al: GO::TermFinder--open source software for accessing Gene Ontology information and finding significantly enriched Gene Ontology terms associated with a list of genes. Bioinformatics 20:3710-3715, 2004.
104. Merico M, Isserlin R, Stueker O, et al: Enrichment map: a network-based method for gene-set enrichment visualization and interpretation. PloS one 5:e13984-e13984, 2010.
105. Pons P, Latapy M: Computing communities in large networks using random walks, Proceedings, 20th International Symposium on Computer and Information Sciences Istanbul, TURKEY, 2005 (available from
106. Gehlenborg N: UpSetR: A More Scalable Alternative to Venn and Euler Diagrams for Visualizing Intersecting Sets. . http://CRAN.R-project.org/package=UpSetR, 2016.
107. Gu Z, Eils L, Roland Schlesner R, et al: circlize Implements and enhances circular visualization in R. Bioinformatics 30:2811-2812, 2014.
108. Gu Z: ComplexHeatmap: Making Complex Heatmaps. R package v1.6.0. 2015, https://github/jokergoo/ComplexHeatmap.
109. Rhee SY, Wood V, Dolinski K, et al: Use and misuse of the gene ontology annotations. Nat Rev Genet 9:509-515, 2008.
110. Gilbert S: Developmental Biology (ed 10th Edition.). Sunderland, MA, Sinauer Assoc, Inc. , 2014.

111. Danisovic L, Varga I, Zamborsky R, et al: The tissue engineering of articular cartilage: cells, scaffolds and stimulating factors. Exp Biol Med (Maywood) 237:10-17, 2012.
112. Ortved K, Nixon AJ: Minimally Invasive Implantation of Autologous Chondrocytes Transduced with rAAV5-IGF-I Improves Longterm Cartilage Repair in Full-Thickness Chondral Defects in the Equine Model. Molecular Therapy 21:S113-S113, 2013.
113. Lohan P, Treacy O, Lynch K, et al: Culture expanded primary chondrocytes have potent immunomodulatory properties and do not induce an allogeneic immune response. Osteoarthritis and Cartilage 24:521-533, 2016.
114. Ryan AE, Lohan P, O/'Flynn L, et al: Chondrogenic Differentiation Increases Antidonor Immune Response to Allogeneic Mesenchymal Stem Cell Transplantation. Mol Ther 22:655-667, 2014.
115. Kopesky PW, Vanderploeg EJ, Kisiday JD, et al: Controlled Delivery of Transforming Growth Factor beta 1 by Self-Assembling Peptide Hydrogels Induces Chondrogenesis of Bone Marrow Stromal Cells and Modulates Smad2/3 Signaling. Tissue Engineering Part A 17:83-92, 2011.
116. Tekari A, Luginbuehl R, Hofstetter W, et al: Transforming Growth Factor Beta Signaling Is Essential for the Autonomous Formation of Cartilage-Like Tissue by Expanded Chondrocytes. Plos One 10:17, 2015.
117. Coates E, Fisher JP: Gene expression of alginate-embedded chondrocyte subpopulations and their response to exogenous IGF-1 delivery. Journal of Tissue Engineering and Regenerative Medicine 6:179-192, 2012.
118. Ortved KF, Nixon AJ, Mohammed HO, et al: Treatment of subchondral cystic lesions of the medial femoral condyle of mature horses with growth factor enhanced chondrocyte grafts: A retrospective study of 49 cases. Equine Veterinary Journal 44:606-613, 2012.
119. Kopesky PW, Lee HY, Vanderploeg EJ, et al: Adult equine bone marrow stromal cells produce a cartilage-like ECM mechanically superior to animal-matched adult chondrocytes. Matrix Biology 29:427-438, 2010.
120. Herlofsen SR, Kuchler AM, Melvik JE, et al: Chondrogenic differentiation of human bone marrow-derived mesenchymal stem cells in self-gelling alginate discs reveals novel chondrogenic signature gene clusters. Tissue Eng Part A 17:1003-1013, 2011.
121. Watts AE, Ackerman-Yost JC, Nixon AJ: A Comparison of Three-Dimensional Culture Systems to Evaluate In Vitro Chondrogenesis of Equine Bone Marrow-Derived Mesenchymal Stem Cells. Tissue Engineering Part A 19:2275-2283, 2013.
122. Hegewald AA, Ringe J, Bartel J, et al: Hyaluronic acid and autologous synovial fluid induce chondrogenic differentiation of equine mesenchymal stem cells: a preliminary study. Tissue & Cell 36:431-438, 2004.
123. Marlovits S: Keynote: Biomaterials for autologous matrix-associated chondrocyte transplantation. Journal of Tissue Engineering and Regenerative Medicine 6:53-53, 2012.
124. Streit A, Stern CD: Transplantation of Neural Tissue: Quail-Chick Chimeras, in Sprecher SG (ed): Brain Development: Methods and Protocols, Vol 1082, 2014, pp 235-251.
125. Wa Q, Gao M, Dai X, et al: Induction of chondrogenic differentiation of mouse embryonic mesenchymal stem cells through an in vitro pellet model. Cell Biol Int 39:657-665, 2015.
126. De Schauwer C, Meyer E, Cornillie P, et al: Optimization of the Isolation, Culture, and Characterization of Equine Umbilical Cord Blood Mesenchymal Stromal Cells. Tissue Engineering Part C-Methods 17:1061-1070, 2011.
127. Berg LC, Koch TG, Heerkens T, et al: Chondrogenic potential of mesenchymal stromal cells derived from equine bone marrow and umbilical cord blood. Veterinary and Comparative Orthopaedics and Traumatology 22:363-370, 2009.

128. Hoynowski SM, Fry MM, Gardner BM, et al: Characterization and differentiation of equine umbilical cord-derived matrix cells. Biochemical and Biophysical Research Communications 362:347-353, 2007.
129. Underhill M, Dranse, HJ, Hoffman, LM: Analysis of Chondrogenesis Using Micromass Cultures of Limb Mesenchyme. Methods Mol Biol 1130:251-265, 2014.
130. Vidal MA, Kilroy GE, Johnson JR, et al: Cell growth characteristics and differentiation frequency of adherent equine bone marrow-derived mesenchymal stromal cells: adipogenic and osteogenic capacity. Vet Surg 35:601-610, 2006.
131. Favi PM, Benson RS, Neilsen NR, et al: Cell proliferation, viability, and in vitro differentiation of equine mesenchymal stem cells seeded on bacterial cellulose hydrogel scaffolds. Materials Science & Engineering C-Materials for Biological Applications 33:1935-1944, 2013.
132. Vidal MA, Robinson SO, Lopez MJ, et al: Comparison of Chondrogenic Potential in Equine Mesenchymal Stromal Cells Derived from Adipose Tissue and Bone Marrow. Veterinary Surgery 37:713-724, 2008.
133. Arnhold SJ, Goletz I, Klein H, et al: Isolation and characterization of bone marrow-derived equine mesenchymal stem cells. American Journal of Veterinary Research 68:1095-1105, 2007.
134. Bourzac C, Smith LC, Vincent P, et al: Isolation of equine bone marrow-derived mesenchymal stem cells: a comparison between three protocols. Equine Veterinary Journal 42:519-527, 2010.
135. Decker RS, Koyama E, Pacifici M: Genesis and morphogenesis of limb synovial joints and articular cartilage. Matrix Biol 39C:5-10, 2014.
136. Koyama E, Shibukawa Y, Nagayama M, et al: A distinct cohort of progenitor cells participates in synovial joint and articular cartilage formation during mouse limb skeletogenesis. Developmental Biology 316:62-73, 2008.
137. Betteridge K, MD E, MitchellD, et al: Development of horse embryos up to twenty two days after ovulation: observations on fresh specimens. Journal of Anatomy 135:191-209, 1982.
138. Stewart MS, KM. Burton-Wurster, N. MacLeod, JN. , 15:116-174: Phenotypic stability of articular chondrocytes in vitro: the effects of culture models, BMP-2 and serum supplementation. Journal of Bone and Mineral Research 15:116-174, 2000.
139. Giovannini S, Brehm W, Mainil-Varlet P, et al: Multilineage differentiation potential of equine blood-derived fibroblast-like cells. Differentiation 76:118-129, 2008.
140. Worster AA, Nixon AJ, Brower-Toland BD, et al: Effect of transforming growth factor beta 1 on chondrogenic differentiation of cultured equine mesenchymal stem cells. American Journal of Veterinary Research 61:1003-1010, 2000.
141. Jones M, Calabresi P: Agar-gelatin for embedding tissues prior to paraffin processing. BioTechniques 42:569-570, 2007.
142. Rosenberg LC: Chemical Basis for the Histological Use of Safranin O in the Study of Articular Cartilage. The Journal of Bone & Joint Surgery 53:69-82, 1971.
143. Grogan S, Barbero A, Winkelmann V, et al: Visual Histological Grading System for the Evaluation of in Vitro–Generated Neocartilage. TISSUE ENGINEERING 12:2006.
144. Bustin SA, Benes V, Garson J, et al: The need for transparency and good practices in the qPCR literature. Nature Methods 10:1063-1067, 2013.
145. Ramakers C, Ruijter JM, Deprez RHL, et al: Assumption-free analysis of quantitative real-time polymerase chain reaction (PCR) data. Neuroscience Letters 339:62-66, 2003.

146. Livak KJ, Schmittgen TD: Analysis of Relative Gene Expression Data Using Real-Time Quantitative PCR and the 2−ΔΔCT Method. Methods 25:402-408, 2001.
147. Li S, Sengers BG, Oreffo RO, et al: Chondrogenic potential of human articular chondrocytes and skeletal stem cells: A comparative study. J Biomater Appl 29:824-836, 2015.
148. Shell K, Raabe O, Freitag C, et al: Comparison of Equine Adipose Tissue-Derived Stem Cell Behavior and Differentiation Potential Under the Influence of 3% and 21% Oxygen Tension. Journal of Equine Veterinary Science 33:74-82, 2013.
149. Braunschweig L, Meyer AK, Wagenfuhr L, et al: Oxygen regulates proliferation of neural stem cells through Wnt/beta-catenin signalling. Mol Cell Neurosci 67:84-92, 2015.
150. Buckley CT, Vinardell T, Kelly DJ: Oxygen tension differentially regulates the functional properties of cartilaginous tissues engineered from infrapatellar fat pad derived MSCs and articular chondrocytes. Osteoarthritis Cartilage 18:1345-1354, 2010.
151. Kumar H, Choi DK: Hypoxia Inducible Factor Pathway and Physiological Adaptation: A Cell Survival Pathway? Mediators Inflamm 2015:584758, 2015.
152. Cote AJ, McLeod CM, Farrell MJ, et al: Single-cell differences in matrix gene expression do not predict matrix deposition. Nat Commun 7, 2016.
153. Kisiday JD, Kopesky PW, Evans CH, et al: Evaluation of adult equine bone marrow- and adipose-derived progenitor cell chondrogenesis in hydrogel cultures. J Orthop Res 26:322-331, 2008.
154. Mambelli LI, Santos EJC, Frazao PJR, et al: Characterization of Equine Adipose Tissue-Derived Progenitor Cells Before and After Cryopreservation. Tissue Engineering Part C-Methods 15:87-94, 2009.
155. Pacifici M, Golden EB, Oshima O, et al: Hypertrophic Chondrocytes. Annals of the New York Academy of Sciences 599:45-57, 1990.

VITA

Place of birth: Melton Mowbray, England

Educational institution	***Degree***
Royal Veterinary College, University of London	BVetMed

Professional positions held

Surgeon/Internist	Clinique Veterinaire de la Cote Fleurie, Deauville, France.
Surgeon/Internist	Rhinebeck Equine Clinic, Rhinebeck, NY
Surgeon/Internist	Equine Sports Medicine & Surgery, Weatherford, TX

Scholastic and professional honors

Diplomate, American College of Veterinary Internal Medicine

Diplomate, American College of Veterinary Surgeons

Professional publications

Johnson CB, **Adam EN**, Taylor PM. Evaluation of a modification of the Hudson demand valve on ventilated and spontaneously breathing horses. Vet Rec 135:569-572; 1994.

Adam EN, Morley PS, Chmielewski KE, Carman J, Gonzales G. Detection of a cold-adapted vaccine-strain influenza virus using two commercial assays. Equine Vet J 34(4): 400-404; 2002.

Adam EN, Southwood LL. Surgical and traumatic wound infections, cellulitis, and myositis. Vet Clin N Am: Equine Pract 22:335-361; 2006.

Adam EN, Southwood LL. Primary and secondary limb cellulitis: 44 cases (2000-2006). J Am Vet Med Assoc 231(11):1696-1703;2007.

Levine J, **Adam EN**, MacKay R, Walker M, Cohen N. Confirmed and presumptive cervical vertebral compressive myelopathy in older horses: a retrospective study (1992-2004). J Vet Intern Med 21(4)**:**812-9; 2007.

Levine DG, Smith JJ, Richardson DW, Brown V, Beech J, Habecker P, **Adam E**. Suspected panosteitis in a camel. J Am Vet Med Assoc 231(3):437-41; 2007.

Dahlberg JA, **Adam EN**, Palmer JE, Parente EJ. Gastrointestinal nonrotation in a neonatal foal. Equine Vet J. 21(10):508-512; 2009.

Adam, EN. Bone and Bisphosphonates. Invited article for the Grayson-Jockey Club Foundation website. 2015. https://www.grayson-jockeyclub.org/resources/bones.pdf

Adam, EN. Genomics in Equine Veterinary Medicine. A review article for equine clinicians to enjoy a better understanding of genomics. Equine Veterinary Education. 2016. DOI: 10.1111/eve.12578

Adam EN. Osteoarthritis. In: Davidson EJ (ed): Five Minute Veterinary Consult. Elsevier. 2008

Emma Noble ADAM